

DISS ETH NO. 27252

***Functional characterization of the ubiquitin ligase Nedd4-1 in skin homeostasis and repair***

A thesis submitted to attain the degree of  
**DOCTOR OF SCIENCES OF ETH ZURICH**

(Dr. sc. ETH Zurich)

presented by

***Shen Yan***

Master of Natural Science, Xiamen University

born on 25.12.1989

citizen of the People's Republic of China (PRC)

accepted on the recommendation of

*Prof. Dr Sabine Werner, examiner*

*Prof. Dr. Cornelia Halin Winter, co-examiner*

*Prof. Dr. Liliane Michalik, co-examiner*

2020

*(Year of acceptance of the doctoral thesis by the Department Conference)*

*To my family.*

# Acknowledgments

I would like to thank all those who gave constructive opinions on the project and those who supported me in pursuing and finishing the PhD. Without their help and encouragement, there wouldn't be today's achievements.

Foremost, I would like to thank Prof. Dr. Sabine Werner for giving me this opportunity to do a PhD thesis in her laboratory, and in particular, thank her for her continuous support, regular discussion and advice on this project. Young scientists in our group, including myself, are deeply inspired by her enthusiasm for science. Her positive influence was not only helpful for the scientific research during my PhD, but also for the life-long academic career.

I would also like to thank Prof. Dr. Cornelia Halin Winter and Prof. Dr. Liliane Michalik for agreeing to become members of my doctoral thesis committee and for their important comments, discussions and suggestions regarding the results and priorities during my three committee meetings.

Of course, I would like to thank all the collaborators outside of ETH for the generous support to the project. Thanks to my home country for its financial support for my PhD and the project.

A special thanks to Dr. Paul Hiebert and Hayley Hiebert for all their useful suggestions and technical help on the project. Thanks to Dr. Michael Cangkrama and Dr. Maya Ben-Yehuda Greenwald for their inputs and contributions to the project and to Dr. Mateusz Wietecha, Dr. Mattia R. Bordoli, Dr. Svitlana Kurinna, Prof. Dr. Ulrich auf dem Keller and PD Dr. Matthias Schäfer for their kind and valuable suggestions. Thanks to Dr. Corinne Urwyler for sharing her experience, as well as for scientific research help and suggestions.

I also want to thank Dr. Michael Meyer and Dr. Luigi Maddaluno for their care and help in the first year when I joined the group, not only in experimental technology but also in scientific thinking and daily life. Special thanks to Dr. Michael Meyer for introducing me to the field of skin research and local culture, showing me the laboratory at the beginning, working together, and for lots of Assbar cake moments. Not forgotten is Dr. Jitka Sulcova, for introducing me to the lab in the first month when I came to the group. A lot of thanks to Dr. Natasha Joshi for her help and the nice memories of running in the Käferberg forest and long-distance running together in Zurich Marathon.

Thanks to my master student Raphael Ripamonti, who worked with me for six months, for his contribution to the project. Moreover, except science, we both enjoyed the superkondi, body combat sport and Sushi time.

Sincere thank you to all animal caretakers for taking care of the mice in the EPIC facility, and special thanks to Sol Taguinod for his responsible work.

Thanks to Salome Brüschi, Selina Gurri, Catharina Sängler, Irina Heggli, Stefanie Trautweiler and all the girls in the lab for their company. All these wonderful time toETHger inside or outside the laboratory built very nice memories. Sweet thanks to Sophia Pantasis and Theresa Rauschendorfer, for the warm company, caring, wine and polyball moments. Thanks to Dr. Beat Siegenthaler and Dr. Sukalp Muzumdar for their nice suggestions regarding research, and to Erik Slabber, Till Wüstemann, Michael Koch, and Luca Ferrarese for the wonderful atmosphere in the laboratory. And my thanks also go to Dr. Michèle Telorack, Dr. Marc Bachofner, Dr. Eric Haertel,

Dr. Fabian Egli and Dr. Mira Rocha Sabino Fábio. Thanks to all the team members who have been in the lab, for creating a nice scientific research atmosphere.

Lots of thanks to Ursula Scheier for her arrangements and help with the contract, insurance and other regular lab arrangements. I still remember the time clearly when she picked me up at the airport and introduced me to the local place on the first day when I came to Switzerland. Learned lots of folk-customs from her.

My thanks also go to all the people at HPL, especially to Rolf Huber, IT support and daily maintenance people for their great work to keep the system operating properly.

Thanks to my friends Dr. Wenshu Luo, Dr. Jing Xue, Dr. Wenfei Sun, Dr. Hua Dong and Dr. Tong Liang for their company over the past few years. The time we spent together for chatting, hiking, cooking and playing games remain fresh in the memory. Thanks Dr. Jian Yu, Yuliang He for help with bioinformatics. Thanks to Dr. Yue Xu (National Institute of Biological Sciences, Beijing) for the fruitful discussion about different research topics and sharing common interests in biology since high school.

I apologize to those that I have not personally mentioned here, also thanks to them.

At the end, I would like to thank my parents, my relatives and friends far away in China. Very special thanks go to my parents for their endless support for me studying abroad and pursuing my dreams. I am compunctious to them for my being in a foreign country and unable to accompany them often, especially I felt so sad and guilty as a daughter not able to accompany them during a hard time in 2018. Thanks to my grandmother for setting herself an example to let me know that learning is a lifetime thing. And a lovely thank to Han Zheng for shining into in my life, comforting me when upset, influencing me by his pure love for physics.

# Contents

<b>SUMMARY</b>	<b>i</b>
<b>ZUSAMMENFASSUNG</b>	<b>iii</b>
<b>1. INTRODUCTION</b>	<b>1</b>
1.1 THE MAMMALIAN SKIN	1
1.1.1 Skin architecture	1
1.1.2 Skin function	6
1.2 CUTANEOUS WOUND HEALING	6
1.2.1 Inflammatory phase	6
1.2.2 Proliferation phase	7
1.2.3 Remodeling phase	8
1.2.4 Signaling molecules and cross-talks between skin cells during wound healing	9
1.3 UV IRRADIATION OF THE SKIN	9
1.3.1 Photobiology of solar UV radiation	9
1.3.2 Effects of UV radiation on the skin	10
1.4 UBIQUITINATION AND UBIQUITIN E3 LIGASES	12
1.4.1 Ubiquitination	12
1.4.2 HECT E3 Ligases	14
1.4.3 Nedd4 E3 Ligases	14
1.4.4 Neural precursor cell expressed developmentally down-regulated protein 4-1 (NEDD4-1)	16
1.5 AIM OF THIS THESIS	18
1.5.1 Project 1	18
1.5.2 Project 2	19
<b>2. MATERIALS</b>	<b>20</b>
2.1 CHEMICALS AND OTHER CONSUMABLES	20
2.2 ENZYMES AND GROWTH FACTORS	21
2.3 KITS AND PREFABRICATED PRODUCTS	22
2.4 CELL CULTURE MEDIA AND ADDITIVES	23
2.5 BUFFERS AND SOLUTIONS	23
2.6 ANTIBODIES	26
2.6.1 Primary antibodies	26
2.6.2 Secondary antibodies	27
2.7 OLIGONUCLEOTIDES	27
2.7.1 Primers for genotyping	27
2.7.2 Primers for real-time RT-PCR	27
2.7.3 siRNA	28
2.7.4 shRNA	28
2.8 LABORATORY EQUIPMENT AND MATERIALS	28
2.9 SOFTWARE	29
<b>3. METHODS</b>	<b>29</b>
3.1 ANIMAL EXPERIMENTS	29
3.1.1 Mouse lines	29

3.1.2	Mouse genotyping .....	30
3.1.3	Wounding .....	32
3.1.4	UV irradiation .....	32
3.1.5	Transepidermal water loss (TEWL) analysis.....	32
3.1.6	Tissue collection after animal experiments.....	32
3.1.7	Separation of epidermis and dermis .....	33
3.1.8	Identification of proliferating cells.....	33
<b>3.2</b>	<b>RNA METHODS</b> .....	<b>33</b>
3.2.1	RNA isolation from tissue.....	33
3.2.2	RNA isolation from cultured cells.....	34
3.2.3	Quantification and quality analysis of isolated RNA.....	34
3.2.4	Reverse transcription .....	34
3.2.5	Quantitative Real-Time PCR (qRT-PCR).....	35
<b>3.3</b>	<b>PROTEIN METHODS</b> .....	<b>35</b>
3.3.1	Preparation of protein lysates from skin tissue or cultured cells .....	35
3.3.2	Determination of protein concentrations .....	36
3.3.3	Western blot (WB) .....	36
<b>3.4</b>	<b>CELL CULTURE</b> .....	<b>37</b>
3.4.1	Isolation of primary murine keratinocytes.....	37
3.4.2	Isolation of primary dermal fibroblasts .....	37
3.4.3	Cultivation of murine immortalized keratinocytes.....	38
3.4.4	Cultivation of murine immortalized fibroblasts .....	38
3.4.5	Passaging of cells.....	38
3.4.6	Freezing and thawing of cells.....	38
3.4.7	siRNA-mediated knockdown .....	39
3.4.8	pInducer20/ 21 Nedd4-1 cloning .....	39
3.4.9	Lentiviral transduction of cultured cells.....	41
3.4.10	Growth factor treatment.....	41
3.4.11	Cell culture assays .....	42
<b>3.5</b>	<b>HISTOLOGY</b> .....	<b>43</b>
3.5.1	Hematoxylin and eosin (HE) – staining .....	43
3.5.2	Masson Trichrome staining.....	44
3.5.3	Herovici staining .....	44
3.5.4	Immunofluorescence and immunohistochemistry.....	45
<b>3.6</b>	<b>MICROSCOPY</b> .....	<b>46</b>
<b>3.7</b>	<b>STATISTICAL ANALYSIS</b> .....	<b>46</b>
<b>4.</b>	<b>PROJECTS</b> .....	<b>47</b>
4.1	NEDD4-1 IS A KEY REGULATOR OF EPIDERMAL HOMEOSTASIS, WOUND REPAIR AND UV RESPONSE .....	47
4.2	NEDD4-1 IS A KEY REGULATOR OF FIBROBLAST FUNCTION <i>IN VITRO</i> AND DURING MOUSE DEVELOPMENT .....	86
<b>5.</b>	<b>DISCUSSION AND OUTLOOK</b> .....	<b>116</b>
5.1	ROLE OF NEDD4-1 IN KERATINOCYTES.....	116
5.1.1	Keratinocyte-derived Nedd4-1 in skin development and homeostasis .....	116
5.1.2	Keratinocyte-derived Nedd4-1 in wound healing .....	118
5.1.3	Nedd4-1 in UV-induced apoptosis.....	120
5.2	ROLE OF NEDD4-1 IN FIBROBLASTS.....	121
5.3	POTENTIAL ROLE OF NEDD4-1 IN SKIN CANCER .....	123
5.4	MECHANISM OF ACTION OF NEDD4-1 IN SKIN CELLS .....	124

5.4.1 *Nedd4-1 regulates skin cell behavior*.....124  
5.4.2 *Finding targets of Nedd4-1 in skin cells* .....125  
5.5 CONCLUSION.....127

**COMPLETE BIBLIOGRAPHY** I

**CURRICULUM VITAE AND PUBLICATIONS** XI

# Summary

The skin is the largest organ of the body and forms a protective barrier against invading pathogens, allergens, and toxins, as well as harmful UV irradiation, and it protects from excessive water loss from the inside. Any insult to this barrier is therefore a major challenge and requires rapid and efficient repair.

Wound healing is a complex and dynamic biological process, and various cellular pathways are activated after injury to restore tissue integrity. Different cell types, including keratinocytes, fibroblasts, endothelial cells and immune cells, migrate, proliferate and differentiate to reach this goal. These cells produce various growth factors and cytokines, which are important for intercellular communication. An imbalance in the regulation and expression pattern of these signaling molecules causes impaired repair and even results in the formation of non-healing ulcers. Interestingly, it has recently been shown that growth factor signaling is regulated by various types of post-translational protein modifications. One of them is protein ubiquitination, and the previous work of our laboratory identified the ubiquitin ligase Nedd4-1 as a positive regulator of epidermal growth factor receptor (EGFR) signaling with a key function in liver regeneration. However, the function of the E3 ubiquitin ligase Nedd4-1 in the skin has not been well studied. Therefore, this thesis project aimed to study the function of Nedd4-1 in skin development, homeostasis, injury and repair.

Expression studies revealed that Nedd4-1 is strongly expressed in the epidermis and even more in the dermis of mouse skin as well as in cultured keratinocytes and fibroblasts. This is functionally relevant, since knockout of Nedd4-1 in keratinocytes or fibroblasts and other mesenchymal cells in mice had various severe consequences. Mice with Nedd4-1 deficiency in keratinocytes exhibit reduced epidermal thickness and attenuated terminal differentiation of keratinocytes as well as abnormalities in hair follicle cycling. In particular, healing of full-thickness excisional wounds was strongly impaired in the mutant mice, mainly as a result of impaired re-epithelialization, but also of reduced wound contraction. The re-epithelialization defect resulted from reduced proliferation and migration of keratinocytes as shown *in vivo* and in knock-down studies with cultured keratinocytes. Loss of Nedd4-1 in keratinocytes also aggravated UVB-induced keratinocyte apoptosis. Functional *in vitro* studies suggest that the beneficial activities of Nedd4-1 in wound repair and UV response are at least in part mediated by impaired EGFR-induced Erk1/2 signaling. These results identify a crucial function of Nedd4-1 in epidermal homeostasis, UV response and wound healing.

Knockout of Nedd4-1 in mesenchymal cells caused early postnatal lethality, and E18.5 embryos exhibited strong growth retardation and malformation of various organs. In particular, bone and lung development were impaired in the mutant mice. The skin of these mice exhibited dermal atrophy, and concomitantly severe impairments of keratinocyte differentiation, resulting in a hyperthickened epidermis. These abnormalities are at least in part a consequence of the reduced proliferation and migration of Nedd4-1-deficient fibroblasts, as revealed by knock-down studies in cultured fibroblasts. The reduction in the number of fibroblasts and/or abnormal function of these cells is likely to affect the epidermis by alterations in paracrine-acting factors or extracellular matrix proteins. Impaired EGFR – Erk1/2 signaling is a possible cause for the proliferation and migration deficiency of Nedd4-1 deficient fibroblasts, although additional, as yet unknown mechanisms may well be involved.



Taken together, the results of this thesis revealed novel roles of Nedd4-1 in fibroblasts and keratinocytes, which are relevant for skin development, wound healing and UVB response, and they emphasize the relevance of protein ubiquitination in these processes.

# Zusammenfassung

Die Haut ist das grösste Organ des menschlichen Körpers und bildet eine schützende Barriere gegen Krankheitserreger, Allergene, und Giftstoffe. Sie schützt zudem vor schädlicher UV-Strahlung und vor zu starkem Wasserverlust. Jede Verletzung dieser Barriere muss daher rasch und effizient repariert werden.

Die Wundheilung der Haut ist ein komplexer und dynamischer Prozess, während dessen viele zelluläre und molekulare Signalwege aktiviert werden, um die Integrität des Gewebes wiederherzustellen. Verschiedene Zelltypen, insbesondere Keratinozyten, Fibroblasten, Endothelzellen und Immunzellen, wandern in die Wunde ein, teilen sich und differenzieren, um dieses Ziel zu erreichen. Diese Zellen produzieren verschiedene Wachstumsfaktoren und Zytokine, die wichtig sind für die interzelluläre Kommunikation. Ein Ungleichgewicht im Expressionsmuster dieser Signalmoleküle verursacht Wundheilungsstörungen und kann zur Bildung von nicht heilenden Geschwüren führen.

Interessanterweise konnte kürzlich gezeigt werden, dass die Wachstumsfaktor-Wirkung durch verschiedene posttranslationale Proteinmodifikationen reguliert werden kann. Eine davon ist Protein-Ubiquitylierung, und vorausgehende Arbeiten identifizierten die Ubiquitin-Ligase Nedd4-1 als einen positiven Regulator der Signaltransduktion durch den Rezeptor für den Epidermalen Wachstumsfaktor (EGF). Unsere Arbeitsgruppe hat gezeigt, dass dieser Regulations-Mechanismus für die Leberregeneration von entscheidender Bedeutung ist. Über die Funktion von Nedd4-1 in der Haut und bei der Wundheilung ist jedoch bisher sehr wenig bzw. gar nichts bekannt. Daher war es das Ziel dieser Doktorarbeit, die Funktion von Nedd4-1 bei der Entwicklung, Homöostase, Verletzung und Reparatur der Haut zu untersuchen.

Expressions-Untersuchungen zeigten, dass Nedd4-1 in der Epidermis und noch stärker in der Dermis der Mauhaut exprimiert wird, sowie in kultivierten Keratinozyten und Fibroblasten. Dies ist funktionell relevant, da der Knockout von Nedd4-1 in Keratinozyten oder Fibroblasten und anderen mesenchymalen Zellen von Mäusen schwerwiegende Konsequenzen hatte. Mäuse, denen Nedd4-1 in Keratinozyten fehlt, zeigten eine reduzierte epidermale Dicke und eine defekte terminale Differenzierung der epidermalen Keratinozyten, sowie Abnormitäten im Haarzyklus. Insbesondere war die Heilung von Exzisions-Hautwunden verzögert, was auf Defekten in der Re-epithelialisierung sowie der Wundkontraktion beruht. Der Re-epithelialisierungs-Defekt basiert auf der verlangsamten Migration und Teilung von Keratinozyten, was sowohl im Wundgewebe der Knockoutmäuse also auch in kultivierten Keratinozyten mit Nedd4-1 Knock-down gezeigt werden konnte. Der Verlust von Nedd4-1 in Keratinozyten führte auch zu einer verstärkten UVB-induzierten Apoptose dieser Zellen *in vivo*. Resultate, die in funktionellen *in vitro* Experimenten erzielt wurden, sprechen dafür, dass die Wundheilungsstörung und die verstärkte UV-induzierte Apoptose in Nedd4-1 Knockoutmäusen möglicherweise zumindest teilweise auf eine weniger effiziente Aktivierung des Erk1/2 Signalweges durch den EGF Rezeptor zurückzuführen ist.

Der Knockout von *Nedd4-1* in mesenchymalen Zellen führte dazu, dass die Mäuse während der späten embryonalen Entwicklung oder direkt nach der Geburt starben. Achtzehn Tage alte Embryonen zeigten deutliche Entwicklungsstörungen in verschiedenen Organen. Auffallend waren die Knochenabnormitäten sowie Defekte in der Lunge, und auch die Haut zeigte eine stark reduzierte Zellularität in der Dermis und eine verdickte Epidermis. Die dermalen Defekte sind

vermutlich auf die verlangsamte Migration und Teilung von Nedd4-1-defizienten Fibroblasten zurückzuführen, wie in Nedd4-1 Knock-down Experimenten mit kultivierten Hautfibroblasten gezeigt werden konnte. Die Reduktion der Zahl der Fibroblasten oder funktionelle Defekte dieser Zellen könnten dann zu einer reduzierten Produktion von parakrin wirkenden Faktoren oder extrazellulären Matrixproteinen führen, welche wiederum die Epidermis beeinflussen. Die ineffiziente Erk1/2 Aktivierung durch den EGF Rezeptor ist auch hier ein möglicher Grund für die Abnormitäten in den Fibroblasten, obwohl vermutlich noch weitere, bisher unbekannte Mechanismen involviert sind.

Zusammenfassend konnten in dieser Doktorarbeit wichtige Funktionen von Nedd4-1 in Fibroblasten und Keratinozyten identifiziert werden, die von grosser Relevanz sind für die Hautentwicklung, die Wundheilung und die UV Antwort der Haut. Dies zeigt die grosse Bedeutung von Protein-Ubiquitylierung bei diesen Prozessen.

# 1. Introduction

## 1.1 The mammalian skin

Over the last few decades, research in the areas of skin biology and clinical dermatology developed rapidly. Our largest organ, the skin, protects the body against mechanical, chemical and microbial insults from the external environment. Any insult to this barrier is therefore a major challenge and requires rapid and efficient repair. The development of strategies to improve the repair process requires a thorough understanding of the underlying molecular and cellular mechanisms, and this thesis project aimed to contribute to this knowledge by characterizing a novel regulator in skin homeostasis and wound repair.

### 1.1.1 Skin architecture

The average thickness of human skin is 2.5 mm and it contributes about 6% to our total body weight [1]. From top to bottom, the skin comprises the epidermis, the dermis and the hypodermis (Figure 1). The skin develops and forms the stratified structures with appendages after gastrulation [2]. About three weeks after fertilization, the epiblast invaginates along the primitive streak, and epiblast cells proliferate and migrate downward to form three germ layers: the ectoderm, mesoderm, and endoderm. Organs, including skin, develop from these three germ layers [3]. The epidermis originates from the ectoderm, while the dermis and the hypodermis originate from the mesoderm [2, 4].

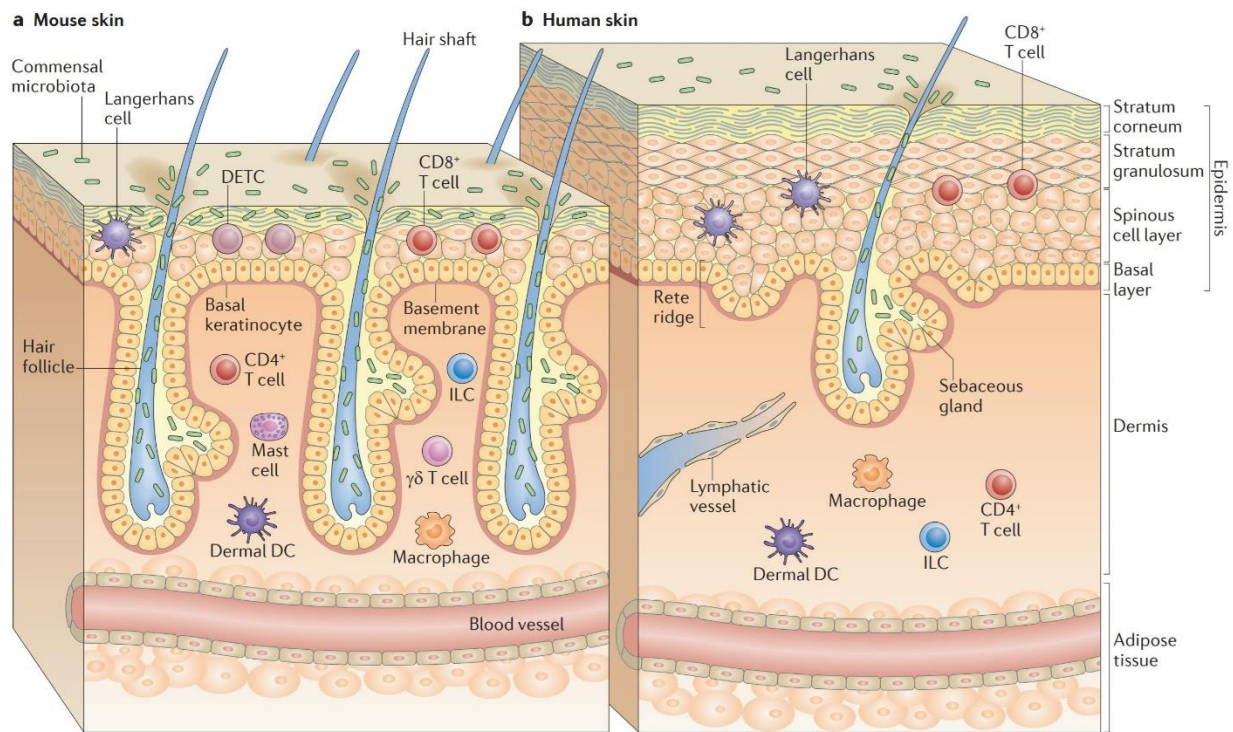


Figure 1. Skin structure, its appendages and cellular components.

The skin's longitudinal structure with its appendages is shown for the mouse (a) and human (b) skin. Human epidermis and dermis are thicker than in the mouse, while mice have more hair follicles than humans and they are more densely packed. Except for hair follicles, various accessory structures, including sebaceous glands, blood vessels, and lymphatic vessels, are present in the skin. The stratified epidermis can be generally divided into *stratum corneum* (cornified layer), *stratum granulosum* (granular layer), *stratum spinosum* (spinous layer), and *stratum basale* (basal layer). Langerhans cells, dendritic epidermal T cells (DETCs; in mouse skin) and CD8<sup>+</sup>T cells distribute among keratinocytes in the epidermis. The dermis is populated by fibroblasts, macrophages, mast cells, and other immune cells. Reproduced from [5].

### 1.1.1.1 The epidermis

The epidermis is the outermost layer of the body. It is a non-vascularized epithelium built up by keratinocytes that continuously differentiate and form a stratified epidermis. Its thickness is, in most areas, between 75 and 150  $\mu\text{m}$  in humans [1]. It serves as a shield to protect the body from physical and chemical trauma. In human skin, from the bottom to the top, the epidermis contains several layers: *S. basale* (SB), *S. spinosum* (SS), *S. granulosum* (SG) and *S. corneum* (SC) (Figure 1, 2). Keratinocytes are the main cell type (about 90%) of the epidermis. Cells in the lowest layer, the *stratum basale*, proliferate, migrate to the suprabasal layer and start to differentiate, thereby forming the highly organized epidermal structure. During this upward migration and differentiation process, they gradually change their morphology and then start to produce a variety of differentiation-specific keratins and other structural proteins. Keratinocytes are closely connected by desmosomes to maintain relative positions, forming the unique barrier of the epidermis. They play an essential role in rebuilding the new epidermis after trauma [6], a process that will be introduced in section 1.2.

The epidermis is connected to a non-cellular basement membrane (basal lamina), which is required for attachment of epidermal cells and for separating the epidermis from the dermis. The main components of the basement membrane are extracellular matrix (ECM) proteins, such as collagen IV, laminins, tenascin-C and others [7]. Attached to this membrane is the epidermal basal layer (*S. basale* or *S. germinativum*). Cylindrical non-differentiated, but proliferation-competent keratinocytes are the main components of this layer. They express mainly cytokeratin 5 and cytokeratin 14. In the basal layer, stem cells divide slowly and can produce rapidly dividing transit-amplifying cells. They are crucial for carrying out epithelial turnover after injury [8, 9]. Another specialized cell type of the basal layer, melanocytes, are cells that can produce melanin pigment that is transferred to keratinocytes to protect them from UV irradiation. Besides, the basal layer includes Merkel cells, which make synapse-like contacts with myelinated nerve fibers and epithelial cytoskeletal components, functioning as slow-adapting mechanoreceptors. They also have cytoplasmic granules containing neuropeptides that act as neurotransmitters [10, 11].

Above the *S. basale* is the *S. spinosum*, which in humans includes 8 to 10 layers of keratinocytes with a "spiny-like" appearance. They are derived from the transit-amplifying cells, which move to the suprabasal layer and differentiate. In normal skin, cells of the *S. spinosum* have lost their mitotic activity and begin to express other structural proteins, such as cytokeratin 1 and cytokeratin 10. Between these keratinocytes are some Langerhans cells, which are derived from bone marrow and have a long dendritic structure. They act as antigen-presenting cells and thereby protect the skin from foreign entities. When exogenous or endogenous antigens activate the Langerhans cells, they move to the skin lymph nodes to activate T cells. Those activated T cells then migrate to the location of the antigen to elicit an immune response [12].

The next outer part is the *S. granulosum*, which in humans contains 3 to 5 layers of non-dividing keratinocytes with a granular appearance. They contain keratohyalin granules, which include e.g. loricrin and filamentous filaggrin. Filaggrin helps to cross-link keratin filaments, thereby contributing to cell compaction. Keratinocytes of the *S. granulosum* are sealed together by tight junctions, which form an important component of the epidermal barrier [13].

The outmost layer of the epidermis is the *S. corneum*, which contains non-viable corneocytes that have retained some biochemical activities. They are anucleated keratinocytes, which are in the final phase of differentiation. They have degraded their main organelles and therefore cannot produce new proteins. These highly differentiated cells appear flat and cross-connected with each other, forming a tight seal for skin protection [13].

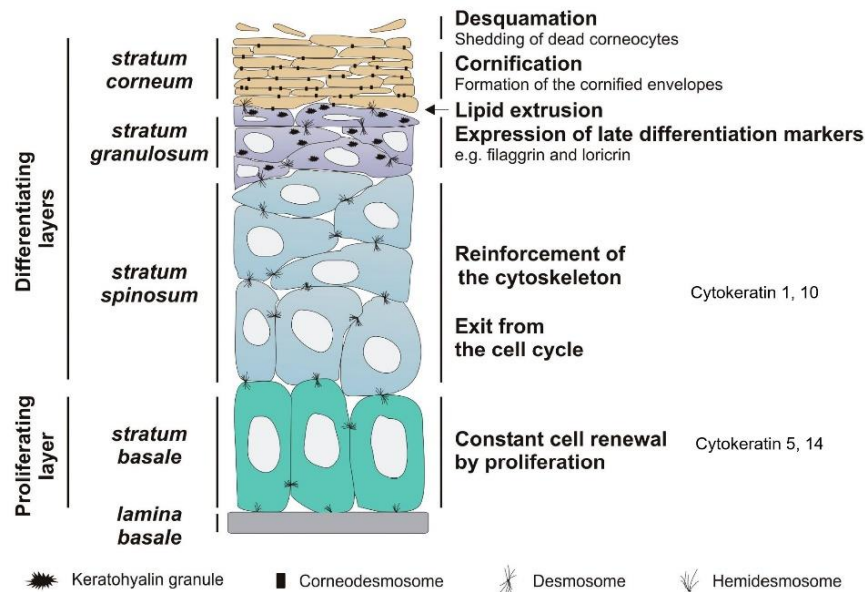


**Figure 2. Structure of epidermis and cellular events associated with the different layers.**

A schematic overview of the four epidermal layers (from bottom to the top): *stratum basale*, *stratum spinosum*, *stratum granulosum* and *stratum corneum*. Desmosomes connect cells, and different layers are shown. Keratinocytes of the epidermis undergo programmed differentiation, and lost cells are replaced by proliferating cells in the basal layer. This allows the constant renewal of the epidermis. The main cellular events associated with each layer and the corresponding markers are indicated on the right-hand side of the figure. Reproduced from [14].

### 1.1.1.2 The dermis

Below the epidermis is the dermis. It provides physical support and nutrition to the epidermis. Its thickness in humans is on average 2 mm. Based on the cell number and connective tissue components, it can be divided into two parts, the upper papillary part and the reticular part below. The dermis serves as a home for many different cell types, e.g. fibroblasts, cells of the blood and lymphatic vessels, macrophages, mast cells, and T cells [15]. Much fewer cells are present in the dermis than in the epidermis. The primary cell type is a heterogeneous migration-competent cell type, called fibroblast. These cells deposit a fibrous and amorphous extracellular matrix (ECM), which occupies most of the space in the dermis [15, 16].

Dermal fibroblasts produce ECM proteins, including collagen type I and type III, fibronectin and various proteoglycans. These fibroblasts are also responsible for the production of most



basement membrane proteins, thereby connecting the dermis to the epidermis. Dermal fibroblasts in normal skin rarely replicate or differentiate, but this is different in the case of trauma. Proliferation, migration, and differentiation of fibroblasts play an essential role during wound healing [17]. For instance, fibroblasts can give rise to myofibroblasts, which are important for the wound to heal. Cross-talk between fibroblasts and keratinocytes through paracrine signaling pathways is also vital for maintaining the homeostasis of the skin, especially during wound healing [18, 19], as described in more detail in section 1.2.

### 1.1.1.3 The hypodermis

Underneath the dermis, anatomists defined a layer called hypodermis/sub-cutis. This fatty tissue connects the dermis to skeletal and muscular parts. The space occupied by the hypodermis is affected by the nutritional supply and other conditions, resulting in major individual differences. In the hypodermis, adipocytes are surrounded by collagens and elastin. The hypodermis is of great significance for water and energy storage. It mainly contributes to thermal insulation [20]. In addition, the thickness of the subcutis is characteristic for the different hair cycle stages in mice. This will be introduced in the next section.

### 1.1.1.4 Skin appendages

Skin is like a small complex ecosystem with multiple appendages, including hair follicles and the associated sebaceous glands as well as sweat glands.

#### Hair follicles

There are approximately five million hair follicles (HF) in human skin, only 2% on the head. The size and distribution of the hairs determine the appearance, rather than their number. In furry animals, hairs play a crucial role in thermoregulation. Significant psychological problems are associated with abnormalities in the number, type or color of hairs. HF plays a crucial role in systemic regulatory networks. Interestingly, cells in the HF can respond to many hormones and also produce lots of hormones themselves, e.g. sexual steroid hormones, prolactin, and  $\alpha$ -melanocyte-stimulating hormone and peptides that are generated upon cleavage of the latter. Besides, neuro-hormones, -peptides, and -transmitters allow HF to adapt to stress. Controlled cell proliferation, differentiation and migration take place in this mini-organ. The HF is the only permanently regenerating organ. Generally, healthy HFs continuously undergo three stages of the growth cycle: anagen (growing), catagen (regression) and telogen (quiescence). This cycling is regulated by several hormones, cytokines, and growth factors, and can be affected by different pharmaceutical products [21-23] (Figure 3). So far, no hypothesis can fully explain the enigmas of controlling hair cycling. The bulge-activation hypothesis is the most popular one and suggests that the stem cell-like epithelial cells in the upper HF bulge are activated at the end of the telogen. Then they proliferate and differentiate to replace the lower part of the HF [24].

The morphogenesis of HF and its cyclic transformations usually follow a regular timeline in mice [21] (Figure 3). In wild-type C57BL/6 mice, the first telogen occurs about three weeks after birth and lasts for a week. The second telogen period is from week 7 to 11. This relatively quiescent phase is usually followed by the anagen period. During telogen, the entire HF without inner root sheath (IRS) is anchored in the dermis. There is a compact dermal papilla (DP) with a ball-shape attached to the cap of hair germ cells. When HF enter the anagen period, keratinocyte stem cells begin to divide and proliferate between the DP and club hair, and this middle part between DP and club hair gradually expands. Differentiating keratinocytes appear around the upper pole of the DP. The IRS gradually forms on the DP, while the DP becomes smaller. The bulb gets a little

closer to the boundary of dermis and subcutis until it breaks through the boundary. During the transition from telogen to anagen, the thickness of the subcutis increases. The gradually differentiated keratinocytes form different layers of the IRS, and the newly-generated hair shaft (HS) is wrapped up by the IRS and grows upward. The growing HS first reaches up to the level of the sebaceous gland, then the hair canal, and at the end emerges through the epidermis. The long and straight HS is the most apparent characteristic of anagen [25]. When this continuous and steady HF cycling is disturbed, it affects the function of the skin. In this thesis, a role of Nedd4-1 in the regulation of HF cycling was identified (see section 3).

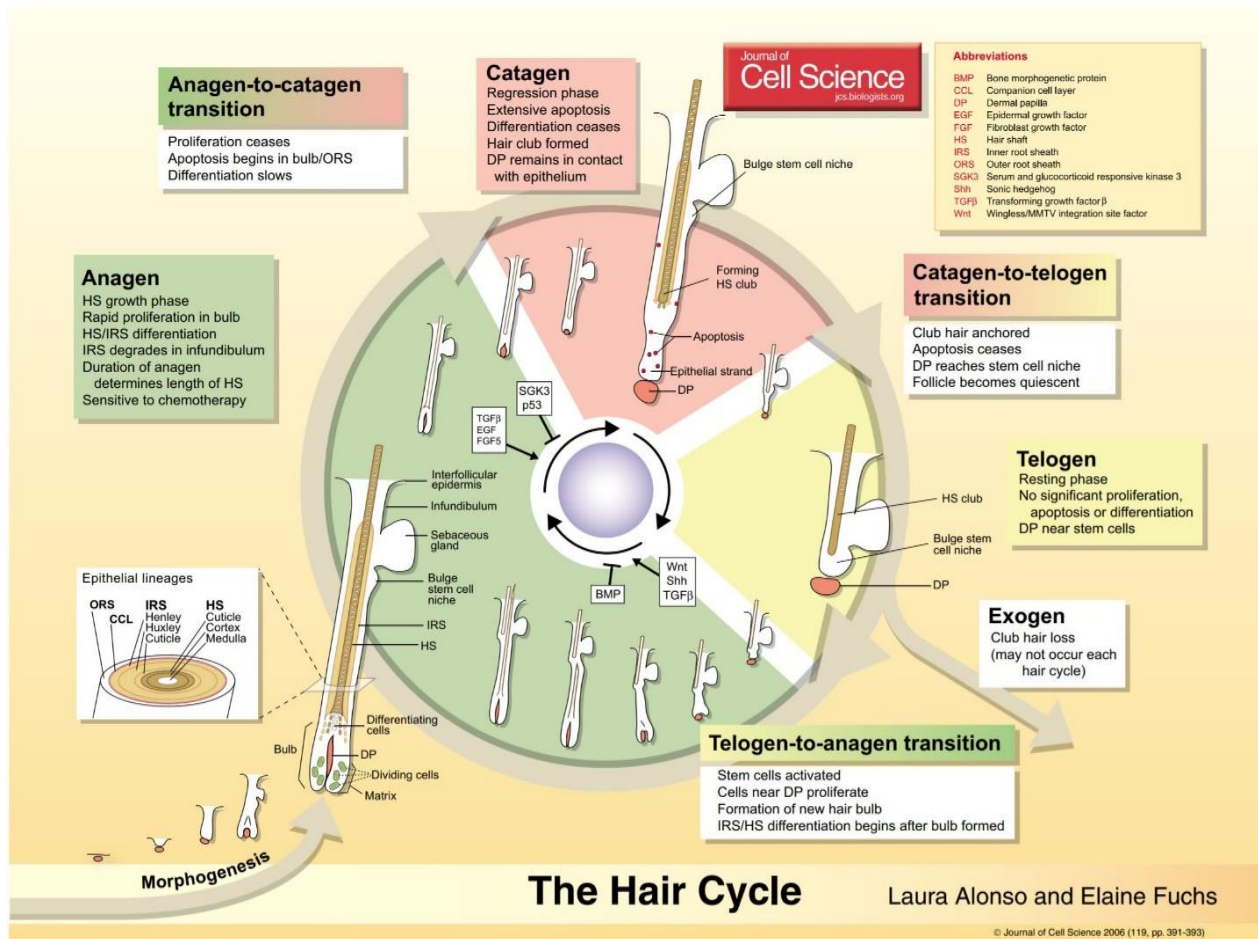


**Figure 3. The hair cycle.**

Schematic representation of the main stages of HF development and cycling with a detailed description. Anagen: the growth phase, catagen: regression phase, telogen: quiescent phase, exogen: active shedding phase. Signals, which regulate these processes, are indicated in the figure. Reproduced from [26].

### Sebaceous glands

There are up to 800 sebaceous glands per square centimeter on the face and scalp in humans associated with the hair follicles. Sebocytes disintegrate and release sebum, a sticky yellow liquid containing sterol esters, free sterols, fatty acids and triglycerides. This secretion manner of the sebaceous gland is unique. Except for secreting sebum, sebaceous glands regulate steroid hormone production, as well as glucose and glutamine metabolism. Moreover, they play a role in



producing anti-inflammatory and pro-inflammatory molecules. In addition to interacting with neuropeptides, they also secrete corticotropin-releasing hormone under stress [1, 27].

### Sweat glands

Sweat glands have a long thin duct connected to the surface of the skin and a supportive coiled part containing secretory cells and myoepithelial cells. There are about three million merocrine glands in human skin. They secrete sweat to keep the core temperature of our body at 37.5°C. The osmotic force pushes the sweat up and out [28]. Sympathetic nerve fibers are wound around the eccrine gland and regulate its activity. This neural stimulation is realized by the neurotransmitter acetylcholine. 99% of the sweat is water, and the rest are electrolytes and other small molecules [1].

## 1.1.2 Skin function

The skin covers the whole body and serves as a barrier against outside pathogens, noxious substances, and harmful UV irradiation, and it protects from excessive water loss from the inside. This barrier is not entirely impermeable to water. It is also possible for water to pass through the epidermis and reach the external environment [29-31]. The skin also acts as a periphery sensor/transducer of the information from the environment because of its delicate network of blood vessels, glands, and nerves. The appendages cooperate to maintain the homeostasis of the body. Finally, the skin plays a central role in the production of vitamin D [32]. Because of these essential functions, any damage to the skin has to be rapidly and efficiently repaired, which is achieved by the wound healing process (introduced in the upcoming section 1.2).

## 1.2 Cutaneous wound healing

Skin, our outermost protective layer, has to remain intact to fulfill its barrier function. Upon injury, a rapid wound healing process is initiated, aiming to restore the damaged body site. Wound healing is a dynamic and complex biological process, and various cellular pathways are activated and synchronized after injury to restore tissue integrity. Different cell types, including keratinocytes, fibroblasts, endothelial cells and immune cells, migrate, proliferate and differentiate to reach this goal. In most mammals, the outcome of the repair process after skin injury that affects the dermis is a scar, a fibrotic tissue that exhibits reduced strength and elasticity compared to non-injured skin and is devoid of all skin appendages. However, some “lower” organisms, such as certain salamanders, can completely regenerate injured tissues, including amputated limbs [33]. In addition, mammals (including humans) up to the end of the third trimester heal wounds without scar formation [34]. Studies of how regeneration starts and how pathways and cells are coordinated and regulated during regeneration vs. repair should improve medical practice in the future.

### 1.2.1 Inflammatory phase

In mammals, wound repair is a continuous process. It is divided arbitrarily into three distinct, but partially overlapping phases: inflammation, proliferation and remodeling (Figure 4).

The first phase of wound repair is the acute inflammatory phase, which starts instantly after tissue injury and lasts 1 to 3 days [35]. Bleeding happens immediately after injury, which triggers the activation of the immune system, inflammatory pathways and the coagulation cascade. Platelets aggregate at the site of injury, initiating haemostasis. They degranulate, and the blood gradually

coagulates, eventually forming a clot that temporarily seals the wound. The clot consists of fibrin that is generated from fibrinogen by thrombin-mediated cleavage. It also includes vitronectin, thrombospondin, fibronectin and other proteins. The fibrin matrix provides a scaffold for cells that infiltrate the wound.

The clot also contains various growth factors released from the degranulated platelets and cytokines secreted by blood cells. Increased vasodilation and permeability, together with these chemotactic cues, cause more circulating immune cells to come to the wound site. Neutrophils are recruited within minutes of injury due to their high abundance in the circulation [35]. They are responsible for clearing contaminating bacteria, and they also produce pro-inflammatory cytokines. The latter activate local fibroblasts and keratinocytes during the repair process [36]. One to three days later, unless the wound is severely infected, neutrophil infiltration stops. Monocytes are also attracted to the wound area and differentiate into tissue macrophages. Macrophages and neutrophils phagocytose pathogens and cell debris, and they release proteases and reactive oxygen species (ROS) to destroy invading pathogens. However, they also secrete various growth factors and cytokines. Together with the earlier cocktail of growth factors and cytokines released by degranulating platelets, they initiate re-epithelialization, granulation tissue formation, and wound contraction.

## 1.2.2 Proliferation phase

The proliferative stage, the second stage, occurs 2 to 10 days after injury. During this phase, various cell types, especially keratinocytes, fibroblasts and endothelial cells, proliferate and migrate to heal the wound [37]. The migration of keratinocytes across the injured dermis is the first event. Keratinocytes at the edge of the wound begin to migrate to the center of the wound under the blood clot, and a new layer of epithelium forms over the denuded wound. This whole process is called re-epithelialization.

Studies indicated that both basal and suprabasal keratinocytes migrate into the wound [38]. Initially, keratinocytes have to dissolve the hemidesmosomes, which connect the keratin cytoskeleton of keratinocytes with laminin 5 in the basement membrane [39]. This action is achieved with the help of matrix metalloproteinases (MMPs) and plasmin [40]. The front-leading keratinocytes also produce new integrins, and those integrins are repositioned in the cell. Together with the contraction of actinomyosin filaments, this allows keratinocytes to migrate over the injured dermis and newly formed granulation tissue [41]. Migrating keratinocytes express keratins 6, 16, and 17. Together with other cellular keratins, they aggregate around the nucleus and retract from the cell edge [42]. This keratin cytoskeletal network provides cell and tissue strength during the re-epithelialization.

In order to supply the newly formed tissue with oxygen and nutrients, the formation of new blood vessels is required. This is mainly achieved by angiogenesis at the wound site. The new capillaries work together with immune cells and fibroblasts to build up granulation tissue and to replace the fibrin-rich provisional matrix with a new matrix composed of collagen III, fibronectin and various other matrix proteins. The proliferating and migrating cells are embedded in this matrix, which has a granular appearance because of the high number of cell nuclei. Therefore, this new tissue is called granulation tissue. Keratinocytes use the granulation tissue as a substrate to migrate during the later phase of repair.

A few hours after the onset of migration, keratinocytes behind the migratory tongue begin to proliferate to replenish the wound with new cells. When the migrated keratinocytes cover the

wound area, MMP expression decreases. Suprabasal keratinocytes begin to differentiate to form a new stratified epidermal structure. From the edge to the inside, the basement membrane also begins to be synthesized. New hemidesmosomes are built and establish a new connection with laminin-5.

Dermal fibroblasts, which are attracted from the edge of the wound, proliferate. In addition, bone marrow-derived cells are attracted that differentiate into wound fibroblasts [43]. A large percentage of wound fibroblasts differentiate into myofibroblasts, characterized by the expression of alpha-smooth muscle actin. These fibroblasts with smooth muscle cell characteristics contract and draw the wound edges together, thereby promoting wound closure. Fibroblasts and myofibroblasts also produce collagens and other ECM proteins to form the mature scar [44].

### 1.2.3 Remodeling phase

The last period of the wound healing process is the remodeling phase. It starts 1 to 3 weeks after trauma and may last for a year or more. Keratinocytes of the wound epidermis reduce their proliferation rate and re-differentiate, and the epidermis finally reaches its initial thickness. In the granulation tissue, many capillaries regress, while others remain and get stabilized by association with pericytes and smooth muscle cells. Most myofibroblasts and also various immune cells undergo apoptosis during this period. The remaining (myo)fibroblasts express mainly collagen I, which gradually replaces the collagen III of the granulation tissue. Fibroblasts, macrophages, and endothelial cells secrete matrix metalloproteinases, and the acellular matrix is actively remodeled. However, the strength and elasticity of new tissue are not the same as in normal skin, and the appendages do not regenerate [45-47].

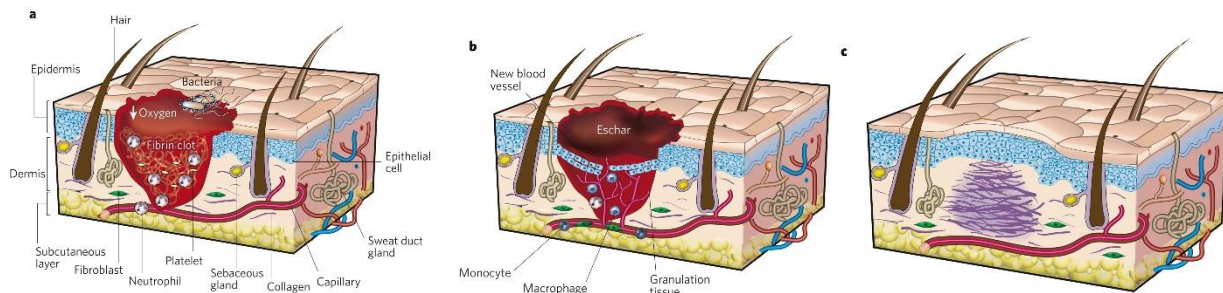


**Figure 4. Classic stages of wound repair.**

Overview of the three classic stages of wound healing: inflammation (a), new tissue formation (b) and remodelling (c). (a) The inflammatory phase is initiated during the first 2 days after a trauma. A formed fibrin clot provides a provisional seal. Hair follicles, sweat glands and other appendages are retained in the normal skin tissue around the wound. (b) In the next 2 to 10 days, the period of new tissue formation, an eschar will form on the wound surface. Keratinocytes migrate below the eschar from the edge of the wound to the middle. Below the eschar is the granulation tissue filled with fibroblasts, capillaries, monocytes/macrophages and other immune cells. The formation of new blood vessels is essential to supply the new tissue with oxygen and nutrients. (c) The remodeling phase lasts up to a year or even longer. The picture shows the outcome of the repair process - a scar. Fibroblasts have migrated into the wound and differentiated into myofibroblasts. The latter have secreted many extracellular matrix proteins and contracted the wound. The re-epithelialized wound is slightly higher than the surrounding area and is devoid of appendages. Reproduced from [47].

## 1.2.4 Signaling molecules and cross-talks between skin cells during wound healing

During the wound healing process, there are intricate cross-talks and interactions between keratinocytes, fibroblasts, immune cells and other cell types. The coordination of different cells is critical for rapid and efficient wound closure. For example, in the early phase of healing, when keratinocytes are activated, they release pre-stored IL-1, which induces the expression of keratins 6 and 16 in migrating keratinocytes. IL-1 activates the surrounding fibroblasts, which in turn upregulate the expression of the keratinocyte mitogen fibroblast growth factor 7 (FGF7). FGF7 promotes the proliferation and migration of keratinocytes [18]. Other regulators of re-epithelialization, of which many are produced by fibroblasts, include hepatocyte growth factor and ligands of the epidermal growth factor receptor (EGFR), such as epidermal growth factor, transforming growth factor- $\alpha$ , and heparin-binding epidermal growth factor. Many growth factors act as mitogens or chemotactic factors for fibroblasts, for example, platelet-derived growth factor [48] and transforming growth factor  $\beta$  [49]. The latter is produced by keratinocytes, fibroblasts and immune cells, and it is of particular importance for the differentiation of fibroblasts into contractile myofibroblasts [49].

Most of these signaling molecules act in an autocrine and/or paracrine fashion, thereby controlling the behavior of the growth factor producing cell and its neighbors. Growth factors and cytokines work together with their tightly regulated receptors during the whole process of wound healing. An imbalance in the regulation and expression pattern of these signaling molecules causes impaired repair and even results in the formation of non-healing ulcers. Interestingly, it has recently been shown that growth factor signaling is regulated by various types of post-translational protein modifications. However, the role of such modifications in the repair process has been poorly characterized. In this thesis, I characterized the role of the E3 ubiquitin ligase Nedd4 in the skin repair process. This protein had previously been shown to regulate EGFR signaling in the regenerating liver [50]. Nedd4-1 will be introduced in section 1.4. I also investigated the role of Nedd4-1 in the UV response of the skin, which will be introduced below.

## 1.3 UV irradiation of the skin

### 1.3.1 Photobiology of solar UV radiation

Sunlight is of considerable significance to the activities of life on earth. Plants need photosynthesis to survive and grow, and the sunlight is also essential for animal life. Humans require sun exposure to promote the production of vitamin D, and also to stimulate the production of hormones that regulate the biological rhythm and mood [51]. Conversely, excessive sun exposure can cause skin damage.

Sunlight is a mixture of continuously changing light of different wavelengths: infrared (IR,  $\lambda$  760–10<sup>6</sup>nm), visible (Vis,  $\lambda$  400–760 nm), and ultraviolet (UV,  $\lambda$  100–400 nm) light. Although the solar spectrum has a wide wavelength range from a few angstroms to ten meters, the distribution of radiant energy according to wavelength is uneven. The region with the immense radiant energy is in the visible part, accounting for about 48%, the radiant energy in the ultraviolet spectrum region is about 8%, and the radiant energy in the infrared spectrum region is about 44% [52].

Depending on the wavelength, UV radiation (UVR) is further divided into UVC (100–290 nm), UVB (290–320 nm), and UVA (320– 400 nm) [53]. UVR is affected by many factors, such as atmospheric conditions, time of day, season, altitude, and latitude. Thanks to the presence of the ozone layer, UVC is absorbed and does not reach the surface of the earth [54]. Rather, UVR that reaches the skin includes 95% UVA and 5% UVB. The multi-layered unique structure of the skin allows sunlight to be absorbed, reflected or scattered, thereby protecting our body from solar radiation. The most penetrating is the near-infrared radiation (NIR, 760–1440 nm), which can reach the subcutaneous tissue [55]. The second is UVA, which can reach the papillary dermis. The last one is UVB, which only penetrates the epidermis and the most upper part of the dermis. However, the radiant energy is in the opposite order of intensity, so the strongest is UVB, followed by UVA and NIR [52].

### 1.3.2 Effects of UV radiation on the skin

Although UV radiation is required for vitamin D production and hormone regulation, excessive UV radiation can cause damage to skin macromolecules, including DNA. UVB is considered the leading cause of skin cancer. However, UVA can penetrate deeper into the skin, so UVA and UVB radiation together have far-reaching effects on both photo-aging and skin carcinogenesis (Figure 5) [56, 57].

The effects of solar radiation on the skin can be roughly divided into acute and chronic. Acute reactions caused by excessive UV radiation include sunburn and epidermal hyperplasia. It is associated with DNA damage, which in most cases gets rapidly repaired. Chronic UV exposure causes skin aging, repeated DNA damage that may exceed the DNA repair capacity and immunosuppression, and eventually leads to skin cancer [58, 59]. These acute or chronic effects are due to the direct or indirect reaction between the UV light and the biomolecules in the skin cell. The direct effects result from the absorption of UVB by DNA. This results in the formation of pyrimidine dimers and other photoproducts [59]. This will be further described in 1.3.2.1. Indirect effects result from the formation of ROS upon UV irradiation. These highly aggressive molecules react with cellular DNA, proteins and membrane lipids, thereby causing cell damage at multiple levels [60]. Therefore, effective and rapid protective responses are needed to maintain skin homeostasis and to avoid tumor formation.

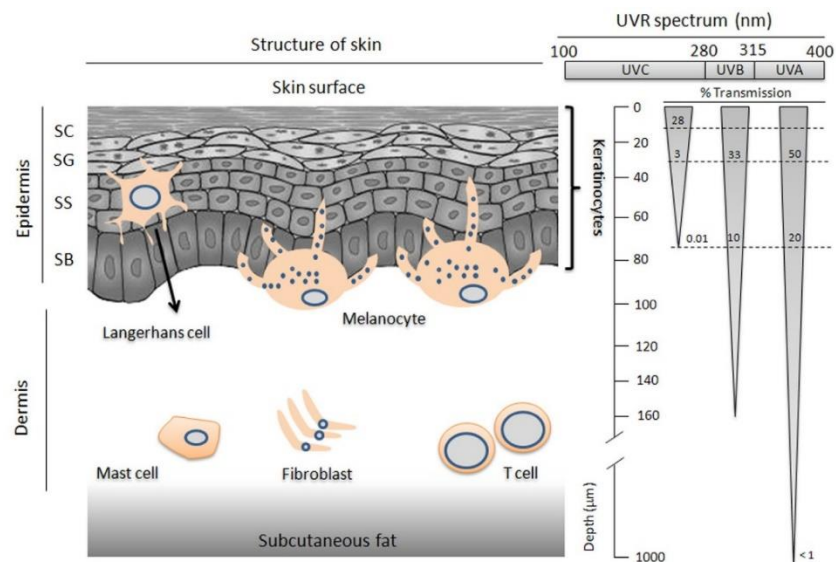




### Figure 5. Penetration of solar UV light into the skin

The general structure of the skin is shown on the left. Melanocytes are at the bottom of the epidermis, and they secrete melanin that is transferred to keratinocytes. Langerhans cells (LC) play a role in antigen presentation in the middle layer of the epidermis. Fibroblasts, mast cells and T cells locate in the dermis. The penetration of UVR into the skin is shown on the right. UVC has the shortest wavelength, but the highest energy; most UVC is absorbed by the ozone layer. The UVB energy and wavelength rank middle. UVB can penetrate through the epidermis and reach the upper layer of the dermis. UVB is the leading cause of DNA damage. UVA can penetrate deeply into the skin, but it carries the lowest energy [61].

#### 1.3.2.1 UVR-induced DNA damage and repair

UVB irradiation of cells induces the formation of two major types of DNA lesions - cyclobutane pyrimidine dimers (CPDs) and pyrimidine (6-4) photoproducts among adjacent pyrimidine residues [62]. C to T and CC to TT mutations at dipyrimidine sequences are a frequent consequence [63]. CPDs have particularly strong mutagenic effects, because they are very frequent and are only slowly repaired [64]. There are mechanisms for the repair of damaged DNA inside the cell, such as direct excision of nucleic acids or bases, repair of mismatched bases, and repair of double-strand breaks. The tumor suppressor protein p53 plays an important role in the repair of DNA damage [65]. When UV radiation is excessive, p53 protein is stabilized and activated. It stops cell cycle progression until the damaged DNA is repaired. In response to DNA damage, p53 induces the expression of its downstream target genes *Gadd45* and *p21* [66]. It has also been shown that p53 or p53-regulated proteins enhance nucleotide excision repair (NER). However, if the DNA damage is too severe, the cell can not repair it. In this case the cell activates the apoptosis pathway, thereby eliminating the damaged cell. This will be further described in 1.3.2.2.

#### 1.3.2.2 UVR-induced apoptosis

The process of terminal keratinocyte differentiation, which was described in 1.1.1.1, is an example for a physiological form of programmed cell death [67]. Under pathological conditions, however, an apoptotic process is initiated to eliminate cells with DNA damage. This is important to prevent the proliferation of mutated cells, which may give rise to malignant tumors. For example, the formation of epidermal sunburn cells is a form of keratinocyte apoptosis after excessive exposure to the sun and is required to prevent skin cancer.

Depending on the UV dose and the type of irradiated cells, different pro-apoptotic signaling pathways are activated. UV-induced apoptosis can be executed by extrinsic and/or intrinsic pathways. Various cell membrane receptors play key roles in the extrinsic apoptosis pathway. For example, CD95 is a cell membrane receptor for members of the tumor necrosis factor (TNF) family. UV radiation causes the multimerization of CD95. Multimerized CD95 then binds to the adaptor Fas-associated protein with death domain (FADD), which activates a downstream caspase cascade [68]. Upon UVB irradiation, TNF receptor (TNFR) clusters in keratinocytes and recruits TNFR1-associated death protein and TNFR-associated factor-2 (TRAF-2) [69]. In addition, TRAIL receptors are also affected by UV radiation. Two receptors act as decoy receptors, competitively binding to block apoptosis, and UVR will change the balance and cause apoptosis [70, 71]. The intrinsic apoptosis pathway is usually initiated by the damage of DNA and the release of cytochrome C from mitochondria [72, 73]. Released cytochrome C from the outer mitochondrial membrane forms an apoptosome together with apoptotic protease activating factor-1 (Apaf-1). This apoptosome recruits and activates caspase 9 [74]. Pro-apoptotic proteins, such as Bax, Bak and Bid promote apoptosis. By contrast, Bcl-2 inhibits caspase 3 and caspase 8 activities, and Bcl-x partially inhibits the release of cytochrome C [75]. Studies have shown that UVB induces

apoptosis by inhibiting Bcl-2 and activating caspase 8 in primary keratinocytes [76]. UV also induces the generation of ROS, which induce cytochrome C release from mitochondria. Mitochondrial DNA deletions are frequent in sun-exposed skin [77, 78]. Together with oxidative stress, they cause mitochondrial dysfunction and also promote apoptosis of damaged skin cells after UV irradiation [79-81]. Upon UV-induced activation of p53, this protein directly acts on mitochondria to induce apoptosis, and it also regulates mitochondria through proteins of the BCL-2 family [82, 83]. Studies have shown that p53 regulates apoptosis through the interaction with Bcl-2 and Bcl-xL proteins [84, 85].

### 1.3.2.3 Ubiquitin ligases in apoptosis

Excessive or insufficient apoptosis disrupts tissue homeostasis in multicellular organisms, and therefore, this process has to be tightly regulated. Among other regulatory mechanisms, post-translational protein modification through ubiquitination plays an essential role in regulating apoptosis. Among the players, ubiquitin E3 ligases are particularly important since they determine substrate specificity. One of these E3 ligases is MDM2. MDM2 is the primary ubiquitin ligase targeting p53. *Mdm2* knockout mice are embryonic lethal, which was rescued by crossing with *p53* knockout mice, thus confirming that p53 is a major target protein of MDM2 [86, 87]. Subsequently, other target proteins of MDM2 were discovered, including MDMX [88], FOXO [89] and insulin-like growth factor 1 receptor (IGF1R). The absence of MDM2 is necessary for IGF1R to induce apoptosis and clear damaged DNA [90]. Another target protein of MDM2 is S7, which enhances apoptosis under stress conditions [91]. In response to DNA damage, it has also been reported that the SCF- $\beta$ TRCP ubiquitin ligase complex promotes the degradation of MDM2, resulting in enhanced p53 levels, repair of DNA, or promotion of apoptosis [92]. Another E3 ligase that plays an essential role in regulating apoptosis is ITCH. It belongs to the HECT family (introduced below) and can ubiquitinate the p53-related proteins p63 and p73. It also regulates the stability of FLIP. When TNF- $\alpha$  activates the JNK signaling pathway, JNK phosphorylates ITCH and enhances its activity. Then ITCH ubiquitinates FLIP and leads to its degradation by the proteasome, thus avoiding the inhibitory effect of FLIP on caspase 8 [93]. ITCH is a member of the NEDD4 family. The founding member of this family, NEDD4-1, has a similar structure as ITCH. In this thesis, a role of the ubiquitin ligase Nedd4-1 in UV-induced apoptosis of mouse keratinocytes was identified (see section 3). The process of ubiquitination and the biological functions of Nedd4-1 will be introduced below.

## 1.4 Ubiquitination and ubiquitin E3 ligases

### 1.4.1 Ubiquitination

Ubiquitination is a type of post-translational protein modification, and it is one of the most compelling ways to control various cellular signaling pathways. It is an energy-dependent process, which involves the covalent attachment and sequential transfer of activated ubiquitin to different proteins. There are three key players in the ubiquitination pathway, the ubiquitin-activating enzyme (E1), the ubiquitin-conjugating enzyme (E2) and the ubiquitin ligase (E3). E3 is the most crucial component determining the specificity of substrate proteins, since the transfer of ubiquitin to one or more Lys residues in the substrate is facilitated by E3. Ubiquitin binds to the substrate protein through a covalent peptide bond between the  $\epsilon$ -amino of a Lys residue in the substrate and the carboxyl group of a Gly residue at the C-terminus of ubiquitin [94]. Usually, lysine residues

in the substrate are the first options, but serine, cysteine or threonine residues can also be targeted. Monoubiquitination is the addition of one ubiquitin molecule to one Lys of the target protein, while multi-monoubiquitination is the addition of a single ubiquitin to several Lys residues of a protein. Poly-ubiquitination is the addition of a chain of ubiquitin molecules to a target protein through a sequential transfer of ubiquitin. Poly-ubiquitination codes differ in length, linkage or branches.

Different types of ubiquitination lead to different fates of the substrate protein. The effects of monoubiquitination include DNA repair, protein trafficking, and transcription. Multi-monoubiquitination may lead to protein endocytosis and degradation. Polyubiquitination of misfolded or damaged proteins usually leads to the proteasomal degradation of these proteins. There are seven Lys residues in ubiquitin, and the Lys48 and Lys63 are the most popular ones. The substrate protein, which contains Lys48-linked ubiquitin chains, usually undergoes proteasome-mediated degradation. Lys63-linked monoubiquitination and polyubiquitination are more likely to play a role in endocytosis and vesicular sorting [95] (Figure 6). Ubiquitination can affect the function of a protein by changing its spatial configuration. The ubiquitinated protein may also interact with receptors that have ubiquitin-binding domains (UBD). These interactions will ultimately affect the activity of the target proteins, their ability to form complexes and the location within the cell [96].

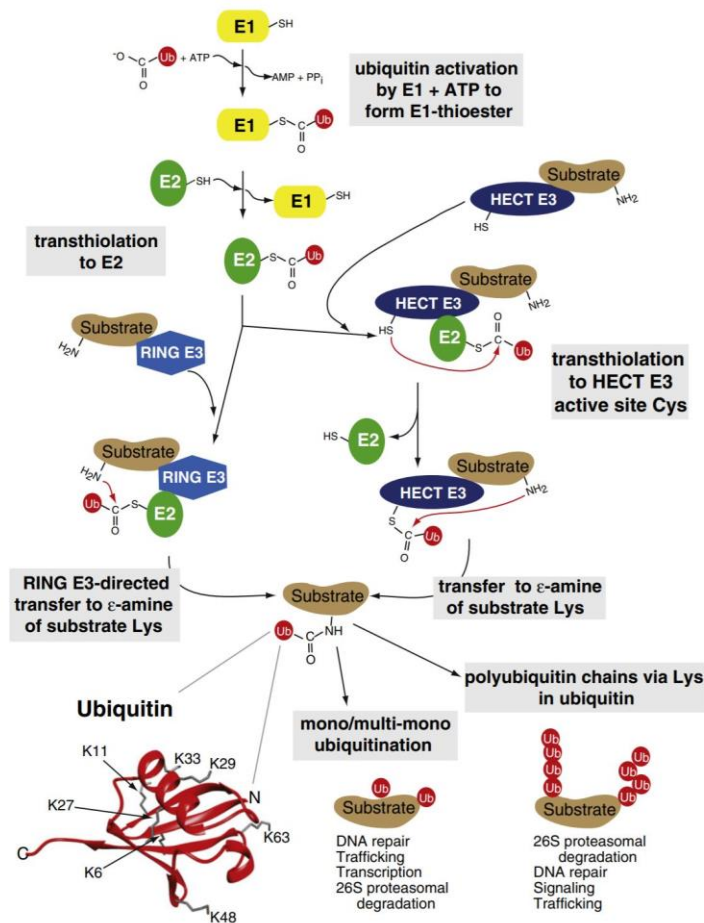




### Figure 6. Ubiquitination pathway

Ubiquitination involves a series of energy-consuming reactions that are carried out by three classes of enzymes. First, the active Cys of a ubiquitin-activating enzyme (E1) gets connected to the C-terminus of ubiquitin through a thioester bond. Then the ubiquitin is transthiolated to the Cys of the ubiquitin-conjugating enzyme (E2). In the end, ubiquitin ligases (E3) transfer the ubiquitin to a specific target after the interaction with E2-ubiquitin and the substrate protein. The HECT E3 ligases serve as a covalent intermediate; they first catalyze the reaction between ubiquitin and Cys on E3 via a transthiolation, and then they transfer ubiquitin to the target. The RING E3 ligases directly catalyze the transfer of ubiquitin from E2 to the substrate. Ubiquitin contains seven Lys residues, with Lys48 and Lys63 being the most popular ones. The monoubiquitination of Lys63 is important for DNA repair, protein trafficking and also targets receptors and endocytic proteins for lysosomal degradation. Multi-monoubiquitination can also lead to protein degradation. Polyubiquitination through Lys48 leads to degradation of the target protein [97].

## 1.4.2 HECT E3 Ligases

Ubiquitin E3 ligases determine the specificity of the substrate, and therefore, cells have a large number of ubiquitin ligases, but less E1 and E2 enzymes. In humans, there are two potential E1s, about thirty E2s and more than 600 E3s [98]. The E3 ligases were classified into three main types: HECT E3s, RING E3s and RBR E3s. There are 28 members of the HECT family in humans, and most of the other E3s belong to the RING family [98]. Unlike RING E3s that directly transfer the ubiquitin from E2 to the substrate, firstly, there is an intermediate thioester bond formed between the Cys residue of HECT E3s ligases and the C terminus of ubiquitin, and then HECT E3s ligases catalyze substrate ubiquitination. Because of the conserved HECT domain at their C-terminus, these E3s were named HECT E3 ligases. The HECT domain contains approximately 350 amino acids, which was first described in human papillomavirus (HPV) E6-associated protein (E6AP), the founding member of HECT E3s [99]. The HECT domain has a bilobal structure. It has a conserved Cys residue that forms thioester complexes with ubiquitin, while its N-terminus binds the E2 enzyme. In the HECT domain of E6AP, a flexible hinge loop connects the N and C lobes, forming an L-shaped structure [100]. The N-terminal domain is responsible for protein-protein interaction or protein-lipid binding. Based on the N-terminal structure, the human HECT E3s were divided into three subgroups: the NEDD4 family, the HERC family and other HECTs. HECT E3s polyubiquitinate substrates in several ways. For example, the HECT domain of Rsp5 (the *Saccharomyces cerevisiae* orthologue of NEDD4) often builds Lys63-linked chains, which is not the case for E6AP [101]. However, the functions of most HECT E3s are still poorly understood.

## 1.4.3 Nedd4 E3 Ligases

The Nedd4 family is a subfamily of the HECT E3 ligases. The members of this group contain a C-terminal HECT domain, an N-terminal C2 domain and two to four WW domains (Figure 7). The C2 domain binds to phospholipid membranes and mediates the intracellular trafficking, usually targeting to the plasma membrane, endosomes and multivesicular bodies (MVBs) [102, 103]. The WW domains bind to PY motifs of the target proteins, thereby determining the specificity of the substrate [104, 105]. In mammals, there are nine Nedd4 family proteins: NEDD4 (also known as NEDD4-1), NEDD4L (also known as NEDD4-2), WWP1, WWP2, SMURF1, SMURF2, ITCH, NEDL1 (also known as HECW1) and NEDL2 (also known as HECW2). They regulate signaling pathways and influence cell proliferation, animal development and cancer [106].

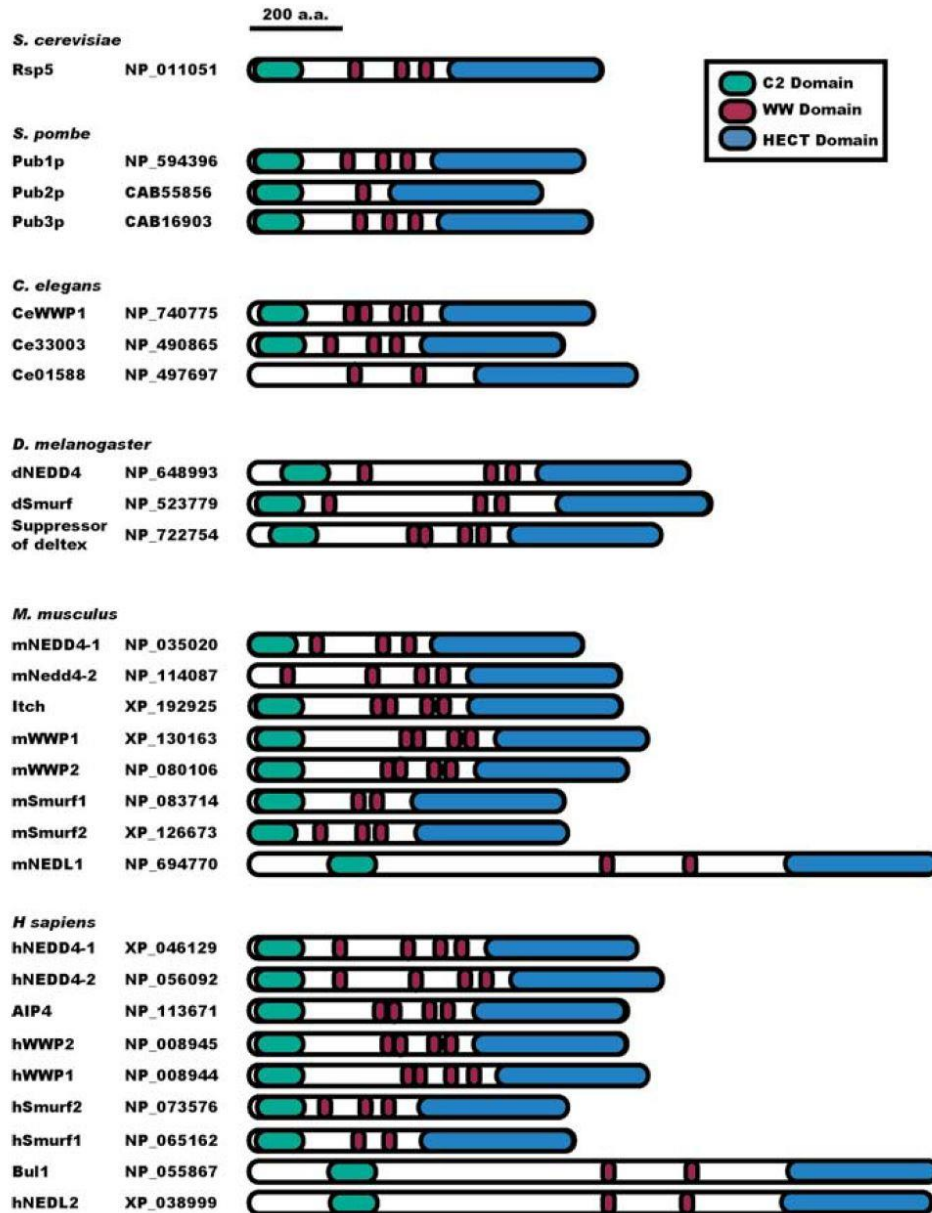


**Figure 7. The Nedd4 E3 ubiquitin ligase family.**

The names, accession numbers and domain architectures of Nedd4 E3 ligases are shown. The relative position of the C2 (green), WW (red), and HECT (blue) domains were obtained by blasting the indicated sequences against the Conserved Domain Database. The bar on the top indicates 200 amino acids. Reproduced from [107-109].

Among the NEDD4 E3 family members, there are some particularly popular proteins, for example, ITCH and RSP5. ITCH mediates FLIP degradation, which controls TNF- $\alpha$ -induced apoptosis (described in 1.3.2.2). Notch and the p53 relatives p63 and p73 are also substrates of ITCH, reflecting the crucial role of ITCH in regulating DNA damage, cell cycle arrest and apoptosis. The other well-characterized NEDD4 family member is RSP5. It regulates endocytosis and the sorting of several membrane proteins in yeast. Some other mammalian NEDD4 proteins seem to have conserved functions. For example, it is well known that NEDD4L can bind to the PY motifs of the epithelial Na<sup>+</sup> channel (ENaC), and then ubiquitinates ENaC and promotes its endocytosis and

degradation [104]. This is essential to maintain the body's salt and fluid balance and prevent Na<sup>+</sup> overload [110-113].

#### 1.4.4 Neural precursor cell expressed developmentally down-regulated protein 4-1 (NEDD4-1)

The *NEDD4-1* gene locates on human chromosome 15q21.3. It contains 30 exons, and the encoded protein NEDD4-1 (also named NEDD4) has a molecular weight of 120 kDa. "NEDD" stands for "Neural precursor cell expressed developmentally down-regulated". Its name results from the down-regulated expression in the murine central nervous system during development [114].

##### 1.4.4.1 Nedd4-1 structure

The *Nedd4-1* gene was first cloned from mouse embryos in 1992 [114]. At that time, the known information about its encoded protein was the C2 domain at its N-terminus and the three repeated similar parts in the middle of the protein. One repeat contains about 40 amino acids with two tryptophan (W) residues that are highly conserved. These three repeats are now widely known as WW domains [115] and are present in most Nedd4 family members. The C-terminal part is similar to human E6-AP, and this domain was named HECT (homologous to the E6-AP C-terminus) [99].

According to the NCBI database, there are five NEDD4 protein variants. From the first WW domain until the end, they have identical sequences; the only difference is at the N-terminus. The C2 domain, the Ca<sup>2+</sup>-dependent lipid-binding domain, contains 116 amino acids. In addition to protein-protein interactions [116], it brings E3 to phospholipid membranes [103], which is important for its function.

The number of WW domains can vary between different species. There are three WW domains in mouse, zebrafish, and *Drosophila* and four in humans and chicken [117]. WW domains specifically bind to proline-rich PY motifs (PPxY). They can also interact with phospho-serine/-threonine residues in substrates [118].

Similar to the other HECT E3 members, the HECT domain of Nedd4-1 also contains 350 amino acids and has a conserved cysteine residue. This cysteine residue can form an intermediate thioester bond with ubiquitin upon activation by E2, and the ubiquitin is then transferred to the substrate. NEDD4-1 is mainly localized in the cytoplasm, and especially in the perinuclear region [119]. It was also found in exosomes when recruited by NEDD4 family-interacting protein 1 (NDFIP1) [120].

##### 1.4.4.2 Nedd4-1 functions

Nedd4-1 is ubiquitously expressed in mammalian tissues. In order to study its physiological functions, numerous studies have been done *in vivo* and *in vitro*. People initially used conventional knockout mice to study the function of Nedd4-1 *in vivo*. The first mice with global *Nedd4-1* knockout that were generated showed neonatal lethality, accompanied by delayed embryonic development, reduced body weight and growth [121]. Embryonic fibroblasts isolated from these mice had an impaired proliferation capacity [121]. Another independently generated *Nedd4-1* knockout mouse line exhibited embryonic lethality, and the embryos had significant vascular malformations and heart development defects [122]. All these findings suggest that Nedd4-1 is necessary to regulate the proliferation of cells and the development of organisms.

NEDD4-1 is well known for its function in various types of cancer. For example, it is involved in the regulation of HER3 expression in breast cancer [123, 124]. In prostate cancer, it has been reported that the anti-cancer drug diosgenin inhibits the expression of NEDD4-1 to achieve anti-tumor activity through cell cycle arrest, growth inhibition and apoptosis [125]. In melanoma, NEDD4-1 was shown to bind to glucocorticoid-induced TNFR-related protein (GITR), resulting in its ubiquitination with concomitant suppression of T cell-targeted GITR, which is an important target for immunotherapy of melanoma. They also found that NEDD4-1 is highly expressed in metastatic melanoma, further confirming that the high expression of this protein is associated with poor prognosis of cancer patients [126]. Overall, NEDD4-1 plays a key role in tumorigenesis, and therefore it is an important therapeutic target [127].

NEDD4-1 is also involved in other human diseases. For example, inhibiting the expression of NEDD4-1 reduced the autophagy of cardiomyocytes caused by angiotensin II treatment [128]. Increased NEDD4-1 levels significantly reduced basal angiotensin converting enzyme 2 (ACE2) activity, and the NEDD4-1-mediated ubiquitination of ACE2 was independent of angiotensin (Ang)-II treatment. Overexpression of NEDD4-1 reduced the levels of ROS and apoptosis caused by angiotensin II, thus protecting the endothelial cells [129]. Nedd4-1 and Nedd4L are expressed in crypt stem cells in the mouse gut and were shown to regulate stem cell priming by degrading the intestinal stem cell (ISC) marker protein Lgr5. Therefore, loss of Nedd4-1 and Nedd4L promoted ISC growth [130].

However, the function of the E3 ubiquitin ligase Nedd4-1 in the skin has not been well studied. Therefore we focused on the role of this protein in skin homeostasis and repair.

#### 1.4.4.3 Nedd4-1 binding partners

With the advancement of proteomics-related technologies, many new approaches for studying protein-protein interactions have emerged, and more Nedd4-1 interacting proteins and substrates have been discovered.

Nedd4-1 interacting proteins and substrates are involved in the regulation of growth factor signaling. Firstly, it was shown that Nedd4-1 regulates IGF signaling. IGF1 is well-known for its proliferation promoting effect. Reduced amounts of IGF1 receptor on the cell surface and reduced IGF1 signaling have been found in *Nedd4-1<sup>-/-</sup>* embryos [121]. Another example is that EGFR endocytosis and degradation are regulated by Nedd4-1. It has been reported that NEDD4-1 plays a pivotal role in EGFR degradation in triple-negative breast cancer and in non-small cell lung cancer drug response and resistance [131, 132]. Knock-down of Nedd4-1 decreased the levels of activated Cdc42-associated tyrosine kinase (ACK) and of EGFR through ubiquitination and lysosomal degradation of these proteins [133]. In liver regeneration, our laboratory found that the failure to regenerate the liver upon knock-down of Nedd4-1 in hepatocytes resulted at least in part from impaired internalization of major growth factor receptors, in particular EGFR, and a subsequent reduction in Erk signaling pathway activation. This is most likely due to impaired ubiquitination of adaptor proteins involved in EGFR internalization in the absence of Nedd4-1. Since EGFR signaling is of key relevance for wound healing (see above), it was of interest to study the role of Nedd4-1 in this process.

Interaction with the endocytosis machinery is one of the first discovered functions of Nedd4-1. It has been reported that Nedd4-1 can mono-ubiquitinate the adaptor protein Eps15 [134, 135]. Eps15 contains a UIM domain. When this UIM domain binds to a ubiquitin molecule, it triggers the mono-ubiquitination of Eps15. The ability of monoubiquitinated Eps15 to interact with EGFR in endosomes is impaired. It is not clear whether Eps15 binds to the EGFR at the plasma

membrane directly or through another protein [136]. A similar finding was obtained for the adaptor protein Hgs, which is involved in the selection and transportation of endocytic bodies, which are part of the “endosomal sorting complexes required for transport” (ESCRT) machinery. The ubiquitination of Hgs suppressed EGFR degradation [137]. Nedd4-1 is also involved in regulating the transport of some transmembrane proteins, such as lysosomal protein transmembrane 5 (LAPTM5), from the Golgi to the lysosome [138]. There, the related LAPTM4B protein serves as a scaffold protein, recruiting Nedd4-1 to the endosome and inducing the monoubiquitination of Hgs. Ubiquitinated Hgs cannot bind EGFR, thus inhibiting the lysosomal degradation of EGFR [139].

The connection between Nedd4-1 and the Hippo signaling pathway also attracted people's attention. Hippo signaling, an evolutionarily conserved pathway, regulates cell proliferation, differentiation, apoptosis, stem cell self-renewal and expansion, and controls organ size [140]. It has been reported that YOD1 regulates the Hippo signaling pathway in the kidney by binding to NEDD4-1, followed by its deubiquitination [141]. Under oxidative stress, H<sub>2</sub>O<sub>2</sub> induced *NEDD4-1* expression via NF- $\kappa$ B, thereby facilitating the translocation of yes-associated protein (YAP). This is accompanied by a decrease in the stability of large tumor suppressor kinase (LATS). Phosphorylation of YAP by LATS is decreased, resulting in enhanced transcriptional activity of YAP [142].

Taken together, Nedd4-1 is a multifunctional protein with various activities that are highly relevant for tissue repair and disease.

## 1.5 Aim of this thesis

NEDD4-1 is an evolutionarily highly conserved and ubiquitously expressed HECT E3 ligase. It plays critical roles in organ development, tissue homeostasis and cancer [143]. Previous studies identified an essential role of protein ubiquitination pathways and especially of Nedd4-1 in mouse liver regeneration. A large-scale proteomics analysis was performed in our laboratory, and it was shown that the levels of Nedd4-1 were strongly upregulated in the liver within 24h after partial hepatectomy. Functional studies using nanoparticle-mediated delivery of siRNA to mouse liver identified an essential function of Nedd4-1 in liver regeneration through its effect on hepatocyte proliferation and survival [50]. Due to the superior repair capacity of the liver compared to other tissues, such as the skin, it is of major interest to explore the expression and function of this protein in the repair of other organs. Since the function of Nedd4-1 in the skin is largely unknown, the overall aim of this thesis was to investigate the role of this E3 ubiquitin ligase in skin homeostasis and repair.

### 1.5.1 Project 1

The goal of the first part of this thesis was to identify the functions of Nedd4-1 in epidermal homeostasis, wound re-epithelialization and UV response. Mice with keratinocyte-specific *Nedd4-1* knockout were generated. This mouse model allowed us to study the role of Nedd4-1 in keratinocytes during wound healing and in the UV response *in vivo*. Stable Nedd4-1 knock-down keratinocyte cell lines were generated and functionally characterized to unravel the molecular mechanisms underlying the phenotype of the *Nedd4-1* mutant mice.

## 1.5.2 Project 2

There is still limited information about Nedd4-1 regulation and function in fibroblasts, except that a potential role of NEDD4-1 in the pathogenesis of keloid scars has been reported [144, 145]. Therefore, its function in skin fibroblasts attracted our interest. To address this question, mice lacking *Nedd4-1* in mesenchymal cells were generated, and this mouse model was used for *Nedd4-1* loss-of-function studies *in vivo*. Stable Nedd4-1 knock-down fibroblast cell lines were generated and functionally characterized to elucidate the mechanisms underlying the phenotype of the *Nedd4-1* mutant mice.

The results obtained in those two projects revealed novel functions of Nedd4-1 in skin homeostasis, wound healing and UV response.



## 2. Materials

### 2.1 Chemicals and other consumables

Chemical / Consumable	Source
2-Mercaptoethanol ( $\beta$ -Mercaptoethanol)	SIGMA, Buchs, Switzerland
5-Bromo-2'-deoxyuridine (BrdU)	SIGMA, Buchs, Switzerland
Acetic acid	FLUKA CHEMIE AG, Buchs, Switzerland
Acrylamide/bisacrylamide	PANREAC APPLICHEM ITW REAGENTS, Darmstadt, Germany
Agarose	BIO & SELL, Nuremberg, Germany
Ammonium persulfate (APS)	SIGMA, Buchs, Switzerland
Boric acid	MERCK, Darmstadt, Germany
Bovine serum albumin (BSA)	SIGMA, Buchs, Switzerland
Bovine serum albumin fraction V	PAN-BIOTECH, Aidenbach, Germany
Bromophenol blue	SIGMA, Buchs, Switzerland
Chloroform	SIGMA, Buchs, Switzerland
Cholera toxin	SIGMA, Buchs, Switzerland
Collagen IV	SIGMA-ALDRICH, St. Louis, MO, USA
D,L-Dithiothreitol (DTT)	SIGMA, Buchs, Switzerland
Diethylpyrocarbonate (DEPC)	SIGMA, Buchs, Switzerland
Eosin	SIGMA, Buchs, Switzerland
Ethanol	MERCK, Darmstadt, Germany
Ethidium bromide	SIGMA, Buchs, Switzerland
Ethylenediamine tetraacetic acid (EDTA)	ROTH, Karlsruhe, Germany
Fetal calf serum	GIBCO, Grand Island, NE, USA
Formaldehyde	SIGMA, Buchs, Switzerland
Glycerol	PANREAC APPLICHEM ITW REAGENTS, Darmstadt, Germany
Hematoxylin	ROTH, Karlsruhe, Germany
HEPES	SIGMA, Buchs, Switzerland
Hoechst 33342	SIGMA, Buchs, Switzerland
Hydrochloric acid	MERCK, Darmstadt, Germany
Magnesium chloride	FLUKA CHEMIE AG, Buchs, Switzerland

Methanol	BRENNTAG, Basel, Switzerland
Milk powder (RAPILAIT)	MIGROS, Zurich, Switzerland
Mineral oil	SIGMA, Buchs, Switzerland
Mitomycin C	SIGMA, Buchs, Switzerland
Mowiol	HOECHST, Frankfurt, Germany
N,N,N,N-Tetramethylenediamine (TEMED)	SIGMA, Buchs, Switzerland
NP-40	SIGMA, Buchs, Switzerland
Paraffin	JUNG / LEICA MICROSYSTEMS, Heerbrugg, Switzerland
Paraformaldehyde	SIGMA, Buchs, Switzerland
Phenol	MERCK, Darmstadt, Germany
Ponceau S	SIGMA, Buchs, Switzerland
Propidium iodide	SIGMA, Buchs, Switzerland
Sodium azide	SIGMA, Buchs, Switzerland
Sodium chloride	MERCK, Darmstadt, Germany
Sodium citrate	FLUKA CHEMIE AG, Buchs, Switzerland
Sodium dodecyl sulfate (SDS)	SIGMA, Buchs, Switzerland
Sodium hydroxide	MERCK, Darmstadt, Germany
Tris[hydroxymethyl]aminomethane hydrochloride (Tris-HCl)	PANREAC APPLICHEM ITW REAGENTS, Darmstadt, Germany
Triton X-100	ROTH, Karlsruhe, Germany
Tween 20	ROTH, Karlsruhe, Germany
Xylene	BRENNTAG, Basel, Switzerland

## 2.2 Enzymes and growth factors

<b>Protein</b>	<b>Source</b>
Epidermal Growth Factor (EGF)	PEPROTECH, Rocky Hill, NJ, USA
Deoxyribonuclease (DNase) I	SIGMA, Buchs, Switzerland
Proteinase K	PANREAC APPLICHEM ITW REAGENTS, Darmstadt, Germany
Taq DNA Polymerase	NEW ENGLAND BIOLABS, Ipswich, MA, USA
Trypsin	THERMO FISHER SCIENTIFIC, Waltham, MA, USA



## 2.3 Kits and prefabricated products

Product/Kit	Source
AEC peroxidase substrate kit	VECTOR LABORATORIES, Burlingame, CA, USA
Bicinchoninic acid (BCA) kit	PIERCE, Rockford, IL, USA
Complete, EDTA-free protease inhibitor cocktail	ROCHE, Basel, Switzerland
Eukitt mounting medium	SIGMA, Buchs, Switzerland
Gateway™ LR Clonase™ II Enzyme mix	THERMO FISHER SCIENTIFIC, Waltham, MA, USA
GeneRuler 100bp DNA ladder	LIFE TECHNOLOGIES, Carlsbad, CA, USA
iScript cDNA synthesis kit	BIORAD, Reinach, Switzerland
KAPA Mouse Genotyping Kit	KAPA BIOSYSTEM, Wilmington, MA, USA
LightCycler 480 SYBR Green	ROCHE, Basel, Switzerland
Lipofectamine RNAiMAX	THERMO FISHER SCIENTIFIC, Waltham, MA, USA
Lipofectamine 2000	THERMO FISHER SCIENTIFIC, Waltham, MA, USA
Masson Goldner Trichrome Staining Kit	ROTH, Karlsruhe, Germany
Mycoplasma Test Kit I/C	PROMOCELL GMBH, Heidelberg, Germany
Nitrocellulose Transfer Membrane	SIGMA, Buchs, Switzerland
One Shot™ TOP10 Chemically Competent <i>E. coli</i>	THERMO FISHER SCIENTIFIC, Waltham, MA, USA
Page Ruler Prestained Protein Ladder	THERMO FISHER SCIENTIFIC, Waltham, MA, USA
Page Ruler Plus Pre-stained Protein Ladder	THERMO FISHER SCIENTIFIC, Waltham, MA, USA
Penicillin-Streptomycin (P/S)	SIGMA, Buchs, Switzerland
pENTR™/D-TOPO™ Cloning Kit	THERMO FISHER SCIENTIFIC, Waltham, MA, USA
PhosStop, phosphatase inhibitor	ROCHE, Basel, Switzerland
Phusion® High-Fidelity DNA Polymerase	NEW ENGLAND BIOLABS, Ipswich, MA, USA
Pierce BCA Assay kit	THERMO FISHER SCIENTIFIC, Waltham, MA, USA
RNeasy Mini Kit	QIAGEN, Hilden, Germany
RNase-free DNase set	QIAGEN, Hilden, Germany
TeloCol® Collagen Solution	ADVANCED BIOMATRIX, San Diego, CA, USA
Tissue freezing medium	JUNG / LEICA MICROSYSTEMS, Heerbrugg, Switzerland
T-PER lysis buffer	THERMO FISHER SCIENTIFIC, Waltham, MA, USA

## 2.4 Cell culture media and additives

Medium	Source
Defined Keratinocyte-SFM	THERMO FISHER SCIENTIFIC, Waltham, MA, USA
Dulbecco's Modified Eagle Medium (DMEM, D6429)	SIGMA, Buchs, Switzerland
Spinner's MEM (M8167)	SIGMA, Buchs, Switzerland

## 2.5 Buffers and solutions

Buffer	Chemical	Concentration /Amount
ADS (10x)	BSA	12% (w/v)
	NP-40	0.1%
	NaN <sub>3</sub>	0.02% (w/v)
	in PBS-T	
Borate buffer (0.1 M, pH 8.5)	Boric acid	61.83 g
	ddH <sub>2</sub> O	950 ml
	Adjust pH to pH 8.5 with 1M NaOH	
Herovici staining solution A	Celestine blue	1.25 g
	Iron alum	15 g
	ddH <sub>2</sub> O	300 ml
	Heat and boil this solution for 3 min to dissolve and let cool	
	Glycerol	60 ml
Herovici staining solution B1 (Weigert's Iron Hematoxylin solution A)	Hematoxylin	1 g
	95% EtOH	100 ml
Herovici staining solution B2 (Weigert's Iron Hematoxylin solution B)	FeCl <sub>3</sub>	2.5 g
	FeSO <sub>4</sub>	4.5 g
	37% HCl	2 ml
	ddH <sub>2</sub> O	298 ml
Herovici staining solution B	Mix Herovici staining solution B1 and B2 together.	
Herovici staining solution C	Metanil yellow	1.25 g

	Acetic acid	25 drops
	ddH <sub>2</sub> O	300 ml
Herovici staining solution D	Acetic acid	9 ml
	ddH <sub>2</sub> O	1800 ml
Herovici staining solution E	Saturated aqueous Li <sub>2</sub> CO <sub>3</sub>	1 ml
	ddH <sub>2</sub> O	500 ml
Herovici staining solution F1	Methyl blue	0.15 g
	ddH <sub>2</sub> O	150 ml
Herovici staining solution F2	Acid fuchsin	0.2 g
	Saturated aqueous picric acid	150 ml
Herovici staining solution F	Mix Herovici staining solution F1 and F2 together.	
	Glycerol	30 ml
	Saturated aqueous Li <sub>2</sub> CO <sub>3</sub>	0.15 ml
Herovici staining solution G	Acetic acid	10 ml
	ddH <sub>2</sub> O	1 l
Laemmli buffer (5x)	Glycerol	50%
	SDS	7.5 g/l
	Tris/HCl pH 6.8	250 mM
	Bromophenol blue	0.5 mg/ml
	β-Mercaptoethanol	10%
Phosphate buffered saline(PBS)	NaCl	137 mM
	KCl	2.7 mM
	Na <sub>2</sub> HPO <sub>4</sub>	10 mM
	KH <sub>2</sub> PO <sub>4</sub>	2 mM
Phosphate buffered saline Tween (PBS-T)	NaCl	137 mM
	KCl	2.7 mM
	Na <sub>2</sub> HPO <sub>4</sub>	10 mM
	KH <sub>2</sub> PO <sub>4</sub>	2 mM
	Tween-20	0.1%
Protein lysis buffer	Tris-HCl pH 8.8	50 mM
	NaCl	150 mM

	EDTA (pH 8.0)	1 mM
	NP-40	1%
	DOC	0.5%
	SDS	0.1%
SBA buffer	NaCl	140 mM
	Boric acid	0.8 M
Scott water	NaHCO <sub>3</sub>	24 mM
	MgCl <sub>2</sub>	95 mM
SDS PAGE -Running gel (10%)	Acrylamide 30%	33%
	Tris/HCl pH 8.8	375 mM
	SDS	0.1% (w/v)
	APS	0.1% (w/v)
	TEMED	0.04%
SDS PAGE -Running buffer	Tris	25 mM
	Glycine	192 mM
	SDS	0.10% (w/v)
SDS PAGE -Transfer buffer	Tris	5 mM
	Glycine	38 mM
	Methanol	20%
Tris buffered saline Tween (TBS-T)	Tris	20 mM
	NaCl	150 mM
	Tween-20	0.1%
Trizol	Phenol in saturated buffer	38%
	Guanidine thiocyanate	0.8M
	Ammonium thiocyanate	0.4M
	Sodium acetate pH 5.0	0.1M
	Glycerol	5%
	DEPC-H <sub>2</sub> O	Filled to 1l
TBE buffer	Tris/HCl, pH 8.0	90 mM
	H <sub>3</sub> BO <sub>3</sub>	80 mM
	EDTA	3 mM

Mowiol solution	Tris-HCl pH 8.5	0.2 M
	Glycerol	15.2%
	Mowiol	10% (w/v)

## 2.6 Antibodies

### 2.6.1 Primary antibodies

Antibody	Host	Catalog Nr	Source
anti- $\beta$ -actin	mouse	A5316	SIGMA, Buchs, Switzerland
anti-GAPDH	mouse	#5G4	HYTEST, Turku, Finland
anti-Nedd4	mouse	611480	BD BIOSCIENCES, San Jose, CA, USA
anti-Nedd4	rabbit	ab27979	ABCAM, Cambridge, UK
anti-Nedd4	rabbit	HPA039883	SIGMA, Buchs, Switzerland
anti-BrdU-FITC	mouse	11202693001	SIGMA, Buchs, Switzerland
anti-BrdU-POD	mouse	11585860001	ROCHE, Basel, Switzerland
anti-cl. caspase 3	rabbit	9661L	CELL SIGNALING, Danvers, MA, USA
anti-Erk1/2	rabbit	9102S	CELL SIGNALING, Danvers, MA, USA
anti-p-Erk1/2 (T202/Y204)	rabbit	9101S	CELL SIGNALING, Danvers, MA, USA
anti-total EGFR	rabbit	sc-03	SANTA CRUZ BIOTECHNOLOGY, Santa Cruz, CA, USA
anti-pEGFR	rabbit	4407S	CELL SIGNALING, Danvers, MA, USA
anti-Eps15	rabbit	12460S	CELL SIGNALING, Danvers, MA, USA
anti-Keratin 6A	rabbit	PRB-169P	BIOLEGEND, San Diego, CA
anti-Keratin 10	mouse	M7002	DAKO, Glostrup, Denmark
anti-Keratin 14	rabbit	PRB-155P	BABCO, Covance, CA, USA
anti-Keratin 15	mouse	MA1-90929	INVITROGEN
anti-Loricrin	rabbit	PRB-145P	BABCO, Covance, CA, USA
anti-Ki67	rabbit	ab15580	ABCAM, Cambridge, UK
anti- $\alpha$ SMA-FITC	mouse	F3777	SIGMA, Buchs, Switzerland
anti-Meca32	rat	553849	BD BIOSCIENCES, San Jose, CA, USA
anti-Ly6G	rat	ab2557	ABCAM, Cambridge, UK

## 2.6.2 Secondary antibodies

Antibody	Host	Catalog Nr	Source
anti-mouse Cy2 IgG	goat	115-225-166	JACKSON IMMUNORESEARCH, Westgrove, PA, USA
anti-rabbit Cy2 IgG	goat	111-225-003	JACKSON IMMUNORESEARCH, Westgrove, PA, USA
anti-mouse Cy3 IgG	goat	115-166-062	JACKSON IMMUNORESEARCH, Westgrove, PA, USA
anti-rabbit Cy3 IgG	goat	111-065-003	JACKSON IMMUNORESEARCH, Westgrove, PA, USA
anti-rat Cy3 IgG	donkey	712-165-150	JACKSON IMMUNORESEARCH, Westgrove, PA, USA
anti-mouse IgG HRP conjugate	goat	W402B	PROMEGA, Fitchburg, MA, USA
anti-rabbit IgG HRP conjugate	goat	W401B	PROMEGA, Fitchburg, MA, USA
anti-rabbit Alexa Fluor® 647	goat	ab150079	ABCAM, Cambridge, UK
anti-rat-Biotinylated	rabbit	BA-4001	VECTOR LABORATORIES, Burlingame, CA

## 2.7 Oligonucleotides

All primers were synthesized by MICROSYNTH, Balgach, Switzerland.

### 2.7.1 Primers for genotyping

Target		Sequence (5'-3')
Nedd4-1-floxed	<i>forward</i>	GTACATTTTAGTTCATGGTTCTCACAGG
	<i>reverse</i>	CAGAGGTCACATGGCTGTGGG
K5-Cre	<i>forward</i>	AACATGCTTCATCGTCGG
	<i>reverse</i>	TTCGGATCATCAGCTACACC
Col1a2-Cre	<i>forward</i>	TTAGCACCACGGCAGCAGGAG
	<i>reverse</i>	CAGGCCAGATCTCCTGTGCAGCAT

### 2.7.2 Primers for real-time RT-PCR

Target		Sequence (5'-3')
<i>mNedd4-1</i>	<i>forward</i>	CACACACCTGCTTCAATCGC

	<i>reverse</i>	GGAAGAGCCAGTGACCATC
<i>mRps29</i>	<i>forward</i>	GGTCACCAGCAGCTCTAGTG
	<i>reverse</i>	GTCCAACCTTAATGAAGCCTATGTCC

### 2.7.3 siRNA

Target	Forward sequence 5'→3'	Reverse sequence 5'→3'
Nedd4-1 (1)	acAGAUuAAGcGAuuuucudTsdT	AGAAUUCGCUuAAUCUGUdTsdT
Nedd4-1 (2)	gacAccGcAuucuuuucGAdTsdT	UCGAAAAGAAUGCGGUGUCdTsdT
Scrambled	AGGuAGuGuAAucGccuuGdTsdT	cAAGGcGAuuAcAcuAccudTsdT

### 2.7.4 shRNA

Target	Mature antisense 5'→3'
Nedd4-1 sh1	AATCCTCCAGAATGTTTGCGC
Nedd4-1 sh2	ATTCATGGTTTACGTAGTAGG

## 2.8 Laboratory equipment and materials

Equipment	Source
5 mm punch biopsy	LABORATORIOS PROVET, Bogota, Columbia
Axiocam MRm camera	CARL ZEISS GMBH, Oberkochen, Germany
Centrifuge 5810 R	EPPENDORF, Hamburg, Germany
Fusion Solo 6S	WITEC AG, Sursee, Switzerland
HM355 MICROTOME	MICROM, Walldorf, Germany
LightCycler 480 II	ROCHE, Rotkreuz, Switzerland
Nalgene Mr Frosty	SIGMA, Buchs, Switzerland
NanoDrop spectrophotometer ND-1000	THERMO SCIENTIFIC, Allschwill, Switzerland via WITEC AG, Litau, Switzerland
Pegstar PCR machine	AXONLAB, Baden, Switzerland
SpectraMAX 190	MOLECULAR DEVICES, Sunnyvale, CA, USA
STP120 Spin Tissue Processor	MICROM, Walldorf, Germany
Superfrost Plus slides	MENZEL, Braunschweig, Germany
Tewameter	COURAGE AND KHAZAKA ELECTRONIC GMBH, Cologne, Germany
Transwell plates (Costar # 3422)	CORNING, Corning, NY, USA

U 200 S control sonicator	JANKE AND KUNKEL GMBH & CO. KG, IKA Labortechnik, Staufen, Germany
UV-light box	BIORAD, Hercules, CA, USA
Ultra Turrax T25 homogenizer	JANKE AND KUNKEL GMBH & CO. KG, IKA Labortechnik, Staufen, Germany
Zeiss Axiovert 200M	CARL ZEISS GMBH, Oberkochen, Germany
Zeiss Imager.A1 microscope	CARL ZEISS GMBH, Oberkochen, Germany
Zeiss Axioskop 2 microscope	CARL ZEISS GMBH, Oberkochen, Germany

## 2.9 Software

Software	Source
Axiovision 4.6	CARL ZEISS GMBH, Oberkochen, Germany
ImageJ	National Institutes of Health, Bethesda, MA, USA
LightCycler® 450 v.1.5.0 SP4	ROCHE, Basel, Switzerland
Microsoft Excel	MICROSOFT, Redmont, WA, USA
GraphPad Prism 8	GRAPHPAD SOFTWARE INC., San Diego, CA, USA

## 3. Methods

### 3.1 Animal experiments

#### 3.1.1 Mouse lines

All mice were housed under specific pathogen-free (SPF) conditions and maintained according to Swiss animal protection guidelines. All animal experiments had been approved by the local veterinary authorities (Kantonales Veterinäramt Zürich, Switzerland).

##### 3.1.1.1 *Nedd4-1* floxed mice

The *Nedd4-1* floxed mouse strain was kindly provided by Dr. Hiroshi Kawabe (Max-Planck Institute of Experimental Medicine, Goettingen, Germany). We imported the frozen sperm of the floxed *Nedd4-1* mutant mouse line, and *in vitro* fertilization was performed at the ETH Phenomics Center. The floxed *Nedd4-1* mouse line is in the C57BL/6N genetic background. Two *loxP* sites flank exon 9, which encodes the last part of the C2 domain and the linker region between the C2 and the first WW domain [146]. We used the first two *Nedd4-1* *fl/wt* male mice obtained after *in vitro* fertilization for crossing with wild-type female mice when they were 8 weeks old. Heterozygous *Nedd4-1* *fl/wt* mice from the first generation were then intercrossed to generate the homozygous mice, and we continue to keep the homozygous *Nedd4-1* floxed mouse line. These mice are viable and fertile and behave normally. We used them to generate the conditional knockout mice for experiments.



### 3.1.1.2 K5-Cre *Nedd4-1* knockout mice

To study the function of *Nedd4-1* *in vivo*, we mated the *Nedd4-1* floxed mice with transgenic mice expressing Cre under the control of a keratin 5 promoter [147]. We used the first two *Nedd4-1 fl/wt* female mice obtained after *in vitro* fertilization to cross with K5-Cre mice when they were 8 weeks old. Heterozygous K5-Cre; *Nedd4-1 fl/wt* male mice from the first generation were then crossed with female *Nedd4-1 fl/wt* mice (which were replaced by *Nedd4-1 fl/fl* mice whenever possible). In the end, we obtained the K5-Cre; *Nedd4-1 fl/fl* mice (conditional knockout mice). The homozygous knockouts and appropriate controls were used for the analysis of the phenotype and for *in vivo* experiments.

### 3.1.1.3 Col1a2-Cre and Col1a2-CreER *Nedd4-1* knockout mice

To generate fibroblast-specific *Nedd4-1* knockout mice, we first crossed male Col1a2-Cre mice [148] with female *Nedd4-1 fl/wt* mice. Heterozygous Col1a2-Cre; *fl/wt* male mice from the first generation were then crossed with female *Nedd4-1 fl/wt* mice (which were replaced by female *Nedd4-1 fl/fl* mice whenever possible). To analyze their phenotype during development, timed matings were set up, and the mother and the embryos were sacrificed at day 18.5 of pregnancy, and the embryos were used for further analysis. We also generated the inducible fibroblast-specific *Nedd4-1* knockout (Col1a2-CreER) mouse model [149], which allows us to induce the *Nedd4-1* knockout after birth through tamoxifen treatment, although these mice have not been further characterized so far.

## 3.1.2 Mouse genotyping

### 3.1.2.1 Isolation of mouse genomic DNA

The biopsy obtained by mouse clipping was used as the source of genomic DNA. The obtained tissue was digested in 200  $\mu$ l tissue lysis buffer (section 2.5) containing 10  $\mu$ l proteinase K (10 mg/ml) at 55°C in a heating block overnight. Subsequently, the lysates were heated to 95°C for 5 min to inactivate proteinase K, followed by a centrifugation step at 13000 rpm for 5 min. The supernatant was used for PCR analysis.

### 3.1.2.2 Polymerase chain reaction

PCR was performed with K5-Cre, Col1a2-Cre, Col1a2-ER-Cre, *Nedd4-1* primers (section 2.7.1), 1  $\mu$ l of the supernatant including the DNA (out of 200  $\mu$ l, see above) and 15  $\mu$ l PCR reaction mix (see below). PCR was performed using a Pqstar PCR machine.

PCR reaction mix :

Components	Volume
2x KAPA genotyping mix	8 $\mu$ l
genotyping primer (5' and 3', 10 $\mu$ M)	1 $\mu$ l
ddH <sub>2</sub> O	6 $\mu$ l

PCR program:  
*Nedd4-1* floxed

Step	Cycle	Time	Temperature
Initialization	1x	3 min	94°C
Denaturation	5x	20 s	94°C
Primer annealing		20 s	65°C
Elongation		2 min	72°C
Denaturation	5x	20 s	94°C
Primer annealing		20 s	60°C
Elongation		2 min	72°C
Denaturation	25x	20 s	94°C
Primer annealing		20 s	55°C
Elongation		2 min	72°C
Final elongation	1x	7 min	72°C

#### K5-Cre

Step	Cycle	Time	Temperature
Initialization	1x	3 min	94°C
Denaturation	35x	30 s	94°C
Primer annealing		45 s	58°C
Elongation		30 s	72°C
Final elongation	1x	10 min	72°C

#### Col1a2-Cre

Step	Cycle	Time	Temperature
Initialization	1x	5 min	94°C
Denaturation	30x	45 s	94°C
Primer annealing		45 s	65°C
Elongation		45 s	72°C
Final elongation	1x	10 min	72°C

#### Col1a2-ER-Cre

Step	Cycle	Time	Temperature
Initialization	1x	5 min	94°C
Denaturation	30x	45 s	94°C
Primer annealing		45 s	65°C
Elongation		45 s	72°C
Final elongation	1x	10 min	72°C

### 3.1.2.3 Agarose gel electrophoresis

To separate and analyze the amplified DNA fragments obtained from the PCR reaction, 1.5% agarose gels (with 0.5 µg/ml final concentration of ethidium bromide inside) in SBA buffer were used to visualize the DNA fragments. Sixteen µl of the reaction mix were loaded. Five µl of a 100 bp DNA ladder was used as a marker. Electrophoresis was performed at 300 V, and the gels were examined on a UV light box.

### 3.1.3 Wounding

Female mice at 10 weeks of age were anesthetized by intraperitoneal injection of ketamine/xylazine (100 mg ketamine with 5 mg xylazine per kg body weight). After gently shaving and disinfection with 75% ethanol, four full-thickness excisional wounds (5 mm diameter) were generated using a biopsy punch, two wounds on each side of the dorsal midline. Mice were allowed to heal without dressing and sacrificed by CO<sub>2</sub> inhalation at different time points after injury, followed by decapitation. The skin tissue around and under the wound area was excised using iris scissors and processed for further analysis.

### 3.1.4 UV irradiation

Female mice at 8-11 weeks of age were anesthetized by intraperitoneal injection of ketamine/xylazine (100 mg ketamine with 5 mg xylazine per kg body weight). The entire murine back skin was then gently shaved and disinfected with 75% ethanol. Subsequently, the head and tail were covered with aluminium foil, and the back skin was irradiated with 100 mJ/cm<sup>2</sup> UVB. Mice were sacrificed by CO<sub>2</sub> inhalation at certain time points after UV irradiation. Back skin samples were excised and processed for further analysis.

### 3.1.5 Transepidermal water loss (TEWL) analysis

The entire murine back skin was gently shaved before analysis. TEWL was determined using a Tewameter. The probe was placed on the upper, middle and lower part of the dorsal skin, 20-30 consecutive measurements were performed, and the average was calculated after the measurement.

### 3.1.6 Tissue collection after animal experiments

After euthanization, the mouse skin tissue was harvested using surgical scissors. For RNA and protein analysis of whole skin tissue, samples were immediately snap-frozen in liquid nitrogen and stored at -80°C.

For cryo-sections, the freshly isolated skin tissue was excised and mounted on a nitrocellulose membrane, embedded in tissue freezing medium<sup>®</sup> and snap-frozen in liquid nitrogen. Samples were stored at -80°C.

For paraffin sectioning, freshly isolated skin tissue was excised and mounted on a nitrocellulose membrane and fixed overnight at 4°C in paraformaldehyde (4% PFA in PBS) or acetic EtOH (95% ethanol and 1% acetic acid). Fixed samples were dehydrated, processed and embedded in the STP120 Spin Tissue Processor using the following protocol:

Step	Component	Time
1	0.9% NaCl	30 min
2	30% Ethanol / 0.9% NaCl	30 min
3	50% Ethanol / 0.9% NaCl	30 min
4	70% Ethanol / 0.9% NaCl	30 min
5	90% Ethanol / 0.9% NaCl	30 min
6	96% Ethanol / 0.9% NaCl	30 min
7	100% Ethanol	60 min
8	100% Ethanol	30 min

9	Xylene	30 min
10	Xylene	30 min
11	Paraffin 60°C	2.5 h
12	Paraffin 60°C	5 h

The processing of the acidic ethanol-fixed samples started at the 100% ethanol step 7. The tissue blocks were cut using an HM355 microtome. Trimming was normally done at a thickness of 10-30  $\mu\text{m}$ . The thickness of the sections for staining was 7  $\mu\text{m}$ . To improve the quality of the sections, they were heated in a 40°C water bath to allow them to flatten out. They were then transferred onto Superfrost Plus slides. The slide rack was placed into an oven, and slides were dried at 37°C overnight, followed by storage at 4°C.

### 3.1.7 Separation of epidermis and dermis

After sacrifice, adult mice were gently shaved. Freshly isolated whole skin tissue samples were excised and subjected to heat shock. For this purpose, the samples were put into 60°C PBS for 30 s, followed by 1 min incubation in PBS on the ice. Subsequently, the epidermis was scraped off from the dermis with a scalpel. Isolated epidermis and dermis samples were immediately snap-frozen in liquid nitrogen and stored at -80°C.

### 3.1.8 Identification of proliferating cells

Mice were injected intraperitoneally with the thymidine analogue 5-bromo-2'-deoxyuridine (BrdU; 250 mg/kg in 0.9% NaCl). They were sacrificed 2 h after injection. Sectioned skin samples were analyzed by immunofluorescence staining (section 3.5.3.2) using a FITC-coupled BrdU antibody.

## 3.2 RNA methods

### 3.2.1 RNA isolation from tissue

Frozen tissue pieces were homogenized with an Ultra Turrax T25 homogenizer in Trizol reagent supplemented with 0.1 % beta-mercaptoethanol and then incubated for 10 min on ice to let the cell lyse well and allow RNA to dissolve in the aqueous phase. After centrifugation (10 min, 4000 rpm, 4°C), the upper (aqueous) phase was placed into a new 1.5 ml Eppendorf tube. 0.2 x volume of chloroform was added and mixed well. After 2 min incubation at room temperature, samples were centrifuged (10 min, 4000 rpm, 4°C). The aqueous phase was transferred into a new tube, avoiding the inclusion of the interphase. Subsequently, a 0.5 x volume of ice-cold chloroform was added to the mixture and mixed well. This step was repeated. Afterwards, the aqueous phase was carefully transferred into a new tube, and a 0.5 x volume of 100% isopropanol and 0.5 x volume of 0.8 M sodium citrate or 1.2 M NaCl were added, mixed well, and the RNA was allowed to precipitate for 30 min to several hours at -20°C. After centrifugation (1 h, 4000 rpm, 4°C), the liquid phase was discarded, the pellet was washed with 1 ml of 75% EtOH and centrifuged again (10 min, 4000 rpm, 4°C). Most of the supernatant was discarded, and after a short centrifugation step, the rest of the liquid phase was also removed. The pellet

was air-dried for 3-4 min and finally dissolved in 50  $\mu$ l DEPC-H<sub>2</sub>O. RNA was stored at -80°C until further use. For longer storage, the RNA was kept in EtOH.

### 3.2.2 RNA isolation from cultured cells

RNA was isolated from cultured skin cells using the RNeasy Mini Kit according to the manufacturer's instructions. DNase digestion was done for 15 min at room temperature using RNase-free DNase provided in the kit. RNA was stored at -80°C until further use.

### 3.2.3 Quantification and quality analysis of isolated RNA

A NanoDrop spectrophotometer ND-1000 was used to determine the concentration of RNA solutions by measuring the absorption at 260 nm. The following approximations apply for RNA concentrations:  $OD_{260} = 1 \approx 40 \mu\text{g RNA/ml}$ . Since proteins in solution absorb light at 280 nm and organic solvents used during RNA extraction absorb light at 230 nm, the ratio between  $OD_{260}$  and  $OD_{280}$  and the ratio between  $OD_{260}$  and  $OD_{230}$  were taken as indicators of RNA purity. The optimal value of both ratios is 2.0. To determine the quality of isolated RNA, 500 ng of each sample was loaded on a 1.5 % agarose gel in TBE buffer (section 2.5). The agarose gels contained 0.5  $\mu\text{g/ml}$  ethidium bromide. After adding the corresponding amount of 6 x loading buffer and DEPC-H<sub>2</sub>O to reach a final sample volume of 16  $\mu$ l, the mixtures were loaded on the gel, and electrophoresis was performed at 100 V for 10-20 min. Gels were examined in a UV-light box.

### 3.2.4 Reverse transcription

We used the iScript<sup>TM</sup> cDNA Synthesis Kit to generate cDNA from purified RNA. The reaction mix for 1  $\mu\text{g}$  RNA sample is shown in the table below. cDNA was synthesized using the RT-PCR program described below using a Peqstar PCR machine.

Reaction mix:

Components	Volume
5x iScript reaction mix	4 $\mu$ l
iScript reverse transcriptase	1 $\mu$ l
RNA template (1 $\mu\text{g}$ )	x $\mu$ l
Nuclease-free water	(15-x) $\mu$ l (the total volume is 20 $\mu$ l)

RT-PCR program:

Step	Temperature	Time
Incubation	25 °C	5 min
Reverse transcription	42 °C	30 min
Inactivation	85 °C	5 min
Cooling	4 °C	$\infty$

### 3.2.5 Quantitative Real-Time PCR (qRT-PCR)

Quantitative real-time PCR was performed to amplify and simultaneously quantify targeted cDNA. Previously generated cDNA samples (see above) were used for qPCR, together with 10  $\mu$ M primers and LightCycler® 480 SYBR Green I Master reaction mix in a reaction volume of 10  $\mu$ l (see below). The qPCR (program see below) was performed in a LightCycler 480 II. Amplification of the *Rps29* cDNA was used for normalization, and PCR products were checked for purity by melting curve analysis and further evaluated using the LightCycler 480 software. The primer sequences are listed in section 2.7.2.

Reaction mix:

Components	Volume
LightCycler® 480 SYBR Green I Master reaction mix	5 $\mu$ l
qRT-PCR primers (5' and 3', 10 $\mu$ M)	0.5 $\mu$ l
Diluted cDNA	4.5 $\mu$ l

qRT-PCR program:

Step	Cycle	Temperature	Time
Pre-incubation	1x	95 °C	3 min
Denaturation	50x	95°C	10 s
Primer annealing		60°C	20 s
Elongation		72°C	20 s
Melting curve	1x	95°C	5 s
		65°C	1 min
		97°C	5 s
Cooling	1x	40°C	30 s

## 3.3 Protein methods

### 3.3.1 Preparation of protein lysates from skin tissue or cultured cells

Cell culture dishes were placed on ice and cells were washed with cold 1x PBS. They were scraped off in one continuous 360° movement using a scraper and rapidly transferred into tubes. Then cells were centrifuged and lysed in protein lysis buffer containing Complete Protease Inhibitor Cocktail and PhosSTOP Phosphatase Inhibitor Cocktail (Roche). Freshly isolated or frozen skin tissue was homogenized in T-PER lysis buffer (the volume of lysis buffer is determined by the size of the tissue) containing protease and phosphatase inhibitor tablets (Roche) in a Greiner tube with the Ultra Turrax T25 homogenizer. The homogenate was then treated with ultrasound (10 pulses, amplitude 30%, each) using a U 200 S control sonicator, and centrifuged for 1 h at 4000 rpm at 4°C. The solution below the lipid layer was transferred to an Eppendorf tube and



centrifuged twice at 13000 rpm for 30 min at 4°C, every time avoiding the lipid layer. The final protein solution was snap-frozen and stored at -80°C until further use.

### 3.3.2 Determination of protein concentrations

The protein concentration was measured using the bicinchoninic acid (BCA) kit (section 2.3) according to the manual. A standard curve was calculated from 9 different dilutions (concentrations: 0, 25, 125, 250, 500, 750, 1000, 1500 and 2000 µg/ml) of BSA in the same buffer as the probe to be analyzed. The concentrations of the probes were in the same range. The lysates were diluted until they were in the range of the standard curve. In all experiments, each standard and lysate were analyzed in triplicates.

The BCA assay uses a buffer with cupric sulfate and bicinchoninic acid.  $\text{Cu}^{2+}$  gets reduced in the presence of proteins, leading to a purple color in combination with bicinchoninic acid as a chelator. The color intensity is measured at 562 nm. Here, 25 µl diluted samples and standards were pipetted into each well before the addition of 200 µl BCA reagent (A: B 1: 50). The plate was incubated at 37°C in the incubator for 30 min, and the absorption was determined in the spectrophotometer.

### 3.3.3 Western blot (WB)

#### 3.3.3.1 Sodium dodecyl sulfate-polyacrylamide gel electrophoresis

SDS-PAGE was used to separate the proteins according to their molecular weight. For this purpose, the corresponding volume of Laemmli buffer was added to the samples and mixed well (section 2.5). The proteins were denatured at 95-100°C for 5-10 min and loaded onto the gel. First, proteins were collected in a stacking gel and separated in a longer separation gel (acrylamide concentration dependent on the size of target proteins). Gel electrophoresis was performed at 60-80 V (stacking gel), 100-120 V (running gel) in SDS-PAGE running buffer (section 2.5). PageRuler (Plus) Prestained Protein Ladder was used for size determination.

#### 3.3.3.2 Protein transfer by wet-blotting

The electrophoretically separated proteins were transferred onto a nitrocellulose membrane (2 µm or 0.45 µm). In order to do so, four Whatman 3MM papers with proper size were soaked in transfer buffer (section 2.5), and two sponges were placed on top and two sponges below the nitrocellulose membrane/gel. To transfer the proteins to the nitrocellulose membrane, they were placed into a wet blot chamber, and the transfer was performed at 300mA for about 120 min at 4°C. Ponceau S staining of the membrane was performed to check the equal loading and transfer efficiency before antibody treatment.

#### 3.3.3.3 Immunodetection of proteins and visualization

The membrane was incubated in a solution of 5% milk powder or BSA (for phospho-antibody detection) in TBST at room temperature for 1 h to block unspecific binding sites. An antibody against the protein of interest was used after blocking. The membrane was transferred to the primary antibody solution and incubated at 4°C overnight on a shaking plate. The membrane was washed in TBST (3x5 min) the next day. The secondary antibody coupled to horseradish peroxidase was added in TBST and incubated for 60 min. The membrane was washed again in TBST (3x10 min). Finally, the membrane was incubated with lumin A and B (1:1) or WesternBright ECL for 1-5 min and the peroxidase



reaction product was then visualized by exposure to an X-ray film and subsequent development. Alternatively, a Fusion Solo S chemiluminescence imager was used.

#### 3.3.3.4 Protein quantification

In order to obtain quantitative values from Western blots, the scanned X-ray films or chemiluminescent images were evaluated. Band intensities were analyzed with ImageJ 1.8.0.

#### 3.3.3.5 Stripping of Western blot membranes

To use the same membrane for the detection of more than one protein, the antibodies can be removed by stripping. For this purpose, the membrane was incubated in a stripping buffer at 55°C for 30 min and then vigorously washed in TBST three to four times at room temperature. Then the blocking and staining procedure was applied again.

### 3.4 Cell culture

#### 3.4.1 Isolation of primary murine keratinocytes

Primary keratinocytes were isolated from mouse skin as described previously [150] with some modifications: Pups at the age of two to four days were sacrificed by decapitation, and appendages were surgically removed with scissors (tails were lysed for genotyping). Subsequently, the samples were disinfected in 70% ethanol (1 min). From the isolated skin, the fat was gently scraped off using a scalpel. Then, the skin was incubated in DMEM containing 0.8% trypsin and P/S (10000 U/ml penicillin/ 10 mg/ml streptomycin) at 37°C for 30 min. From here on, the samples were kept sterile in the cell culture hood. The epidermis was carefully peeled off using forceps and incubated at 37°C for 30 min in DMEM containing DNase (0.025% DNase). The cells were pressed through a 50 µm cell strainer and washed once with DMEM + P/S. Finally, they were plated on collagen IV-coated (2.5 µg per cm<sup>2</sup>) dishes, and cultured in defined keratinocyte serum-free medium contained 10 ng/ml epidermal growth factor and 10<sup>-10</sup> M cholera toxin. After 8-12 h, the cells were washed in 1x PBS twice. After the addition of fresh medium, they were cultivated until the desired confluency was reached. Cells were used for experiments at passage 2-4.

#### 3.4.2 Isolation of primary dermal fibroblasts

Primary fibroblasts were isolated from newborn mice around P2.5. The mice were euthanized by decapitation, and a paper towel was used to remove excessive blood. Toes were clipped off and used for genotyping. The entire skin was removed using sterile forceps and placed in 5% trypsin/EDTA solution at 37°C for 1 h. The epidermis was gently peeled off from the dermis after incubation. The dermis was then minced into small pieces and incubated with 2.5 ml of a collagenase type II solution (500 U/ml) in a 37°C water bath for 1 h. The tubes were shaken up and down every 15 min to physically disrupt the dermis tissue and help release the cells. The cell suspension was poured through a 100 µm cell strainer and the contents were centrifuged at 1,200 rpm for 5 min. After removing the supernatant, the resulting cell pellet was re-suspended in fibroblast medium (DMEM, 10% FBS, 10000 U/ml penicillin, 10 mg/ml streptomycin) and plated onto dishes. The cells were cultured at 37°C under a 5% CO<sub>2</sub> atmosphere overnight. The medium was

changed the following day, and cells were passaged prior to confluency. Primary fibroblasts were used for experiments at passage 2 to 4.

### 3.4.3 Cultivation of murine immortalized keratinocytes

Spontaneously immortalized mouse keratinocytes were obtained by serial passaging of the primary cells. These immortalized cells were seeded and maintained at 37°C under a 5% CO<sub>2</sub> atmosphere in keratinocyte culture medium (one part Spinner's MEM and two parts defined keratinocyte serum-free medium). Spinner's MEM was supplemented with 5 µg/ml insulin, 10 ng/ml EGF, 10 µg/ml transferrin, 10 mM phosphoethanolamine, 10 mM ethanolamine, 0.36 µg/ml hydrocortisone, 200 mM glutamine, 10000 U/ml penicillin, 10 mg/ml streptomycin, 45 µM CaCl<sub>2</sub> and 8% (v/v) chelated fetal calf serum (FCS). The defined keratinocyte serum-free medium is supplemented with 1 ml supplements (provided by the medium manufacturer), 10000 U/ml penicillin, 10 mg/ml streptomycin, 10 ng/ml EGF and 10<sup>-10</sup> M cholera toxin.

### 3.4.4 Cultivation of murine immortalized fibroblasts

Immortalized fibroblasts were seeded and maintained at 37°C under a 5% CO<sub>2</sub> atmosphere in fibroblasts culture medium (DMEM, 10% FBS, 10000 U/ml penicillin, 10 mg/ml streptomycin).

The absence of mycoplasma was confirmed for all cell cultures by PCR using the PCR Mycoplasma Test Kit I/C.

### 3.4.5 Passaging of cells

In order to passage the cultured keratinocytes, they were first washed with 1x PBS and then incubated with 1x PBS containing 0.05% EDTA at 37°C for 10 min. The detachment was achieved by incubation with 1x trypsin (in 1x PBS containing 0.05% EDTA) at 37°C for 10-20 min. Inactivation of trypsin was achieved by adding a culture medium containing 10% FCS. After centrifugation, cells were resuspended in pre-warmed culture medium (section 2.4). Finally, cells were transferred to new culture dishes or flasks at the desired density.

Cultured fibroblasts were first washed once with 1x PBS. The detachment was achieved by incubation with 1x trypsin (in 1x PBS containing 0.05% EDTA) at 37°C for 1-3 min. Inactivation of trypsin was achieved by adding a culture medium containing 10% FBS. After centrifugation, cells were resuspended in a pre-warmed culture medium (section 2.4). Finally, cells were transferred to new culture dishes or flasks at the desired density.

### 3.4.6 Freezing and thawing of cells

To freeze cells, they were detached and centrifuged as described above. The cell pellet was resuspended in a pre-warmed culture medium (section 2.4) containing an additional 10% DMSO. Subsequently, cells were cooled down to -80°C (-1°C /min) using a Nalgene Mr Frosty freezing container and transferred to liquid nitrogen for long-term storage. To thaw frozen cells, they were placed in a 37°C water bath, centrifuged, and after resuspension in a culture medium, plated onto culture dishes.

### 3.4.7 siRNA-mediated knockdown

Skin cells were transfected with siRNAs using Lipofectamine RNAiMAX according to the manufacturer's instructions. Experiments were performed 48h after siRNA transfection. The siRNA duplexes used are listed in section 2.7.3.

### 3.4.8 pInducer20/ 21 Nedd4-1 cloning

The murine Nedd4-1 cDNA was amplified from the template (Plasmid E430021K23, Source BioScience, Cambridge, UK) with CACC extend using Phusion<sup>®</sup> High-Fidelity DNA Polymerase (reaction shown below). The PCR program described below was performed using a Pqstar PCR machine. The PCR product (band size 2668 bp) was purified by gel electrophoresis (1 % agarose gel) and extracted from the gel using a Macherey-Nagel NucleoSpin<sup>®</sup> Gel and PCR Clean-up Kit according to the manufacturer's instructions. The concentration of the PCR product was measured in a NanoDrop spectrophotometer ND-1000.

Reaction mix:

Components	Volume
Murine Nedd4-1 cDNA template	10 ng
10 $\mu$ M Forward Primer Nedd4-1 (with CACC)	2.5 $\mu$ l
10 $\mu$ M Reverse Primer Nedd4-1	2.5 $\mu$ l
10 mM dNTPs	1 $\mu$ l
5x Phusion HF Buffer	10 $\mu$ l
Phusion DNA Polymerase	0.5 $\mu$ l
Nuclease-free water	x $\mu$ l (the total volume is 50 $\mu$ l)

PCR program:

Step	Cycle	Time	Temperature
Lid Heat			110°C
Initialization	1x	30 s	98°C
Denaturation	30x	10 s	98°C
Primer annealing and elongation		100 s	72°C
Final elongation	1x	8 min	72°C

The PCR product was inserted into the pENTR<sup>™</sup>/D-TOPO<sup>®</sup> vector using the pENTR<sup>™</sup> Directional TOPO<sup>®</sup> Cloning Kit (reaction is shown below).

pENTR<sup>™</sup>/D-TOPO<sup>®</sup> cloning reaction mix:

Components	Volume
PCR product (see above)	15 ng (1:1 molar ratio of PCR product and pENTR <sup>™</sup> /D-TOPO <sup>®</sup> vector)
TOPO <sup>®</sup> vector	15 ng
Salt Solution (1.2 M NaCl, 0.06 M MgCl <sub>2</sub> )	1 $\mu$ l
Nuclease-free water	x $\mu$ l (the total volume is 12 $\mu$ l)

The pENTR™/D-TOPO® with inserted murine *Nedd4-1* cDNA was used for the transformation of One Shot® chemically competent *E. coli* bacteria as described in the Invitrogen pENTR™ Directional TOPO® Cloning protocol.

Single colonies were picked from bacterial culture plates and resuspended in 30 µl ddH<sub>2</sub>O (bacteria suspension). To verify the presence of the murine *Nedd4-1* insert, a PCR was performed (PCR reaction and program are shown below).

Reaction mix:

Components	Volume
Bacteria suspension	2 µl
10 µM Forward Primer M13	1 µl
10 µM Reverse Primer Nedd4-1	1 µl
2x KAPA 2G Fast Mix	12.5 µl
Nuclease-free water	8.5 µl (the total volume is 25 µl)

PCR program:

Step	Cycle	Time	Temperature
Lid Heat			110°C
Initialization	1x	3 min	95°C
Denaturation	30x	15 s	98°C
Primer annealing and elongation		40 s	72°C
Final elongation	1x	3 min	72°C

The positive colonies (which showed the murine *Nedd4-1* cDNA insert) were used for large-scale bacterial culture, and the plasmids were purified. Furthermore, the pENTR™/D-TOPO® *Nedd4-1* plasmid was sequenced and showed the fully matched murine *Nedd4-1* coding sequence.

*In vitro* recombination between pENTR™/D-TOPO® *Nedd4-1* (attL1-*Nedd4-1*-attL2) and pInducer20/pInducer21 (attR1-ccdB-attR2) was used to generate the pInducer20/pInducer21 *Nedd4-1* (attB1-*Nedd4-1*-attB2) plasmid. The *in vitro* recombination was performed according to the Invitrogen Gateway™ LR Clonase™ II Enzyme Mix protocol (reaction is shown below).

Reaction mix:

Components	Volume
pENTR™/D-TOPO®- <i>Nedd4-1</i>	150 ng
pInducer20 / pInducer21 vector	150 ng
TE buffer, pH 8.0	x µl (the total volume is 8 µl)

The pInducer20/21 mix with inserted murine *Nedd4-1* cDNA was used for the transformation. Single colonies were picked from bacterial culture plates and resuspended in 30  $\mu$ l ddH<sub>2</sub>O (bacteria suspension). To verify the presence of the murine *Nedd4-1* insert, a PCR was performed (PCR reaction and program are shown below).

Reaction mix:

Components	Volume
Bacteria suspension	2 $\mu$ l
10 $\mu$ M Forward Primer M13	1 $\mu$ l
10 $\mu$ M Reverse Primer Nedd4-1	1 $\mu$ l
2x KAPA 2G Fast Mix	12.5 $\mu$ l
Nuclease-free water	8.5 $\mu$ l (the total volume is 25 $\mu$ l)

PCR program:

Step	Cycle	Time	Temperature
Lid Heat			110°C
Initialization	1x	3 min	95°C
Denaturation	30x	15 s	98°C
Primer annealing and elongation		40 s	72°C
Final elongation	1x	3 min	72°C

The positive colonies (which included the murine *Nedd4-1* cDNA insert) were used for large-scale culture, and the plasmids were purified. Furthermore, the pInducer20 Nedd4-1 and pInducer21 Nedd4-1 plasmids were sequenced and showed the fully matched murine *Nedd4-1* coding sequence.

### 3.4.9 Lentiviral transduction of cultured cells

Cells were cultured in 6 cm dishes and transduced at 30-50% confluency. Four ml virus-containing medium was mixed with 1 ml fresh culture medium and polybrene (final concentration 8  $\mu$ g/ml) and subsequently filtered through a 0.45  $\mu$ m syringe filter to remove cellular debris and particles. The culture medium was removed, and 4 ml of the filtered virus-containing medium was added dropwise to the cells. After overnight incubation, the virus-containing medium was replaced by a fresh culture medium. Forty-eight hours later, cells transduced with viruses containing the pLKO.1 vector [151] were selected for 2 weeks by culturing in a medium containing 2  $\mu$ g/mL puromycin. The shRNAs used are listed in Supplementary Table S4.

### 3.4.10 Growth factor treatment

Cells were cultured as described above. The detachment was achieved by incubation with 1x trypsin (in 1x PBS containing 0.05% EDTA) at 37°C. Inactivation of trypsin was achieved by adding a culture medium containing 10% FBS. After centrifugation, the pellet

was washed with culture medium without serum, and cells were resuspended and plated onto 6-well dishes with a density of  $3.6 \times 10^5$  cells/well. Cells were cultured in the starvation medium at 37°C under a 5% CO<sub>2</sub> atmosphere for 24-48 h. 10 ng/ml murine EGF was added for treatment, and cells were lysed at different time points after EGF treatment. Protein samples were isolated from the EGF treated cells and analyzed by western blotting.

### 3.4.11 Cell culture assays

#### 3.4.11.1 Proliferation

For *in vitro* studies, BrdU at a final concentration of 10 μM was added to the cell culture medium, and cells were incubated for 2 h at 37°C under a 5% CO<sub>2</sub> atmosphere. After washing with 1x PBS, they were fixed by 4% paraformaldehyde (PFA) at room temperature for 10 min. Cells were then permeabilized using 0.1% Triton-X 100 in PBS, followed by incubation with 2M HCl for 30 min. Afterwards the HCl solution was removed, and cells were incubated with borate buffer for 5 min. Blocking was performed using 1% BSA at room temperature for 10 min. Then the cells were incubated with the FITC-coupled BrdU antibody at 4°C overnight. In the end, cells were counterstained using propidium iodide.

#### 3.4.11.2 Migration: Scratch assay

Cells were grown to 100% confluency in the culture medium and treated with 10 μg/ml mitomycin C for 2 h. A scratch was made into the cell layer of each well using a sterile 200 μl pipette tip. Dead cells and debris were washed away with pre-warmed PBS, and fresh pre-warmed culture medium was added. Alternatively, cells were seeded into 24-well plates, grown to 100% confluency, and treated with 10 μg/ml mitomycin C for 2 h. A circular wound was introduced into each well with a 200 μl pipette tip (without filter) mounted on a vacuum pump. The pipette tip was moved perpendicularly on top of the cell monolayer, and the vacuum pump was applied for 5 sec. The medium of each well was replaced with serum-containing medium. Pictures were acquired with an Axiovert 200M inverted microscope at different time points. Wound closure was determined using ImageJ software with the MRI wound healing tool plugin.

#### 3.4.11.3 Migration: Transwell assay

Transwell migration assay (Boyden chamber assay) is used to study cell migration and chemotaxis. Cells were cultured in 6 cm dishes until they were 80-90% confluent. The culture medium was replaced by a starvation medium and cells were incubated for 24 h. Adherent cells were trypsinized, centrifuged, and counted with a hemocytometer. To reach a final concentration of  $4 \times 10^5$  cells/ml, the cells were resuspended in starvation medium. 250 μl cell suspension was added to a transwell plate (6.5 mm Transwell® chambers with 8.0 μm pore polycarbonate membrane inserts). After 1 h of incubation, the transwell inserts were transferred to a well of a 24-well plate with 650 μl serum-containing culture medium. Cells were incubated for several hours, washed twice with 1x PBS, and fixed with cold 100% methanol at room temperature for 15 min. Cell layers were covered with 0.5 % crystal violet solution (500 mg crystal violet, 25 ml methanol, 75 ml H<sub>2</sub>O) for 10 min and washed twice with 1x PBS. Cells on the upper layer were removed with cotton swabs. The transwell inserts were dried for 2 h, and the dried membranes were removed

with a scalpel blade. The cell-free side of the membrane was placed onto a microscope slide, and the cell-containing side was mounted with Mowiol. Images of the migrated cells were taken with an Axioskop 2 inverted light microscope at 20 x magnification. The areas covered by cells on the transwell membrane were measured using ImageJ software with the color deconvolution plugin.

#### 3.4.11.4 Collagen gel contraction assay

Fibroblasts were seeded and maintained in a 10 cm dish and cultured until they reached 75-90% confluency. One ml of 1% BSA was added in advance to each of the wells in a 24-well plate. The 24-well plates with the 1% BSA were incubated at 37°C for at least 30 min. While the 24-well plates were incubated with 1% BSA, the gel solutions were prepared in 1.5 ml tubes (one tube for each gel). The collagen gel recipe for one 500 µl gel (one tube) is shown below. The final collagen concentration of the gel was ~1 mg/ml.

Component	Volume
0.2 M HEPES buffer, pH 8.0	120 µl
DMEM	26 µl
Sterile H <sub>2</sub> O	16 µl
TeloCol® Collagen Solution (3.1 mg/ml)	198 µl
Cells at 4.2 x 10 <sup>5</sup> cells/ml	240 µl

The collagen solution was kept on ice until use. HEPES, DMEM and sterile Milli-Q H<sub>2</sub>O were added to each tube (one tube for one well of a 24-well plate). Cells were then trypsinized, centrifuged, and resuspended in 500 µl medium. Ten µl of the cell-containing medium from each tube was used to count the cell number using a haemocytometer. The total number of cells was divided by 4.2 x 10<sup>5</sup> to calculate the required final volume. The appropriate amount of medium was added to each tube (which contained the initial 500 µl re-suspended cells) so that all tubes had the same cell density. The 1% BSA solution was removed from the 24-well plate. Then, 198 µl of the collagen solution was added to each of the tubes (one tube for one well of 24-well plate), and 240 µl of the cells at 4.2 x 10<sup>5</sup> cells/ml were added to the tubes containing the gel mixtures. The gel mixtures were quickly, but gently mixed, and 500 µl of the mixture was added to the appropriate wells in the 24-well plate. The 24-well plate containing the gels was incubated in the cell culture incubator at 37°C for 30 min until the gels were fully solidified. 500 µl cell culture medium was then added to the wells containing the gels. Gels were photographed together with a ruler at 0 h and at different time points thereafter (e.g., 2, 24, 48 h).

## 3.5 Histology

### 3.5.1 Hematoxylin and eosin (HE) – staining

Hematoxylin and eosin staining was performed according to the following protocol:

Solution	Time
Hematoxylin	1 min
ddH <sub>2</sub> O	10 s



ddH <sub>2</sub> O	10 s
ddH <sub>2</sub> O	10 s
Scott water	30 s
ddH <sub>2</sub> O	10 s
70% EtOH	30 s
Eosin solution	1 min
80% EtOH	10 s
80% EtOH	10 s
95% EtOH	10 s
95% EtOH	10 s
100% EtOH	10 s
100% EtOH	10 s
Xylene	10 min
Xylene	10 min
Dry and mount with Eukitt mounting medium	

### 3.5.2 Masson Trichrome staining

Prior to staining, tissue sections were dewaxed (2x 10 min in xylene) and rehydrated in ethanol/water solutions of decreasing ethanol content (100%, 96%, 90%, 80%, 70%, 50%, 1 min each), and finally washed in water and in 1x PBS for 5 min.

For formalin-fixed tissue, sections were re-fixed in Bouin's solution for 1 h at 60°C to improve the staining quality and then washed in distilled water. To remove the yellow color, the sections were rinsed in running tap water for 5-10 min. And then they were stained in Weigert's iron hematoxylin working solution for 3 min and rinsed in flowing tap water for 10 min. After washing in distilled water for 10 s, they were stained with Biebrich scarlet-acid fuchsin solution (Goldner's stain I) for 5-10 min and rinsed with 1% acetic acid solution for 30 s. They were then incubated in phosphomolybdic-phosphotungstic acid solution (Goldner's stain II) for 1-3 min and rinsed with 1% acetic acid solution for 30 s. In the end, they were counterstained with Goldner's stain III for 2-5 min. Sections were washed with 1% acetic acid solution for 2-5 min. Subsequently, they were dehydrated very quickly through incubation in 95% ethyl alcohol and in absolute ethyl alcohol and cleared in xylene for 2x10 min. Finally, the slides were mounted with a resinous mounting medium.

### 3.5.3 Herovici staining

Prior to staining, tissue sections were dewaxed (2x 10 min in xylene) and rehydrated in ethanol/water solutions of decreasing ethanol content (100%, 96%, 90%, 80%, 70%, 50%, 1 min each).

Herovici staining was performed according to the following protocol: (recipes of the solutions are shown in section 2.5)

Solution	Time
----------	------

Herovici staining solution A	5 min
Running tap water	2 min
Herovici staining solution B	2-5 min
Running tap water	2 min
Herovici staining solution C	2 min
Herovici staining solution D	2 min
Running tap water	2 min
Herovici staining solution F	2 min
Herovici staining solution G	2 min
100% EtOH	1 min
100% EtOH	1 min
Xylene	2 min
Xylene	2 min
Dry and mount with Eukitt mounting medium	

### 3.5.4 Immunofluorescence and immunohistochemistry

#### 3.5.4.1 Immunofluorescence

Prior to staining, tissue sections were dewaxed and rehydrated in ethanol/water solutions of decreasing ethanol content (100%, 96%, 90%, 80%, 70%, 50%, 1 min each), and finally washed in water, or fixed with cold methanol (in case of frozen sections). Unspecific binding sites were blocked with 12% BSA/0.1% NP-40 in PBS at room temperature for 1 h. Sections were then incubated with primary antibodies (section 2.6.1) diluted in the same buffer at 4°C overnight. If necessary, antigen retrieval was performed prior to the blocking procedure by cooking in citrate buffer (10 mM citric acid, pH 6.0) for 1 h at 95°C. After three washing steps with PBST, slides were incubated with secondary antibodies (section 2.7.2) and Hoechst for 1 h at room temperature, and then washed with PBST again and mounted with Mowiol.

#### 3.5.4.2 BrdU staining

Acetic ethanol-fixed paraffin sections were dewaxed and rehydrated as described in section 3.5.3.1. and incubated for 10 min in ice-cold 100% methanol. The sections were treated with 1% H<sub>2</sub>O<sub>2</sub> for 40 min and washed with 1x PBS. After denaturing the DNA in 2 M HCl at 37°C for 1 h, the sections were incubated in 0.1 M borate buffer three times (with each time 10 min incubation). After that, the sections were washed in 1x PBS for 5 min and blocked with 12% BSA at room temperature for 1 h. Proliferating cells were then stained with an anti-BrdU-POD antibody (section 2.6.1) at 4°C overnight. After washing with PBST for 4 x 10 min, the DAB solution was added (buffer - 2 drops, H<sub>2</sub>O<sub>2</sub> - 2 drops, DAB 4 drops in 5 ml of water). After staining, the sections were washed with water, and the H&E staining was performed as follows:

Step content	Time
Hematoxylin	1 min
ddH <sub>2</sub> O	10 s
ddH <sub>2</sub> O	10 s
ddH <sub>2</sub> O	10 s

Scott water	30 s
ddH <sub>2</sub> O	10 s
70% EtOH	10 s
Eosin solution	2 min
80% EtOH	10 s
80% EtOH	10 s
95% EtOH	10 s
95% EtOH	10 s
100% EtOH	10 s
100% EtOH	10 s

Sections were dried and mounted with Eukitt mounting medium.

### 3.6 Microscopy

All sections were photographed using a Zeiss Imager.A1 microscope equipped with an AxioCam MRm camera, Zeiss EC Plan-Neofluar objectives (10x/0.3, 20x/0.5, 40x/1.3 Oil) and Zeiss Plan-APOCHROMAT (60x/1.4 Oil). For data acquisition, the AxioVision Rel.4.8 software was used.

### 3.7 Statistical analysis

Statistical analysis was performed using the GraphPad Prism 8 software. Quantitative data are expressed as mean  $\pm$  SEM. Testing for statistically significant differences between two experimental groups was performed using Student's t-test or non-parametric Mann-Whitney U test that compares two unpaired groups at a confidence level starting at 95% ( $p < 0.05$ ) or using Fisher's exact test. \* $P < 0.05$ , \*\* $P < 0.01$ , and \*\*\* $P < 0.001$ , \*\*\*\* $P < 0.001$ .

## 4. Projects

### 4.1 NEDD4-1 is a key regulator of epidermal homeostasis, wound repair and UV response

**Shen Yan<sup>1</sup>, Raphael Ripamonti<sup>1</sup>, Maya Ben-Yehuda Greenwald<sup>1</sup>, Hiroshi Kawabe<sup>2</sup>,  
and Sabine Werner<sup>1\*</sup>**

<sup>1</sup>Institute of Molecular Health Sciences, Department of Biology, Swiss Federal Institute of Technology (ETH) Zurich, 8093 Zurich, Switzerland

<sup>2</sup>Max-Planck-Institute of Experimental Medicine, Department of Molecular Neurobiology, 37075 Göttingen, Germany

\*Address for correspondence:

Prof. Dr. Sabine Werner

Institute of Molecular Health Sciences

Otto-Stern-Weg 7

8093 Zurich, Switzerland

Phone: +41 44 633 3941

Fax: +41 44 633 1174

E-mail: [sabine.werner@biol.ethz.ch](mailto:sabine.werner@biol.ethz.ch)

Running title: Nedd4-1 in keratinocytes

Manuscript in preparation

Own contributions:

- Generation of mice lacking *Nedd4-1* in keratinocytes and other stratified epithelia (breedings, weaning, biopsy taking, genotyping, regular observation and macroscopic analysis)
- Characterization of normal back skin from adult mutant mice (sample collection, tissue processing, sectioning, staining, microscopy data acquisition; evaluation of stainings, quantification of thickness of skin layers, distance between hair follicles, and proliferating cells; TEWL measurements and epidermal differentiation marker staining)
- Characterization of normal back skin of 3-day-old mice (sample collection, tissue processing, sectioning, stainings, microscopy data acquisition, evaluation of stainings)
- Wound healing studies (3-day, 5-day and 14-day wound sample collection, tissue processing, sectioning, staining, microscopy data acquisition, evaluation of stainings)
- UV irradiation studies (non-UV irradiated, 24h, 72h after UV irradiation-skin sample collection, tissue processing, sectioning, staining, evaluation of the stainings) (performed together with Dr. Maya Ben-Yehuda Greenwald)
- Expression studies using normal back skin and wound samples of adult wild-type C57BL/6 mice (sample collection and preparation, preparation of protein lysates, Western blot analysis)
- Loss-of-function studies of *Nedd4-1* in keratinocytes using siRNA (knock-down efficiency validation, RNA extraction and subsequent quantitative real-time RT-PCR analysis, protein lysate preparation and subsequent Western blot analysis, analysis of cell proliferation and migration)
- Cloning of plasmids for *Nedd4-1* knock-down and overexpression (performed together with my Master student Raphael Ripamonti)
- Generation of lentiviral vectors for *Nedd4-1* knock-down or overexpression (performed together with my Master student Raphael Ripamonti)
- Loss-of-function studies of *Nedd4-1* in keratinocytes using shRNA (generation of stable knock-down keratinocyte cell lines, knock-down efficiency validation, RNA extraction and subsequent quantitative real-time RT-PCR analysis, protein lysate preparation and subsequent Western blot analysis, analysis of cell proliferation and migration) (performed together with my Master student Raphael Ripamonti)
- EGF stimulation experiments in keratinocytes, analysis of Erk1/2 activation
- Experimental design together with S.W.
- Design of the figures and writing of the manuscript together with S.W.

## **Abstract**

Nedd4-1 is an evolutionarily highly conserved and ubiquitously expressed HECT E3 ligase. It plays key roles in organ development, tissue homeostasis and cancer, but its functions in the skin are largely unknown. Here we show that mice with Nedd4-1 deficiency in keratinocytes exhibit perturbed epidermal homeostasis and abnormalities in hair follicle cycling. In particular, healing of full-thickness excisional wounds was delayed in the mutant mice, mainly as a result of impaired re-epithelialization. This resulted from reduced proliferation and migration of keratinocytes as shown *in vivo* and in functional *in vitro* studies. Loss of Nedd4-1 in keratinocytes also aggravated the extent of UV-induced keratinocyte apoptosis. *In vitro* studies suggest that the beneficial activities of Nedd4-1 in wound repair and UV response are at least in part mediated by impaired epidermal growth factor-mediated activation of the Erk signaling pathway. These results identify Nedd4-1 as a key player in in epidermal homeostasis, UV response and wound healing.

## Introduction

The skin is the largest organ of the body and forms a protective barrier against the environment. Its outermost part is the multilayered epidermis, which undergoes continuous self-renewal and forms a seal to prevent water loss from the inside and invasion of allergens, irritants and pathogens from the outside. Therefore, any injury to the skin has to be rapidly and efficiently repaired. This is achieved by an elaborate wound healing process, which involves three partly overlapping stages, including inflammation, new tissue formation and remodeling [47, 152, 153]. Unfortunately, wound repair is frequently impaired in aged individuals and in patients with diabetes or those treated with chemotherapeutic or immunosuppressive agents. This results in the formation of chronic, non-healing skin ulcers, which cause severe morbidity and even mortality. Chronic wounds constitute an enormous burden to the health care system [153, 154] and therefore, the development of novel approaches for the improvement of healing is essential. This requires a thorough understanding of the mechanisms underlying normal and impaired wound repair and the identification of key players involved in this process. In contrast to skin wounding, which leads to scar formation [47], repair of the injured liver allows complete regeneration of the organ if the insult is not too severe [155]. Therefore, genes and proteins, which orchestrate liver regeneration, may be promising targets for promotion of repair in other tissues. In a search for such proteins, our laboratory performed a large-scale proteomics screen using samples from non-injured liver and from liver at different time points after two-third (partial) hepatectomy in mice. Bioinformatics analysis of the data revealed a strong regulation of components involved in protein ubiquitination, with the ubiquitin ligase “neural precursor cell expressed developmentally down-regulated 4-1” (Nedd4-1) being the top up-regulated protein [50]. Importantly, *in vivo* knock-down of Nedd4-1 in hepatocytes caused liver failure after partial hepatectomy [50], demonstrating an essential role of this protein in the regeneration process.

NEDD4-1 is a member of the HECT (Homologous to E6 AP Carboxyl Terminus) E3 ligase family. It is an evolutionarily highly conserved and ubiquitously expressed protein with key functions in organ development, tissue homeostasis and cancer [143, 156]. In the skin, a role in the pathogenesis of keloid scars has been suggested [144, 157], while its role in



epidermal homeostasis and wound healing is unclear. In this study we show that Nedd4-1 in keratinocytes is an important regulator of skin homeostasis, UV response and wound re-epithelialization.

## **Results**

### **Nedd4-1 is expressed in murine skin and in cultured skin cells**

To determine a potential function of Nedd4-1 in the skin, we first analyzed its expression in this tissue. qRT-PCR analysis revealed a similar expression level of *Nedd4-1* in skin and liver of wild-type mice, and expression was seen in the dermis and in the epidermis (Supplementary Fig. S1A, B). This is consistent with RNA sequencing data of cells isolated from mouse skin at embryonic day 14.5 and at postnatal day 5 (P5), which revealed strong expression of *Nedd4-1* in epidermal and hair follicle keratinocytes and in various cell types of the dermis [158, 159]. Expression of Nedd4-1 in keratinocytes of mouse skin was confirmed by immunofluorescence analysis (Supplementary Fig. S1C). Cultured primary mouse keratinocytes and fibroblasts also expressed Nedd4-1 RNA and protein (Supplementary Fig. S1D-F). Immunohistochemical staining of normal human skin showed ubiquitous expression of NEDD4-1 in this tissue, and it was particularly abundant in the granular layer of the epidermis and in dermal fibroblasts (Supplementary Fig. S1G).

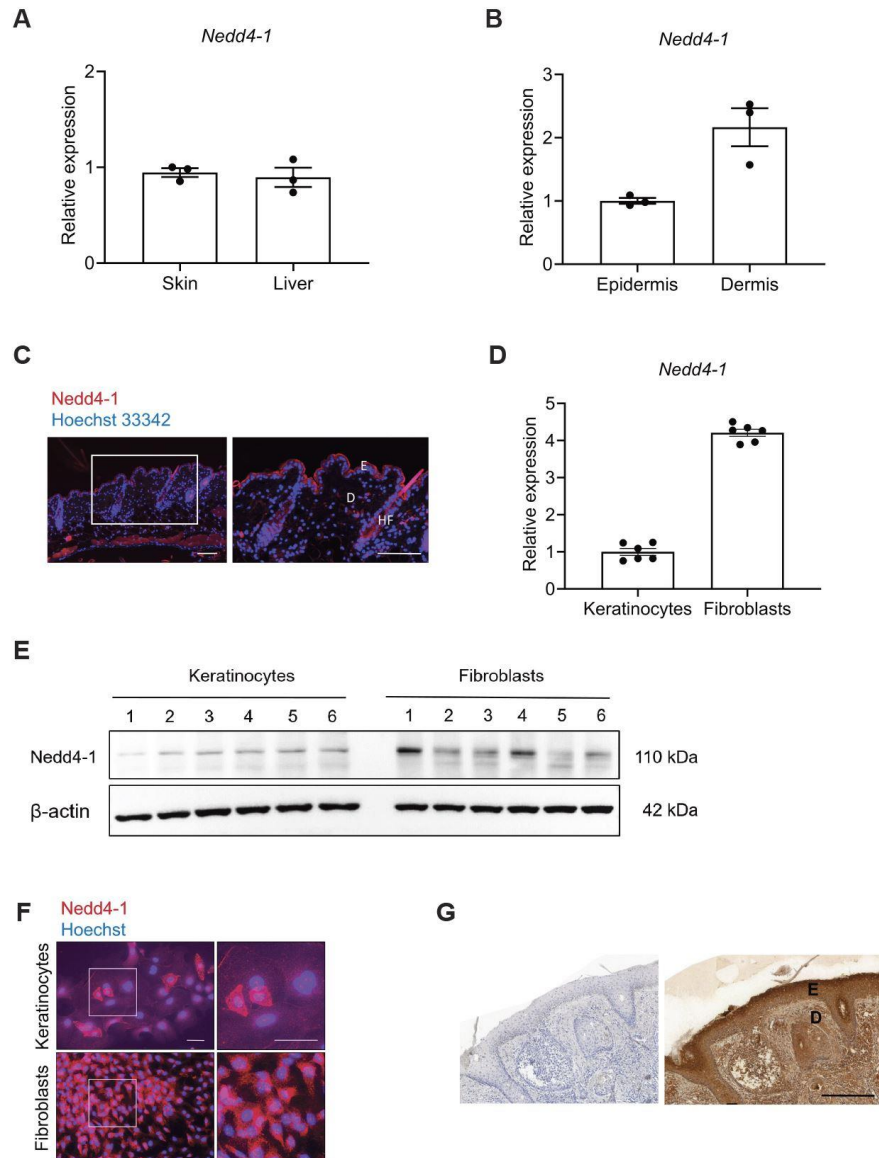


### Fig. S1 Nedd4-1 is strongly expressed in the skin

(A, B) qRT-PCR for *Nedd4-1* relative to *Rps29* using RNA samples from total skin and liver (A) or isolated epidermis and dermis (B) of adult C57BL/6J mice. N = 3 mice.

(C) Immunofluorescence staining of normal back skin of wild-type mice for Nedd4-1 (red). Nuclei were counterstained with Hoechst (blue).

(D, E) qRT-PCR for *Nedd4-1* relative to *Rps29* (D) and Western blot analysis for Nedd4-1 and  $\beta$ -actin (loading control) (E) using RNA samples or protein lysates from cultured primary fibroblasts and keratinocytes of newborn C57BL/6 mice. N = 6 cultures (each from a different mouse).

(F) Immunofluorescence staining of cultured primary mouse keratinocytes and fibroblasts for Nedd4-1 (red). Nuclei were counterstained with Hoechst (blue).

(G) Immunohistochemical staining of normal skin adjacent to a basal cell carcinoma for NEDD4-1, counterstained with hematoxylin (right). The left panel shows the negative control (staining without primary antibody). E: Epidermis; D: Dermis.

Bar graphs show mean  $\pm$  SEM. Mean expression in total skin (A) in the epidermis (B) or in keratinocytes (D) was set to 1.

Magnification bars : 50 $\mu$ m(C, F); 200 $\mu$ m (G).

### **Impaired epidermal homeostasis and hair follicle cycling in mice lacking Nedd4-1 in keratinocytes**

Based on the previously identified key role of Nedd4-1 in hepatocytes for liver regeneration [50], we focused our functional analysis on epithelial cells and determined the consequences of Nedd4-1 deficiency in keratinocytes. By breeding of K5-Cre mice [147] with mice harboring floxed alleles of *Nedd4-1* [146], we generated mice lacking this protein in keratinocytes of the epidermis and hair follicles (Supplementary Fig. S2A). The efficient knockout in the resulting K5cre-Nedd4-1 mice (designated *Nedd4-1* cKO) was verified by PCR, qRT-PCR, Western blot analysis and immunofluorescence staining (Supplementary Fig. S2B-E).

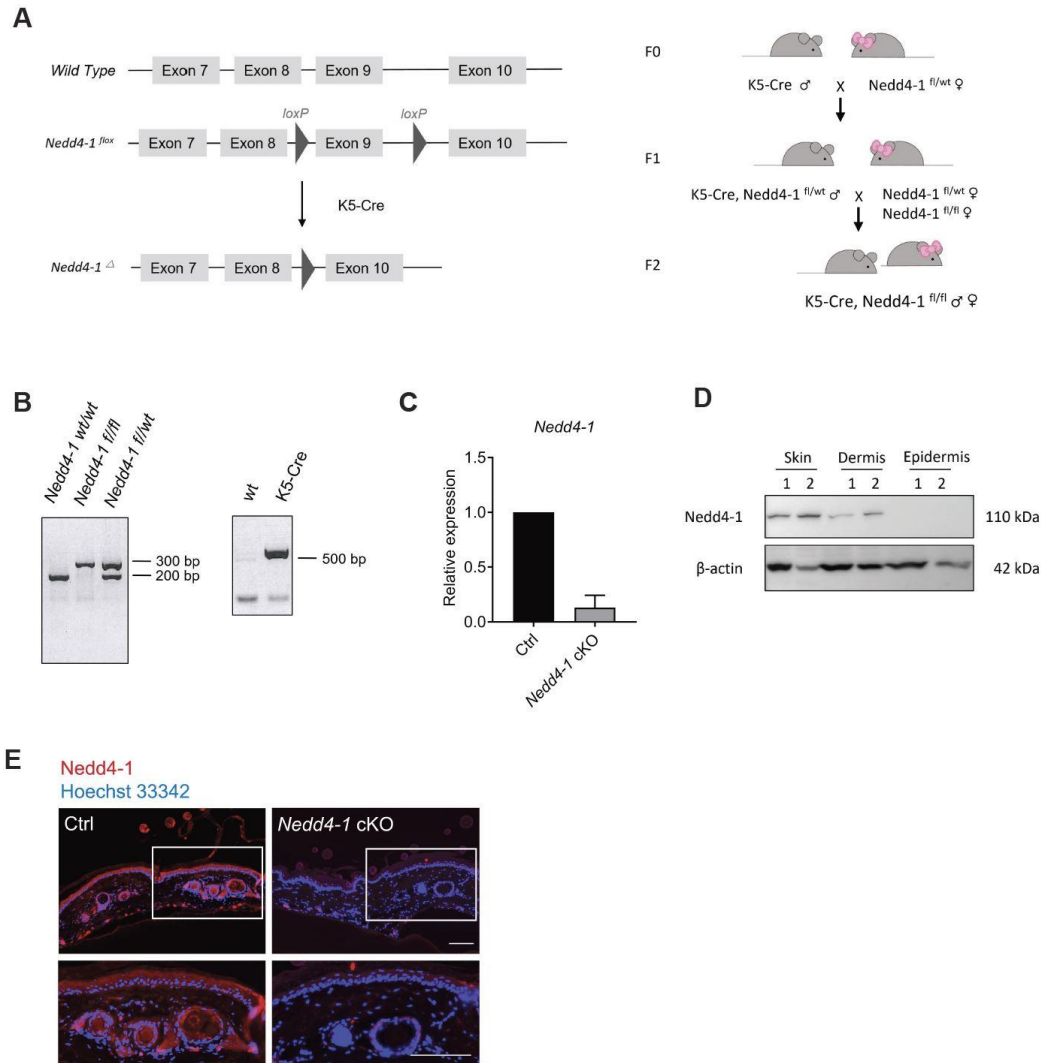


**Fig. S2 Generation of K5cre-Nedd4-1 (*Nedd4-1* cKO) mice**

(A) Schematic representation of the *Nedd4-1* targeting strategy (left) [146], and breeding scheme (right) for the generation of mice lacking *Nedd4-1* in keratinocytes.

(B) PCR analyses of DNA from WT (wt/wt), heterozygous (fl/wt), and homozygous (fl/fl) *Nedd4-1* knockout mice using primers detecting the *Nedd4-1* wild-type (wt) and floxed (fl) alleles (left panel) or the *Cre* transgene (right panel).

(C) qRT-PCR analysis for *Nedd4-1* relative to *Rps29* using RNA samples from isolated epidermis of adult Ctrl and *Nedd4-1* cKO mice. Scatter plot shows mean  $\pm$  SEM. N = 3 mice per genotype. Mean expression in ctrl (fl/fl;wt) mice was set to 1.

(D) Western blot analysis of lysates from isolated dermis and epidermis of adult Ctrl and *Nedd4-1* cKO mice for Nedd4-1 and  $\beta$ -actin (loading control). N = 2 mice per genotype.

(E) Representative immunofluorescence staining of tail skin from adult Ctrl and *Nedd4-1* cKO mice for Nedd4-1 (red). Nuclei were counterstained with Hoechst (blue). The white rectangle indicates the area that is shown at higher magnification below. Magnification bars: 100  $\mu$ m.

The percentage of *Nedd4-1* cKO mice that were detected in the litters did not follow the expected Mendelian ratio (25%) upon weaning and genotyping, but were underrepresented (approximately 15%). This observation suggests that some mice may die *in utero* or immediately after birth and are cannibalized by the mothers. Neonatal *Nedd4-1* cKO mice that survived had a thinner epidermis, mainly because of the thinner cornified layer compared to control mice (Supplementary Fig. S3A-D). Consistently, there was a reduced staining for the late epidermal differentiation marker loricirin in the *Nedd4-1* cKO mice, indicating a defect in terminal keratinocyte differentiation (Supplementary Fig. S3E).

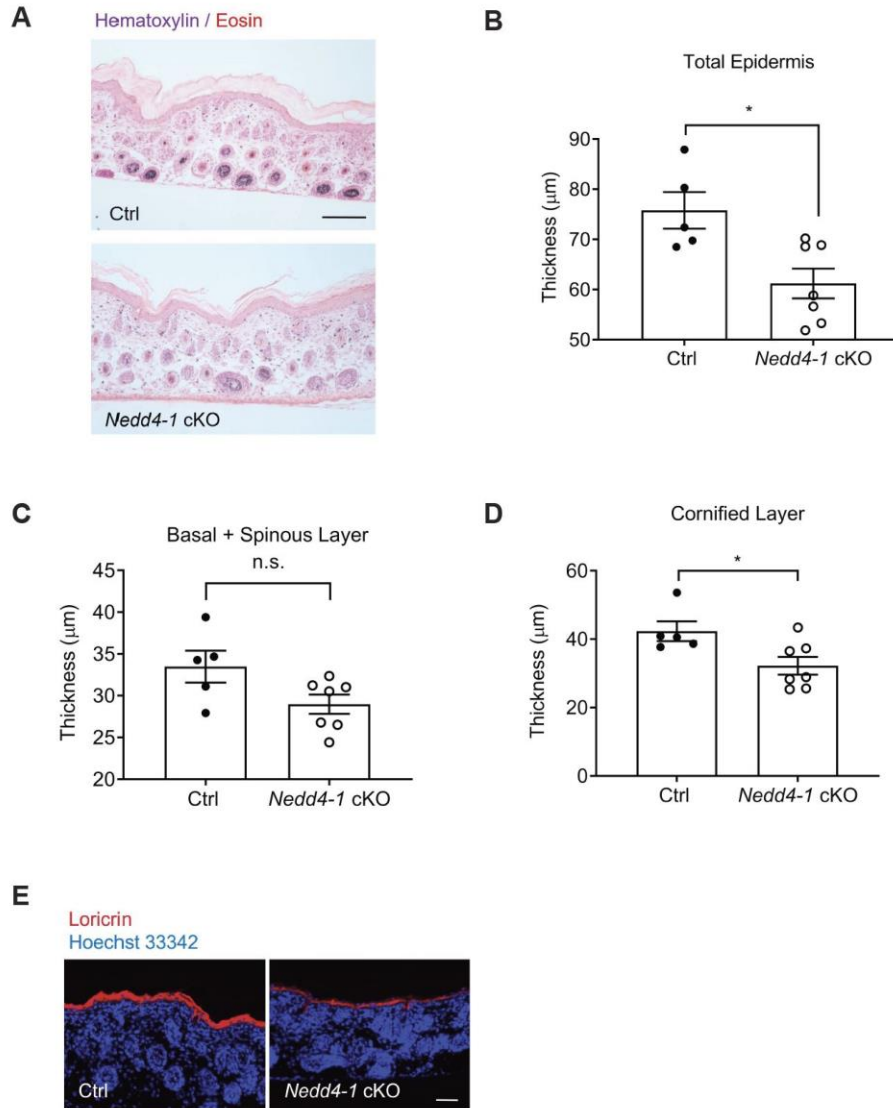


**Fig. S3 Morphogenesis of epidermis and hair follicles is only mildly affected in K5-Cre *Nedd4-1* cKO mice**

(A) Representative photomicrographs of hematoxylin/eosin-stained back skin sections from neonatal Ctrl and *Nedd4-1* cKO mice.

(B) Epidermal thickness of neonatal Ctrl and *Nedd4-1* cKO mice. N = 5-7 mice per genotype.

(C, D) Thickness of basal and spinous layer (C) or cornified layer (D) of neonatal Ctrl and *Nedd4-1* cKO mice. N = 5-7 mice per genotype.

(E) Representative immunofluorescence stainings of back skin sections from neonatal Ctrl and *Nedd4-1* cKO mice for loricrin (red). Nuclei were counterstained with Hoechst (blue).

Scatter plots show mean ± SEM. n.s.: non-significant, \*P < 0.05 (Mann-Whitney U test).

Magnification bars: 100 µm (A) and 50 µm (E).

Adult *Nedd4-1* cKO mice were fertile and they did not exhibit obvious health problems. They were significantly smaller and had a lower body weight at the weaning age (Fig. 1A, B), but this was much less pronounced in adult mice (Fig. 1C, D). At 10 weeks of age, however, when hair follicles of control mice are in the telogen phase of the hair cycle [25], patchy hair growth was seen in shaved *Nedd4-1* cKO mice (Fig. 1E). Histological analysis of the skin at this stage identified anagen hair follicles in *Nedd4-1* cKO, but not in control mice (Fig. 1F), and a significantly lower percentage of the follicles in the mutant mice were in telogen (Fig. 1G). The average distance between hair follicles was not altered, indicating that hair follicle morphogenesis was not affected (Fig. 1H). There was no difference in the thickness of the dermis (Fig. 1I), but the adipose layer of *Nedd4-1* cKO mice was significantly thicker, even in the areas without anagen hair follicles (Fig. 1J). Because the adipose layer increases in mouse skin during the transition to anagen, this finding may reflect the alterations in hair follicle cycling [25].

Histological analysis of the epidermis and hair follicles showed a strong disorganization of the keratinocytes in *Nedd4-1* cKO mice and a reduced thickness of the viable and cornified layers of the epidermis (Fig. 1K). Furthermore, expression of K15, a hair follicle bulge stem cell marker [160], was almost completely absent in their hair follicles (Fig. 1L).



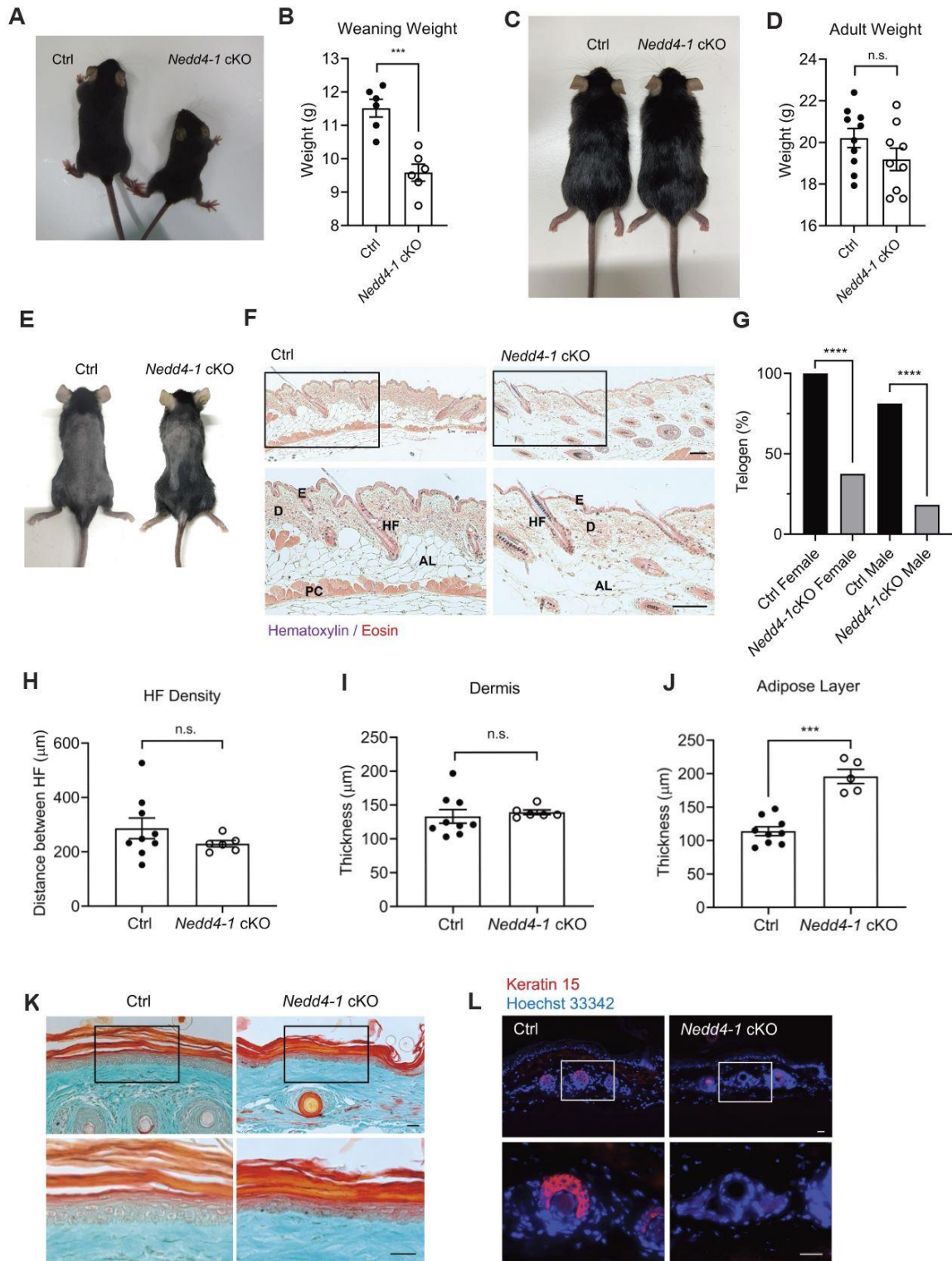


**Fig. 1 Epidermal and hair follicle abnormalities in *Nedd4-1* cKO mice**

(A-D) Macroscopic appearance (A, C) and body weight (B, D) of mice at postnatal day 28 (P28) (A, B) and at 10 weeks of age (C, D). B: N = 6 mice per genotype; D: N = 9-10 mice per genotype.

(E) Macroscopic appearance of 10 week-old Ctrl and *Nedd4-1* cKO mice after shaving. Note the appearance of hair patches in the *Nedd4-1* cKO mice at this stage.

(F) Hematoxylin/eosin staining of longitudinal back skin sections from Ctrl and *Nedd4-1* cKO mice at 10 weeks of age. AL: Adipose layer; D: Dermis, E: Epidermis; HF: Hair follicle.

(G) Percentage of hair follicles in female and male Ctrl and *Nedd4-1* cKO mice, which are in the telogen phase of the hair cycle. N= 11-17 mice per genotype.

(H) Distance between hair follicles in back skin of Ctrl and *Nedd4-1* cKO mice at 10 weeks of age. N = 6-9 mice per genotype.

(I) Dermal thickness of Ctrl and *Nedd4-1* cKO mice at 10 weeks of age. N = 6-9 mice per genotype.

(J) Thickness of the adipose layer in Ctrl and *Nedd4-1* cKO mice at 10 weeks of age. N = 6-9 mice per genotype.

(K) Representative photomicrographs of Masson Trichrome stained tail skin sections from Ctrl and *Nedd4-1* cKO mice at 10 weeks of age.

(L) Representative immunofluorescence stainings of tail skin sections from Ctrl and *Nedd4-1* cKO mice at 10 weeks of age for the bulge stem cell marker keratin15. Nuclei were counterstained with Hoechst.

Magnification bars: 100  $\mu$ m (F) or 20  $\mu$ m (K, L). Areas, which are marked with a rectangle, are shown at higher magnification below.

Scatter plots show mean  $\pm$  SEM. n.s.: non-significant, \*\*\*P<0.001, \*\*\*\*P<0.0001; Mann-Whitney U test (C, D, H, I, J) and Fisher's exact test (G).

## **Nedd4-1 is required for keratinocyte proliferation and differentiation in the epidermis**

Quantification of the epidermal thickness confirmed its significant reduction in adult *Nedd4-1* cKO mice (Fig. 1K and 2A). This is most likely a result of impaired keratinocyte proliferation as determined by Ki67 staining (Fig. 2B), while the number of apoptotic keratinocytes was equally low in the epidermis of mice from both genotypes (Fig. 2C). Analysis of differentiation-specific keratins revealed normal expression of keratin 14 (K14) in the basal layer and of K10 in the superbasal layers (Fig. 2D). Keratin 6, which is only expressed in hair follicles of normal skin, was also restricted to the follicles in *Nedd4-1* cKO mice (Fig. 2D).

However, and consistent with the results obtained with neonatal skin, expression of the late differentiation marker loricrin was strongly reduced in the epidermis of *Nedd4-1* cKO

mice, again pointing to a defect in terminal keratinocyte differentiation (Fig. 2D). This hypothesis is supported by the enhanced transepidermal water loss in *Nedd4-1* cKO mice (Fig. 2E), which reflects a defect in the inside-out barrier of the epidermis.

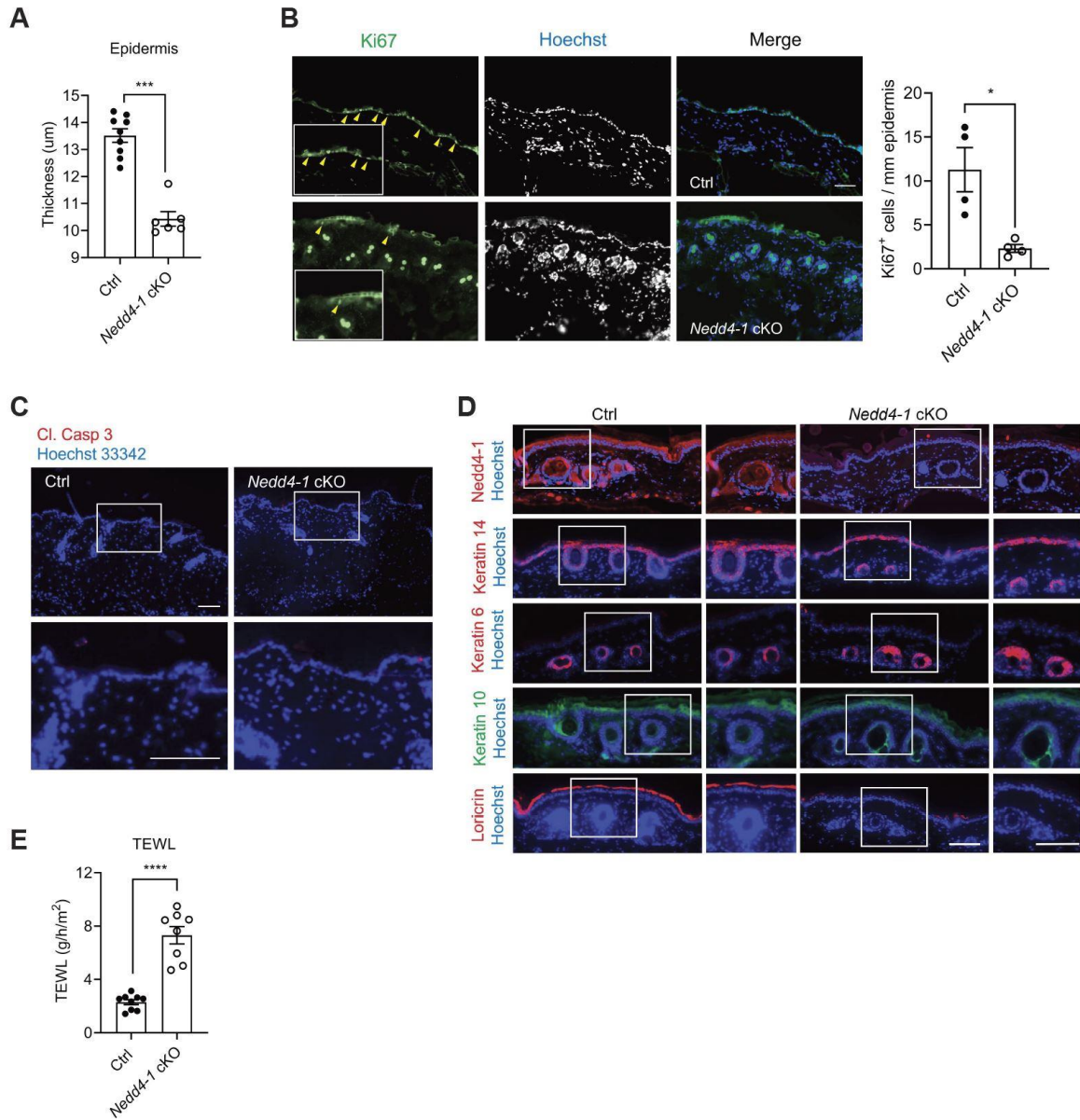


**Fig. 2 Impaired proliferation and terminal differentiation of epidermal keratinocytes in *Nedd4-1* cKO mice**

(A) Epidermal thickness of Ctrl and *Nedd4-1* cKO mice at 10 weeks of age. N = 6-9 mice per genotype.

(B) Representative photomicrographs of Ki67-stained sections from normal skin of Ctrl and *Nedd4-1* cKO mice at 10 weeks of age. Ki67-positive keratinocytes in the epidermis are indicated with yellow arrowheads.

Bar graph shows quantification of Ki67-positive cells in the epidermis. N = 4 mice, n = 4-6 pictures per mouse. Higher magnifications are shown as an indent (white rectangle).

(C) Representative photomicrographs of skin sections stained for cleaved caspase-3 (red). Nuclei were counterstained with Hoechst (blue). Areas, which are indicated by the white rectangles, are shown at higher magnification below.

(D) Representative immunofluorescence stainings of tail skin sections from Ctrl and *Nedd4-1* cKO mice at 10 weeks of age for Nedd4-1, keratin 14 (K14), K6, K10, and loricrin. Nuclei were counterstained with Hoechst (blue). Areas, which are indicated by the white rectangles, are shown at higher magnification at the right hand side.

(E) Transepidermal water loss (TEWL) on the back skin of 10 week-old Ctrl and *Nedd4-1* cKO mice. N = 8-9 mice per genotype.

Scatter plots show mean  $\pm$  SEM. n.s.: non-significant, \*P<0.05, \*\*\*P<0.001, \*\*\*\*P<0.0001 (Mann-Whitney U test). Magnification bars: 100  $\mu$ m (B, C, D).

### Impaired wound healing in *Nedd4-1* cKO mice

To determine a potential role of Nedd4-1 in wound healing, we first analyzed its expression during the healing process of full-thickness excisional wounds in control mice. Western blot analysis of total wound lysates showed strong Nedd4-1 expression during the proliferation and remodeling phase of healing (Supplementary Fig. S4A). This was confirmed by immunofluorescence staining of 5-day wounds (Supplementary Fig. S4B).

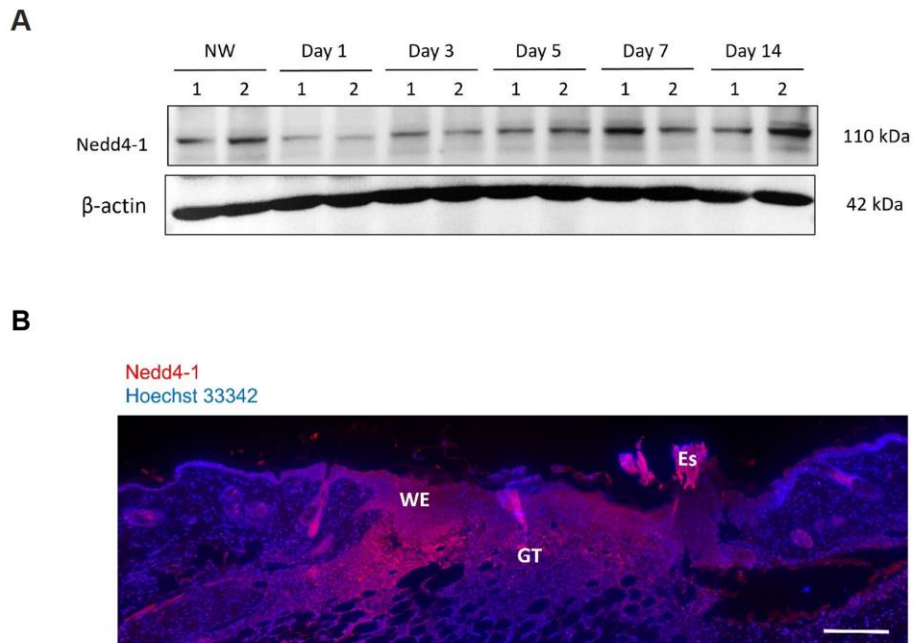


Fig. S4 Expression of Nedd4-1 in skin wounds

(A) Western blot analysis for Nedd4-1 and  $\beta$ -actin (loading control) using total lysates of full-thickness excisional wounds from wild-type C57BL/6J mice at different time points after injury. NW: Non-wounded skin.

(B) Representative immunofluorescence staining of section from a 5-day wound of a wild-type mouse for Nedd4-1 (red). Nuclei were counterstained with Hoechst (blue). Magnification bar: 200  $\mu$ m. WE: Wound epidermis, G: Granulation tissue; Es: Eschar.

We next generated full-thickness excisional wounds in the back skin of female *Nedd4-1* cKo and ctrl mice. Histological and histomorphometric analysis of 3-day wounds (Fig. 3A, B) revealed a mild delay in wound repair at this early stage in *Nedd4-1* cKO mice. The mutant mice showed no significant reduction in wound re-epithelialization and contraction, which both contribute to wound closure in mice to a similar extent (Fig. 3C, D). However, the length of the wound epidermis, which mainly reflects the rate of migration at this stage, as well as the area of the wound epidermis, were significantly reduced in *Nedd4-1* cKO mice, while its thickness was similar in mice of both genotypes (Fig. 3E-G). Keratinocyte proliferation in the wound epidermis was significantly lower in *Nedd4-1* cKO mice (Fig. 3H, I).



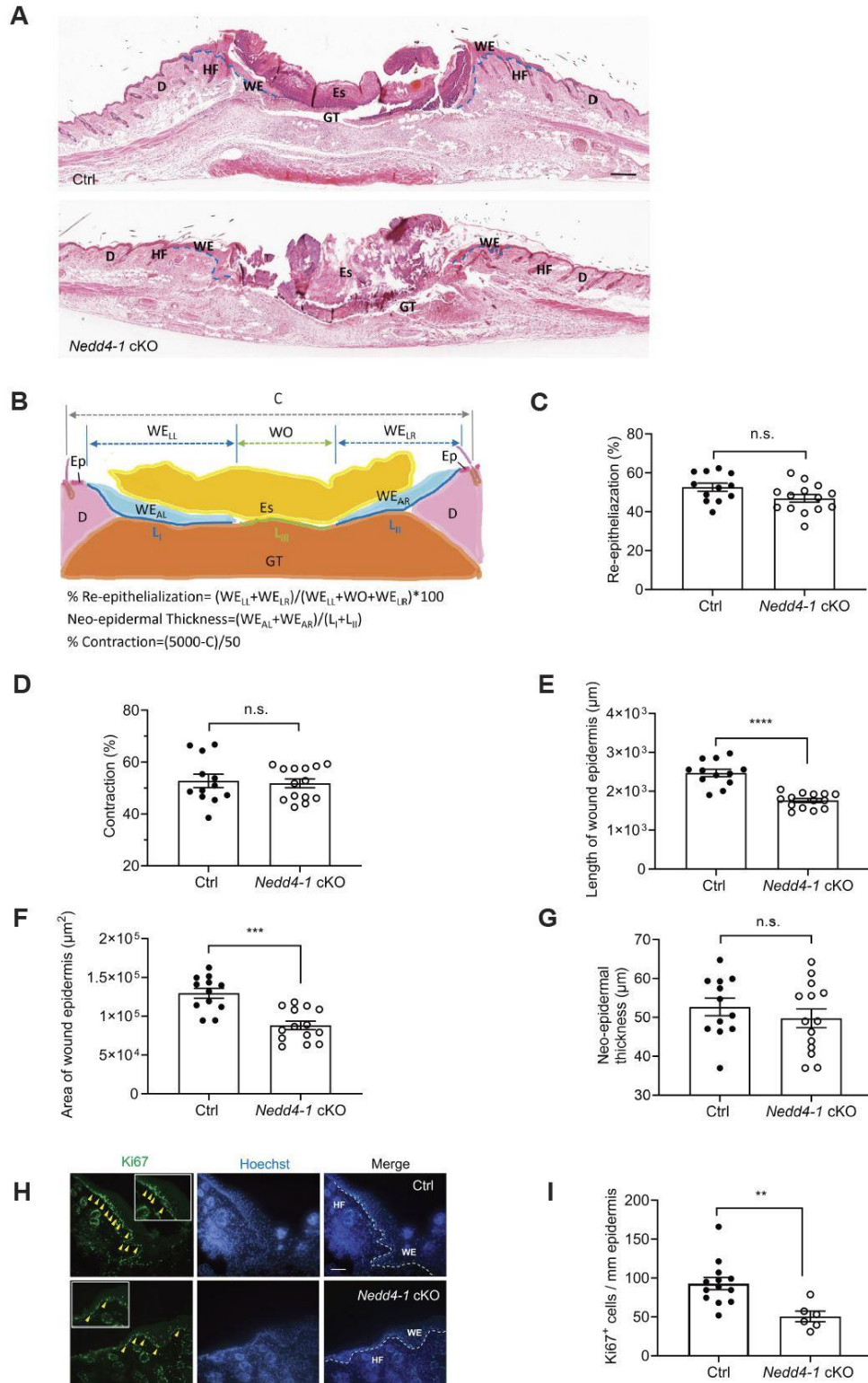


**Fig. 3** The early wound healing phase is delayed in *Nedd4-1* cKO mice

**(A)** Representative hematoxylin/eosin stainings of 3-day wound sections from Ctrl and *Nedd4-1* cKO mice. D: dermis; Es: eschar; GT: granulation tissue; HE: Hyperproliferative wound epidermis; HF: hair follicle; WE: wound epithelium.

**(B)** Schematic representation of a wound section, indicating parameters quantified by histomorphometric analysis. The formulas used to determine percentage of re-epithelialization, neo-epidermal thickness and contraction are given below the figure. D: Dermis; Ep: Epidermis adjacent to the wound; Es: eschar; GT: Granulation tissue; C: Distance between hair follicles,  $WE_{LL}$ : Length of left wound epithelium;  $WE_{LR}$ : Length of right wound epithelium; WO: Length of open wound (gap);  $WE_{AL}$ : Area of left wound epithelium;  $WE_{AR}$ : Area of right wound epithelium;  $L_I$ : Migrated distance of left wound epithelium;  $L_{II}$ : Migrated distance of right wound epithelium.

**(C, D)** Percentage of wound re-epithelialization **(C)** and contraction **(D)** in 3-day wounds of Ctrl and *Nedd4-1* cKO mice. N = 7 mice per genotype.

**(E-G)** Length **(E)**, area **(F)** and thickness **(G)** of wound epidermis of 3-day wounds from Ctrl and *Nedd4-1* cKO mice. N = 7 mice per genotype.

**(H, I)** Representative photomicrographs of Ki67-stained sections from 3-day wounds of Ctrl and *Nedd4-1* cKO mice. Ki67-positive keratinocytes in the wound epidermis are indicated with yellow arrowheads. Bar graphs show quantification of Ki67-positive cells in the wound epidermis. N = 3-4 mice per genotype.

Scatter plots show mean  $\pm$  SEM. n.s.: non-significant, \*\*P < 0.01, \*\*\*P < 0.001, \*\*\*\*P < 0.0001 (Mann-Whitney U test).

Magnification bars: 100  $\mu$ m **(A, H)**.

The delayed wound healing in *Nedd4-1* cKO mice was even more pronounced at day 5 after wounding, and significantly less wounds were fully closed in the mutant mice at this time point (Fig. 4A, B). This was a consequence of reduced re-epithelialization and contraction (Fig. 4C, D). The length of the wound epidermis was even slightly increased in the mutant mice at this time point (Fig. 4E), most likely reflecting the need to re-epithelialize a larger wound area as a consequence of the reduced contraction. There was no difference in the area of the wound epidermis, while its average thickness was reduced in *Nedd4-1* cKO mice (Fig. 4F, G), most likely because of the strongly reduced keratinocyte proliferation (Fig. 4H, I).

In spite of the delayed healing, wounds in mice of both genotypes were fully closed at day 14 after injury, and there was no significant difference in the length, area and thickness of the neo-epidermis between control and *Nedd4-1* cKO mice (Fig. 5A-E). Furthermore, the granulation tissue appeared similar in mice of both genotypes (Fig. 5A, B).

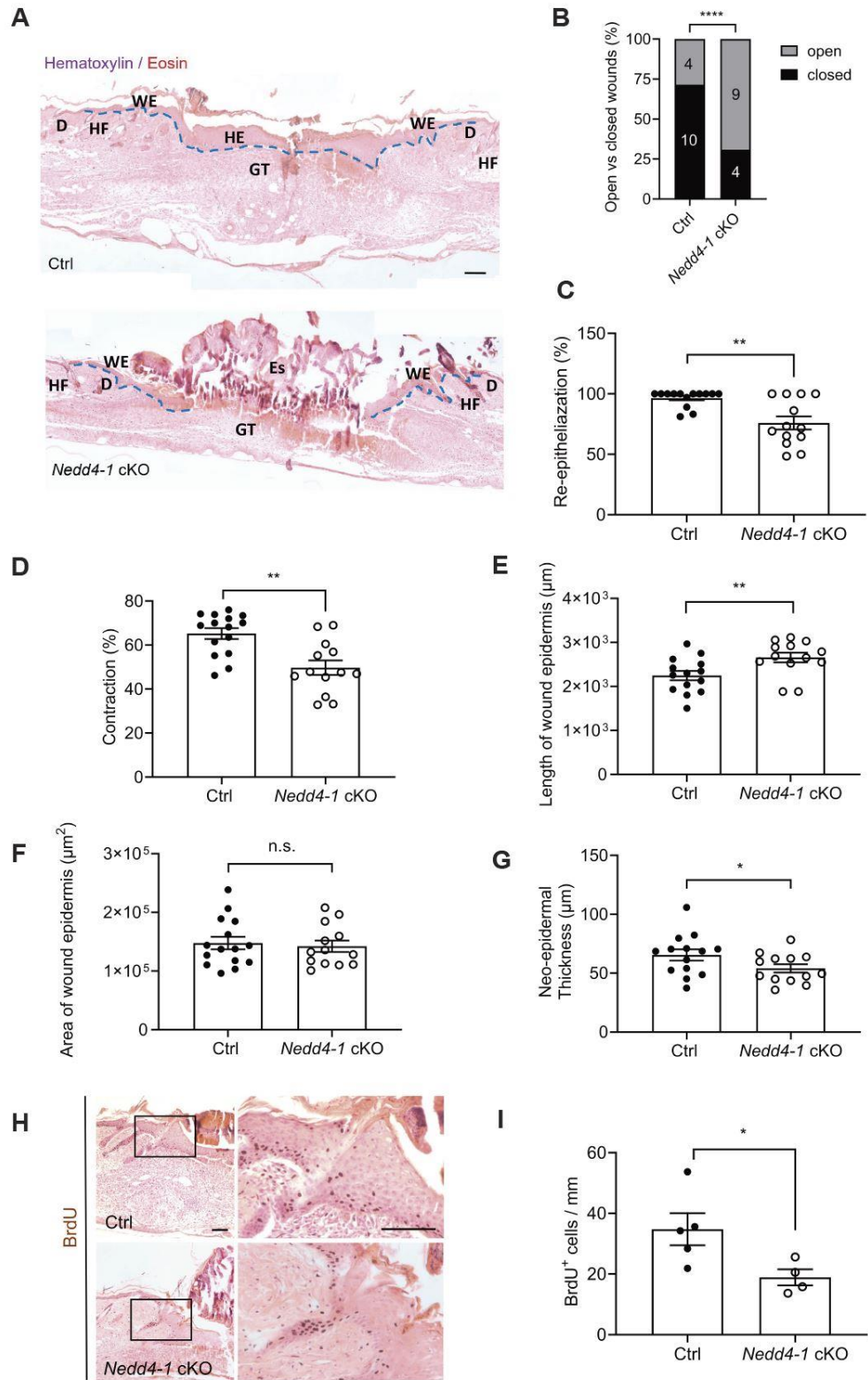


**Fig. 4 Wound closure is delayed in *Nedd4-1* cKO mice**



**(A)** Representative hematoxylin/eosin stainings of 5-day wound sections from Ctrl and *Nedd4-1* cKO mice. D: Dermis; Es: Eschar; GT: Granulation tissue; HE: Hyperproliferative wound epidermis; HF: Hair follicle; WE: Wound epithelium.

**(B)** Numbers and percentages of open and closed 5-day wounds in Ctrl and *Nedd4-1* cKO mice. N = 7-9 mice per genotype.

**(C, D)** Percentage of wound re-epithelialization **(C)** and wound contraction **(D)** in 5-day wounds of Ctrl and *Nedd4-1* cKO mice. N = 7-9 mice per genotype.

**(E-G)** Length **(E)**, area **(F)** and average thickness **(G)** of wound epidermis of 5-day wounds from Ctrl and *Nedd4-1* cKO mice. N = 7-9 mice per genotype.

**(H, I)** Representative photomicrographs of BrdU-stained sections from 5-day wounds of Ctrl and *Nedd4-1* cKO mice **(H)** and quantification of BrdU-positive keratinocytes per length of WE **(I)**. The areas indicated by black rectangles are shown at higher magnification on the right hand side. N = 4-5 mice per genotype. Scatter plots show mean  $\pm$  SEM. \*P < 0.05, \*\*P < 0.01 Mann-Whitney U test **(C, D, E, F, G, I)** and \*\*\*\*P < 0.0001 Fisher's exact test **(B)**.

Magnification bars: 100  $\mu$ m **(A, H)**.

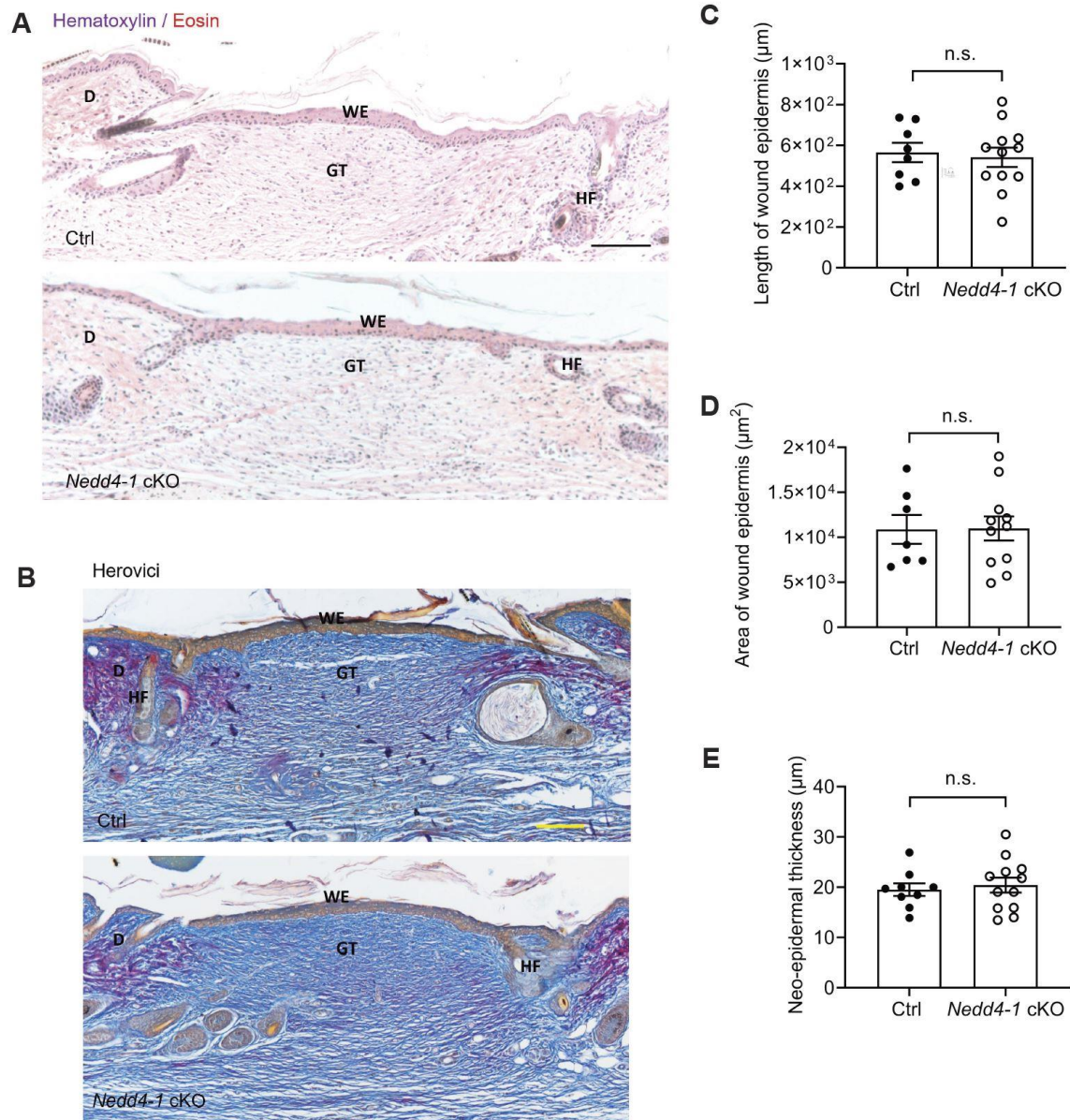


**Fig. 5 Loss of Nedd4-1 in keratinocytes does not affect scar formation**

(A) Representative hematoxylin/eosin stainings of 14-day wound sections from Ctrl and *Nedd4-1* cKO mice. D: dermis; HF: hair follicle; GT: granulation tissue; WE: wound epithelium.

(B) Representative Herovici stainings of 14-day wound sections from Ctrl and *Nedd4-1* cKO mice.

(C-E) Length (C), area (D) and average thickness (E) of wound epidermis in 14-day wounds from Ctrl and *Nedd4-1* cKO mice. N = 4-6 mice per genotype.

Scatter plots show mean  $\pm$  SEM. n.s.: non-significant (Mann-Whitney U test).

Magnification bars: 100  $\mu\text{m}$  (A, B).

## Nedd4-1 protects keratinocytes from UV-induced apoptosis

To further determine the role of Nedd4-1 in keratinocytes under stress conditions, we irradiated the mice with a physiologically relevant dose of UVB (100 mJ/cm<sup>2</sup>). Extremely few apoptotic cells were detected in non-irradiated skin of mice of both genotypes (Fig. 2C and 6A). As expected, the number of apoptotic cells increased strongly within 24h upon UVB irradiation in mice of both genotypes, but this was significantly more pronounced in *Nedd4-1* cKO mice (Fig. 6A, B). The difference was no longer visible at 72h after irradiation (Fig. 6B). There was no significant difference in the UV-induced influx of neutrophils between control and *Nedd4-1* cKO mice (Fig. 6C, D).

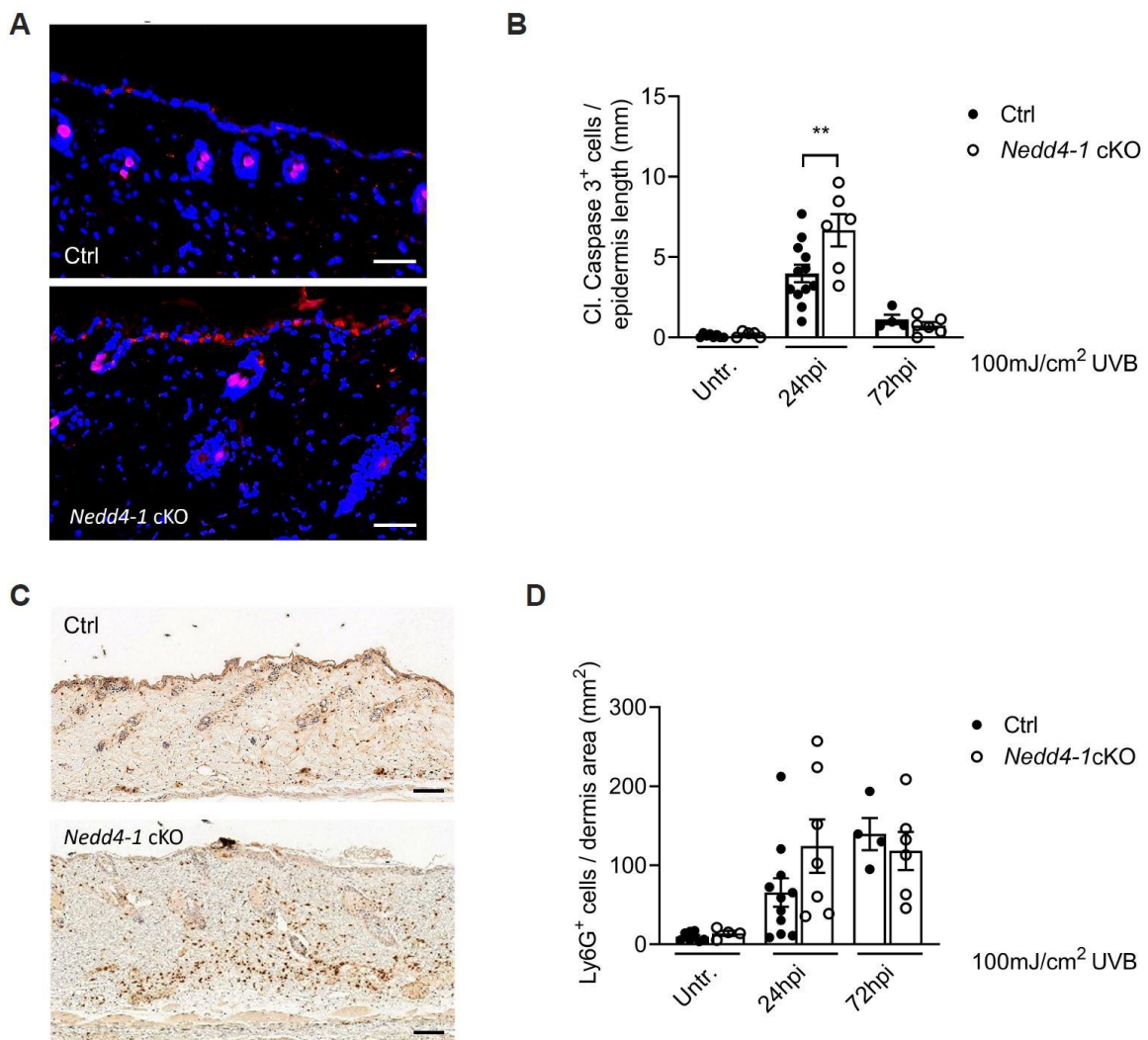


**Fig. 6 Nedd4-1 protects keratinocytes from UVB-induced apoptosis *in vivo***

(A) Cleaved caspase 3 staining and quantification of apoptotic cells per mm epidermis (B) using sections from untreated (untr.) skin or 24 h or 72 h post irradiation with 100 mJ/cm<sup>2</sup> UVB. Nuclei were counterstained with Hoechst (blue). hpi; hours post irradiation. N = 4-12 mice per genotype.

(C) Ly6G staining and quantification of neutrophils in the dermis (D) using sections from untreated (untr.) skin or 24 h or 72 hpi with 100 mJ/cm<sup>2</sup> UVB. N = 4-11 mice per genotype.

Scatter plots show mean ± SEM. Each data point represents the result from an individual mouse.

\*\*P < 0.01 (Bonferroni's multiple comparisons test).

Magnification bars: 50 μm (A) 100 μm (C).

**Knock-down of Nedd4-1 impairs proliferation and migration of keratinocytes**

To unravel the cellular mechanisms underlying the phenotype of *Nedd4-1* cKo mice, we performed siRNA-mediated knock-down experiments in primary mouse keratinocytes from wild-type mice (Fig. 7A-C). Consistent with the *in vivo* data, Nedd4-1 knock-down strongly suppressed proliferation and migration of keratinocytes as shown by BrdU incorporation (Fig. 7D) or scratch wounding (Fig. 7E), respectively. We also generated immortalized murine keratinocyte cell lines with stable shRNA-mediated knockdown of Nedd4-1. Efficient knock-down of this protein (Fig. S5A) did not influence the cell morphology and viability of keratinocytes (Fig. S5B, C). However, it significantly reduced the proliferation rate of two different cell lines (Fig. S5D), and also the migratory capacity as shown in circular wound closure and chemotactic transwell migration assays (Fig. S5E, F).

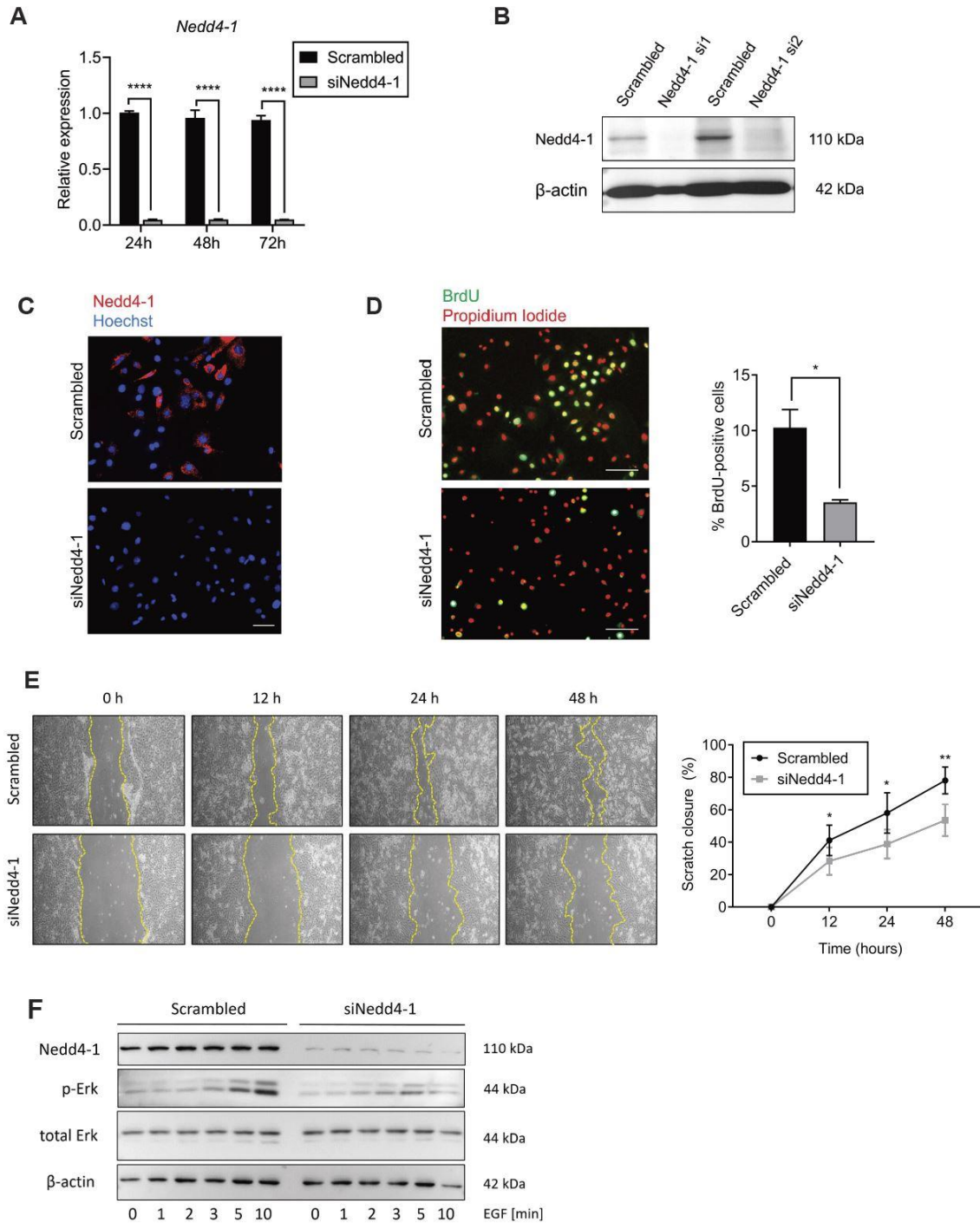


**Fig. 7 Transient knock-down of Nedd4-1 inhibits keratinocyte proliferation, migration and EGF-induced Erk1/2 activation *in vitro***

(A) qRT-PCR analysis for *Nedd4-1* relative to *Rps29* using RNA samples from primary murine keratinocytes transfected with two different *Nedd4-1* siRNAs (si1 and si2) or scrambled siRNA and harvested 24h, 48h or 72h after transfection. N = 3 for each siRNA using cells from 3 different mice.

(B) Western blot analysis of lysates from primary murine keratinocytes transduced with *Nedd4-1* or scrambled siRNAs for *Nedd4-1* and  $\beta$ -actin (loading control).

(C) Representative photomicrographs of Nedd4-1 immunofluorescence staining of keratinocytes transfected with Nedd4-1 or scrambled siRNAs (red). Nuclei were counterstained with Hoechst (blue).

(D) Representative photomicrographs of BrdU-stained primary murine keratinocytes (green) transfected with Nedd4-1 or scrambled siRNAs. Nuclei were counterstained with propidium iodide (red). Quantification of BrdU-positive keratinocytes is shown in the graph. N = 3 for each siRNA using cells from 3 different mice.

(E) Representative photomicrographs of scratch wounded primary murine keratinocytes transfected with Nedd4-1 or scrambled siRNAs and treated with mitomycin C to inhibit cell proliferation. The open area devoid of cells was measured immediately after (0h) and 12h, 24h, and 48h post scratch wounding. Quantification of the percentage of wound closure at the indicated time points is shown in the N = 3 for each siRNA using cells from 2 different mice.

(F) Growth factor-starved primary keratinocytes were treated with epidermal growth factor (EGF) (10 ng/ml) for 0, 1, 2, 3, 5 and 10 min. Cell lysates were analyzed by Western blot for Nedd4-1 and total and phosphorylated Erk1/2.  $\beta$ -actin was used as an additional loading control.

Bar graphs show mean  $\pm$  SEM. \*P < 0.05, \*\*P < 0.01, \*\*\*\*P < 0.0001 (Student's t-test).

Magnification bars: 100 $\mu$ m.



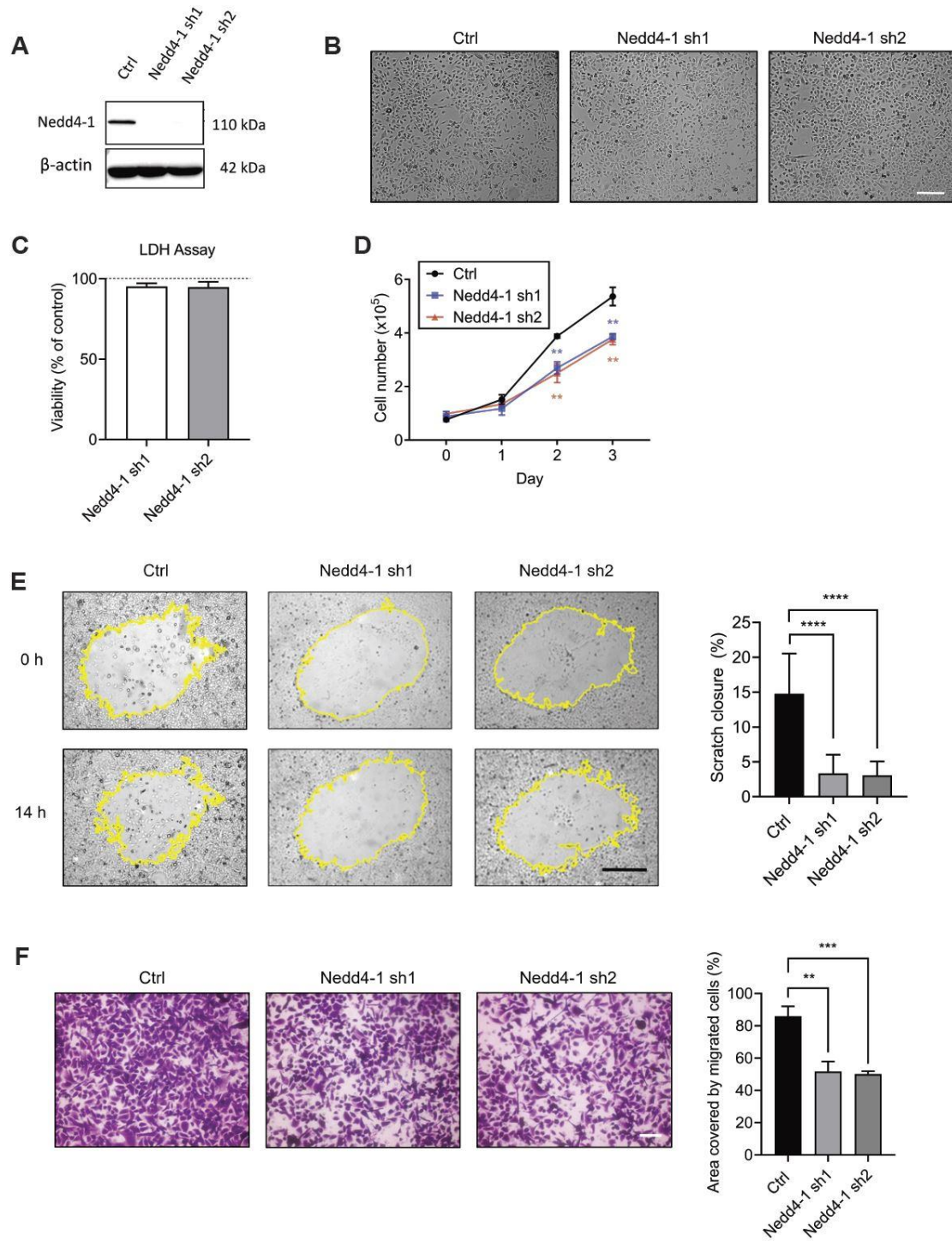


**Fig. S5 Long-term knock-down of Nedd4-1 inhibits keratinocyte proliferation and migration**

(A) Western blot analysis for Nedd4-1 and  $\beta$ -actin (loading control) using lysates of immortalized murine keratinocytes transduced with lentiviruses expressing two different Nedd4-1 shRNAs (sh1 and sh2) or cells transduced with a viral vector expressing ctrl shRNA (Ctrl).

(B) Morphology of Ctrl and Nedd4-1 knock-down keratinocytes under normal culture conditions.

(C) Keratinocyte cell lines with Nedd4-1 knock-down were cultured under normal conditions. The media were analyzed for LDH levels in the supernatant using an LDH cytotoxicity assay. Results are presented as % viability relative to control cells. N = 6 dishes from each cell line.

(D) The total number of Nedd4-1 knock-down and control keratinocytes was counted every 24h after seeding in 12-well-plates under normal culture conditions. N = 3 dishes from each cell line.

(E) Cell migration was determined using a circular wound closure assay. Representative images (left) and quantification of the area covered by migrated cells (scratch closure, right) are shown. N= 8-10 dishes from each cell line.

(F) Cell migration was determined using Millipore transwell chambers. Representative images (left) and quantification of the area covered by migrated cells (right) are shown. N=3 dishes from each cell line.

Bar graphs show mean $\pm$  SEM. \*\*P<0.01; \*\*\*P<0.001, \*\*\*\*P<0.0001 (Student's t-test). Magnification bars: 200  $\mu$ m (B), 500  $\mu$ m (E) and 100  $\mu$ m (F).

### **Mechanism of action of Nedd4-1 in keratinocytes**

We previously showed for hepatocytes that Nedd4-1 is required for efficient internalization of the epidermal growth factor receptor (EGFR) and subsequent activation of Erk1/2 signaling [50]. Since the EGFR-Erk1/2 pathway also controls proliferation, migration and survival of keratinocytes [161, 162], we treated starved keratinocytes with EGF. Indeed, knock-down of Nedd4-1 reduced the extent and duration of EGF-induced Erk1/2 activation (Fig. 7F). This finding suggests that the effect of Nedd4-1 on keratinocyte proliferation may be in part mediated by impaired EGF-induced activation of the Erk signaling pathway.



## Discussion

We identified the ubiquitin ligase Nedd4-1 as a novel player in skin homeostasis, wound repair and UV-response of the skin. This activity involves important cell autonomous functions of Nedd4-1 in keratinocytes, including regulation of proliferation and migration as well as survival after UV irradiation as demonstrated in *in vitro* studies.

Proliferation of keratinocytes was strongly reduced in the skin of *Nedd4-1* cKO mice *in vivo*, resulting in a reduction of epidermal thickness. Furthermore, we detected a defect in terminal differentiation and epidermal barrier function in these mice as revealed by the strongly reduced expression of the cornified envelope protein loricrin and the enhanced transepidermal water loss. It is as yet unclear if Nedd4-1 directly regulates the differentiation process or if the reduced loricrin expression is a consequence of other abnormalities, including the defect in proliferation. A possible direct effect on this process is supported by the strong expression NEDD4-1 in keratinocytes of the granular layer in human skin. The impairment of the epidermal barrier in *Nedd4-1* cKO mice may provide an explanation for their underrepresentation in the litters. Thus, it is possible that some mice have a very pronounced barrier defect, which results in desiccation and perinatal death as seen in other mutant mice with barrier defects, e.g. those lacking receptor-interacting protein kinase 4 [163]. In the future, this should be determined by analysis of the inside-out and outside-in barrier of the mice at a late embryonic stage.

The most striking abnormality that we observed in this study was the strong delay in wound healing of the surviving *Nedd4-1* cKO mice. This was mainly a consequence of delayed re-epithelialization due to impaired proliferation and migration of wound keratinocytes. It remains to be determined if the loss of Nedd4-1 in keratinocytes also increases the number of apoptotic cells in the wound epidermis. This is possible, since UVB-induced keratinocyte apoptosis was significantly increased in *Nedd4-1* cKO mice, demonstrating that Nedd4-1 is also important for keratinocyte survival under stress conditions.

Although we only deleted Nedd4-1 in keratinocytes, the rate of wound contraction was also significantly reduced. This process is mainly achieved by fibroblasts/myofibroblasts of the granulation tissue, which are not targeted by the K5-Cre transgene. Since wound

keratinocytes are major producers of various growth factors involved in fibroblast proliferation and differentiation, such as platelet-derived growth factor and transforming growth factor  $\beta$  [164], the reduced number of keratinocytes in the wounds of *Nedd4-1* cKO mice may result in reduced levels of paracrine-acting growth factors and cytokines. Alternatively, *Nedd4-1* may directly regulate the production of such factors in keratinocytes through as yet unknown mechanisms. In the future, it should be determined if and how the loss of *Nedd4-1* affects cells in the granulation tissue. Our preliminary data suggest that wound angiogenesis is not affected in the mutant mice, but an effect on fibroblasts and/or immune cells can as yet not be excluded.

In spite of the delay in wound closure, wounds in *Nedd4-1* cKO mice finally healed, demonstrating that this protein is important, but not essential for wound re-epithelialization. This is different to the liver, where knock-down of *Nedd4-1* in hepatocytes caused liver failure after partial hepatectomy as a consequence of liver necrosis and impaired hepatocyte proliferation [50]. It is possible that other ubiquitin ligases, e.g. the related *Nedd4-2*, compensate for the loss of *Nedd4-1* in keratinocytes, but not or only to a minor extent in hepatocytes.

A potential mechanism underlying the effect of *Nedd4-1* on keratinocyte proliferation, migration, and survival, is the impairment of EGF-induced Erk1/2 signaling. It was shown in other cell types that *Nedd4-1* ubiquitinates the adaptor protein Eps15, resulting in EGF receptor internalization [135]. In hepatocytes, a defect in this process as a consequence of *Nedd4-1* deficiency caused reduced and more transient Erk1/2 signaling in response to major mitogens, which negatively influenced proliferation and survival [50]. Indeed, EGF-induced Erk1/2 activation was also less pronounced and more transient in *Nedd4-1*-deficient keratinocytes (this study). This is of likely importance, since (i) EGFR-Erk1/2 signaling promotes keratinocyte proliferation, migration and survival after UV irradiation [165-167] and (ii) ligands of the EGFR promote wound re-epithelialization [164]. However, additional *Nedd4-1* targets are probably involved in the wound healing promoting activity of *Nedd4-1*, which remain to be determined.

In addition to keratinocytes, *Nedd4-1* is also expressed in various cells of the dermis and granulation tissue, in particular in fibroblasts. This is most likely important for the wound

healing process, since loss of this protein strongly reduced proliferation of embryonic fibroblasts [121]. Thus, Nedd4-1 seems to be a global regulator of wound healing through its activities in different skin cells. In the future it will be interesting to determine if NEDD4-1 expression is reduced in chronic, non-healing skin wounds and if strategies to promote its expression and/or activity can be used for therapeutic purposes.

## **Materials and Methods**

### **Mouse lines and genotyping**

Mice expressing Cre recombinase under control of keratin 5 promoter (K5-Cre mice) [147] were mated with mice harboring floxed alleles of the *Nedd4-1* gene [146]. All mice were in C57BL/6 genetic background.

For genotyping, DNA was extracted from toe biopsies and amplified by PCR using the KAPA2G FAST Genotyping Mix (Kapa Biosystems, Wilmington, MA) and the primers shown in Supplementary Table S1.

Mice were housed under specific pathogen-free (SPF) conditions and maintained according to Swiss animal protection guidelines. All animal experiments had been approved by the local veterinary authorities (Kantonales Veterinärämte Zürich, Switzerland).

### **Human Skin Samples**

Human skin samples (basal cell carcinomas and adjacent non-tumorigenic skin) were obtained anonymously from the Department of Dermatology, University Hospital Zurich in the context of the biobank project. Use of the samples was approved by the local and cantonal Research Ethics Committees. Informed consent for research was obtained before routine diagnostic services.

### **Wound Healing Experiments**

Female mice at 10 weeks of age were anesthetized by intraperitoneal injection of ketamine/xylazine (100 mg ketamine / 5-10 mg xylazine per kg body weight). After shaving, four full-thickness excisional wounds (5 mm diameter) were generated using a biopsy punch, two wounds on each side of the dorsal midline. Mice were allowed to heal without dressing and sacrificed by CO<sub>2</sub> inhalation followed by decapitation. Wounds were excised and processed for further analysis.

### **UVB Irradiation of Mice**

8 to 11-week-old mice were irradiated with 100 mJ/cm<sup>2</sup> UVB as previously described [168] and sacrificed at different time points after UV irradiation. Back skin samples were excised and processed for further analysis.

### **Analysis of Transepidermal Water Loss (TEWL)**

Mouse back skin was shaved one day before analysis. TEWL was determined using a Tewameter (Courage and Khazaka Electronic GmbH, Cologne, Germany). The probe was placed on the dorsal back skin of shaved mice, and 30-50 consecutive measurements were performed on two different places on the back.

### **Separation of Dermis and Epidermis**

Mice were sacrificed, shaved, and epidermis from back skin was separated from the dermis after heat shock treatment (30 s at 60°C in PBS, followed by 1 min at 4°C in PBS). Isolated epidermis and dermis were immediately frozen in liquid nitrogen and used for RNA isolation.

### **BrdU Incorporation Assay**

Mice were injected intraperitoneally with BrdU (250 mg/kg in 0.9% NaCl; Sigma, Munich, Germany) and sacrificed 2 h after injection. Skin sections were analyzed by immunofluorescence staining (see above) using a FITC-coupled BrdU antibody (#11202693001, Sigma) as previously described [169].

For *in vitro* studies, BrdU was added to the cell culture medium at a final concentration of 10 μM, and cells were incubated for 2 h at 37°C and 5% CO<sub>2</sub>. After washing with PBS they were fixed for 10 min at room temperature with 4% paraformaldehyde (PFA). Cells were then permeabilized using 0.1% Triton-X 100 in PBS, followed by incubation with 2M HCl for 30 min. The HCl solution was removed and cells were incubated with boric buffer (100 mM boric acid, 75 mM NaCl, 25 mM sodium tetraborate, pH 8.5) for 5 min. Blocking was performed using 1% BSA for 10 min, followed by incubation with the FITC-coupled BrdU antibody at 4°C overnight. Cells were counterstained using propidium iodide (#P4170, Sigma).

## **Histology and Histomorphometry**

Tissue samples were fixed in 4% phosphate buffered PFA or 95% ethanol/1% acetic acid for 24 h at 4°C, processed, and embedded in paraffin. Alternatively, they were immediately frozen in tissue freezing medium® (Leica Biosystems, Wetzlar, Germany). Tissue blocks were sectioned (7 µm) and subjected to hematoxylin/eosin or Masson Trichrome staining.

## **Immunofluorescence and Immunohistochemistry**

Tissue sections were deparaffinized and rehydrated, or fixed with cold methanol (in case of frozen sections). Non-specific binding sites were blocked with PBS/12% BSA/0.025% NP-40 for 1 h at room temperature, and sections were then incubated overnight at 4 °C with the primary antibodies (Supplementary Table S2) diluted in the same buffer. If needed, antigen retrieval was performed prior to the blocking procedure by cooking in citrate buffer (1 h at 95 °C). After three washes with PBST (1× PBS/0.1% Triton-X100), slides were incubated for 1 h with secondary antibodies and Hoechst 33342 (B2261, Sigma), washed with PBST and mounted with Vectashield mounting medium (Vector Laboratories, Burlingame, CA). All secondary antibodies were from Jackson ImmunoResearch (West Grove, PA).

Cultured cells were fixed for 10 min with cold 4% PFA, washed twice with PBS, and treated as described above for tissue sections. They were mounted with Mowiol (Hoechst, Frankfurt, Germany).

## **RNA Isolation and qRT–PCR Analysis**

RNA was isolated from cultured cells using the RNeasy Kit (74106, Qiagen, Hilden, Germany) according to the manufacturer's instructions and reverse transcribed using the iScript™ cDNA synthesis kit (# 1708890, BioRad, Hercules, CA). Quantitative PCR was performed using the LightCycler® 480 SYBR Green I Master reaction mix (04707516001, Roche, Rotkreuz, Switzerland) as previously described [169]. Data were quantified using second derivative maximum analysis and normalized to the expression levels of the housekeeping gene *Rps29*. Primers used for qRT PCR are listed in Supplementary Table S3.

### **Preparation of Protein Lysates and Western Blot Analysis**

Cells were trypsinized, centrifuged and lysed in RIPA lysis buffer containing Complete Protease Inhibitor Cocktail (#11836170001, Roche) and PhosSTOP Phosphatase Inhibitor Cocktail, Roche). Frozen tissue was homogenized in T-PER tissue protein extraction reagent (#78510, ThermoFisher Scientific, Waltham, MA) using the same inhibitor cocktails. Lysates were cleared by sonication and centrifugation, snap frozen, and stored at -80°C. The protein concentration was determined using the BCA Protein assay (#23225, ThermoFisher Scientific). Proteins were separated by SDS-PAGE and transferred onto nitrocellulose membranes. Antibodies are listed in Supplementary Table S2 and used according to the manufacturer's instructions. Corresponding secondary antibodies were coupled to horseradish peroxidase (HRP) and the signal was visualized using WesternBright ECL HRP substrate (K-12045-D50, Witec AG, Sursee, Switzerland) and detected using the Fusion Solo S imaging system (Vilber Lourmat, Eberhardzell, Germany). Bands were quantified using ImageJ software (National Institutes of Health, Bethesda, MD).

### **Isolation and Culture of Primary Epidermal Keratinocytes**

Isolation and cultivation of murine primary keratinocytes from 2-4 day-old mice was performed as previously described [170]. Cells were seeded at a density of  $5 \times 10^4$  cells per  $\text{cm}^2$  on collagen IV ( $2.5 \text{ g/cm}^2$ )-coated dishes and incubated for 30 min at 37 °C/5%  $\text{CO}_2$ . Thereafter the medium was replaced, and cells were grown to 90% confluency in defined keratinocyte serum-free medium (Invitrogen, Paisley, UK) supplemented with 10 ng/ml EGF (Sigma) and  $10^{-10}$  M cholera toxin (Sigma). Cells were used for experiments at passage 2-4. Spontaneously immortalized mouse keratinocytes were obtained by serial passaging of the primary cells. Absence of mycoplasma was confirmed for all cell cultures by PCR using the PCR Mycoplasma Test Kit I/C (PK-CA91-1096, PromoKine, Heidelberg, Germany).

### **Lentiviral Transduction of Cultured Cells**

Cells were cultured in 6 cm culture dishes and transduced at 30-50 % confluency. 4 ml virus-containing medium was mixed with 1 ml fresh culture medium and polybrene (final concentration 8 µg/ml) and subsequently filtered through a 0.45 µm syringe filter to remove cellular debris and particles. The culture medium was removed, and 4 ml of the filtered virus-containing medium was added dropwise to the cells. After overnight incubation, the virus-containing medium was replaced by fresh culture medium. Forty-eight hours later, cells transduced with viruses containing the pLKO.1 vector [151] were selected for 2 weeks with 2 µg/ ml puromycin (Sigma). The shRNAs used are listed in Supplementary Table S4.

### **siRNA-Mediated Knockdown**

Skin cells were transfected with siRNAs (Axolabs, Kulmbach, Germany) using Lipofectamine RNAiMAX (# 13778150, ThermoFisher Scientific) according to the manufacturer's instructions. Experiments were performed 48h after siRNA transfection. The siRNA duplexes used are listed in Supplementary Table S5.

### **Growth Factor Treatment**

Cells were cultured as described above. After centrifugation, the pellet was washed with isolation medium before plating the cells on 6-well dishes at a density of  $3.6 \times 10^5$  cells/well. Cells were left to adhere for 3h. After overnight starvation, 10ng/ml murine EGF (315-09, PeproTech, Rocky Hill, NJ) was added, and cells were lysed at different time points after EGF addition and analyzed by western blotting.

### ***In Vitro* Cell Migration Assays**

Cells were grown to 100% confluency in culture medium and treated with 10 µg/ml mitomycin C (Sigma) for 2 h. A scratch was made in the confluent cell layer of each well using a sterile 200 µl pipette tip. Dead cells and debris were removed by washing with pre-warmed PBS, followed by addition of fresh pre-warmed culture medium. Alternatively, cells were seeded into 24-well plates and a circular wound was introduced with a 200 µl pipette tip (without filter) mounted on a vacuum pump. The pipette tip was moved perpendicularly on top of the cell monolayer, and the vacuum pump was applied for 5 sec.



Subsequently, the medium of was replaced with serum-containing medium. Pictures were acquired with an Axiovert 200 inverted microscope (Carl Zeiss AG, Oberkochen, Germany; bright field, 10x magnification) at different time points. Wound closure was determined using ImageJ software with the MRI wound healing tool plugin.

### **Transwell Migration Assay**

Cells were cultured in 6 cm culture dishes until 80-90% confluency in keratinocyte growth medium and then incubated in starvation medium for 24 h. They were trypsinized, centrifuged, counted with a hemocytometer, and resuspended in starvation medium at a final concentration of  $4 \times 10^5$  cells/ml. 250  $\mu$ l cell suspension was added into a transwell plate (6.5 mm Transwell® chambers with 8.0  $\mu$ m pore polycarbonate membrane inserts (Corning, New York, NY; 105 cells/well). After 1 h of incubation the inserts were transferred into 24-well plates with 650  $\mu$ l serum-containing culture medium per well. Cells were incubated for several hours, washed twice with PBS, and fixed with cold 100% methanol for 15 min at room temperature. Cell layers were covered with 0.5 % crystal violet solution 36 (500 mg crystal violet, 25 ml methanol, 75 ml H<sub>2</sub>O) for 10 min and washed twice with PBS. Cells on the upper layer were removed with cotton swabs. The transwell inserts were allowed to dry for 2 h, and the dried membranes were removed with a scalpel blade. The cell-free side of the membrane was placed onto a microscope slide and the cell-containing side was mounted with Mowiol (Sigma). Images of the migrated cells were taken with an Axioskop 2 inverted light microscope (Carl ZeissAG) at 20x magnification. The areas covered by cells on the transwell membrane were measured using ImageJ software with the colour deconvolution plugin.

### **Statistical Analysis**

Statistical analysis was performed using the GraphPad Prism 8 software (GraphPad Software Inc, San Diego, CA). Quantitative data are expressed as mean  $\pm$  SEM. Testing for statistically significant differences between two experimental groups was performed using Student's t-test or non-parametric Mann-Whitney U test for two-tailed, unpaired comparison at a confidence level starting at 95% ( $p < 0.05$ ) or using Fisher's exact test. \* $P < 0.05$ , \*\* $P < 0.01$ , and \*\*\* $P < 0.001$ ; \*\*\*\* $P < 0.001$ .

**Supplementary Table S1: Primers used for Genotyping**

	Forward sequence 5'→3'	Reverse sequence 5'→3'
<i>Nedd4-1</i> floxed	GTACATTTTAGTTCATGG TTCTCACAGG	CAGAGGTCACATGGCTGTGGG
<i>K5-Cre</i>	AACATGCTTCATCGTCGG	TTCGGATCATCAGCTACACC

**Supplementary Table S2: Antibodies**

Antibody	Source	Catalog No.
Anti-β-Actin	Sigma	#A5316
Anti-GAPDH	HyTest, Turki Finland	#5G4
Anti-Nedd4	BD Biosciences, Franklin Lakes, NJ	#611480
Anti-Nedd4	Abcam, Cambridge, UK	#ab27979
Anti-pErk1/2	Cell Signaling, Danvers, MA	#9101S
Anti-total Erk1/2	Cell Signaling	#9102S
Rabbit anti-keratin 6A	BioLegend, San Diego, Ca	#PRB-169P
Mouse anti-keratin 10	DAKO, Glostrup, Denmark	#M7002
Rabbit anti-keratin 14	BABco, Covance, CA	#PRB-155P
Mouse anti-keratin 15	Invitrogen	#MA1-90929
Rabbit anti-loricrin	BABco	#PRB-145P
Anti-rabbit Cy3	Jackson ImmunoResearch	#111-065-003
Anti-mouse Cy3	Jackson ImmunoResearch	#711-165-152
Anti-rabbit Cy2	Jackson ImmunoResearch	#715-165-150
Anti-mouse Cy2	Jackson ImmunoResearch	#115-225-003
Normal rabbit IgG	Sigma	#12-370
Anti-mouse IgG HRP conjugate	Promega, Fitchburg, MA	#W402B
Anti-rabbit IgG HRP conjugate	Promega	#W4011
Anti-rabbit Alexa Fluor® 647	Abcam	#ab150079
Anti-BrdU-FITC	Sigma	#11202693001
Rat-anti-mouse-Ly6G	Abcam	#Ab2557
Rabbit anti-rat-Biotinylated	Vector Laboratories	#BA-4001
Donkey-anti-rat Cy3	Jackson ImmunoResearch	#712-165-150
Rabbit-anti-mouse Cleaved Caspase 3	Cell Signaling	#9661
Anti-Ki67	Abcam	#Ab15580

**Supplementary Table S3. Primers used for qRT-PCR**

Target gene	Forward sequence 5'→3'	Reverse sequence 5'→3'
<i>Nedd4-1</i>	CACACACCTGCTTCAATCGC	GGGAAGAGCCAGTGACCATC
<i>Rps29</i>	GGTCACCAGCAGCTCTAGTG	GTCCAACCTAATGAAGCCTATGTCC

**Supplementary Table S4. shRNA sequences**

	Mature antisense 5'→3'
Nedd4-1 shRNA 1	AATCCTCCAGAATGTTTGCGC
Nedd4-1 shRNA 2	ATTCATGGTTTACGTAGTAGG

**Supplementary Table S5. siRNA sequences**

	Forward sequence 5'→3'	Reverse sequence 5'→3'
Nedd4-1 siRNA 1	acAGAUuAAGcGAuuuucudTsdT	AGAAAUUCGCUuAAUCUGUdTsdT
Nedd4-1 siRNA 2	gacAccGcAuucuuuuucGAdTsdT	UCGAAAAGAAUGCGGUGUCdTsdT
Scrambled siRNA	AGGuAGuGuAAucGccuuGdTsdT	cAAGGcGAuuAcAcuAccudTsdT

## **Acknowledgements**

We thank Drs. Michael Meyer and Paul Hiebert, ETH Zurich, for invaluable experimental help, Drs. Angel Ramirez and José Jorcano, CIEMAT, Madrid, Spain, for the K5-Cre mice and Dr. Gaetana Restivo, University Hospital Zurich, for the human skin samples. This work was supported by the Swiss National Science Foundation (310030\_132884 and 31003A-169204/1 to S.W) and a Chinese Government Predoctoral Fellowship (to S.Y.)

## **Author Contributions:**

S.Y., R. R. and M. B-G. performed experiments and analyzed the data.

H. K. provided floxed *Nedd4-1* mice.

S. Y. wrote the manuscript together with S.W.

S.W. designed and supervised the study, wrote the manuscript together with S.Y. and provided the funding.

All authors made important suggestions to the manuscript.

## **Disclosure:**

The authors confirm that there are no conflicts of interest.

## 4.2 Nedd4-1 is a key regulator of fibroblast function *in vitro* and during mouse development

Shen Yan<sup>1</sup>, Raphael Ripamonti<sup>1</sup>, Peter Angel<sup>2</sup>, Hiroshi Kawabe<sup>3</sup>, Michael  
Cangkrama<sup>1</sup> and Sabine Werner<sup>1\*</sup>

<sup>1</sup>Institute of Molecular Health Sciences, Department of Biology, Swiss Federal Institute of Technology (ETH) Zurich, 8093 Zurich, Switzerland

<sup>2</sup>German Cancer Research Institute, Department of Signal Transduction and Growth Control, 69120 Heidelberg, Germany

<sup>3</sup>Max-Planck-Institute of Experimental Medicine, Department of Molecular Neurobiology, 37075 Göttingen, Germany

\*Correspondence to [sabine.werner@biol.ethz.ch](mailto:sabine.werner@biol.ethz.ch)

Running title: Nedd4-1 in fibroblasts

Manuscript in preparation

Own contribution:

- Generation of mesenchymal cell-specific conditional *Nedd4-1* knockout mouse line (breedings, weaning, biopsy taking, genotyping, regular observation and macroscopic analysis)
- Timed pregnancy experiments (matings, macroscopic analysis of embryos, embryo sample collection, tissue processing, sectioning, stainings, microscopy data acquisition, evaluation of stainings)
- Characterization of normal back skin of embryos (sample collection, tissue processing, sectioning, stainings, microscopy data acquisition, evaluation of stainings)
- Histological analysis of organs from late embryos and newborn mice (sample collection, tissue processing, sectioning, staining, microscopy data acquisition, evaluation of stainings)
- Analysis of back skin of newborn pups (sample collection, tissue processing, sectioning, stainings, microscopy data acquisition, evaluation of stainings, RNA extraction and subsequent quantitative real-time RT-PCR analysis)
- Loss-of-function studies of *Nedd4-1* in fibroblasts using siRNA (analysis of knock-down efficiency, RNA extraction and subsequent quantitative real-time RT-PCR analysis, protein lysate preparation and subsequent Western blot analysis, analysis of proliferation, migration, and collagen gel contraction)
- Loss-of-function and gain-of-function studies of *Nedd4-1* in fibroblasts using shRNA (generation of stable knock-down keratinocyte cell lines, analysis of knock-down efficiency, RNA extraction and subsequent quantitative real-time RT-PCR analysis, protein lysate preparation and subsequent Western blot analysis, analysis of cell proliferation and migration) (together with my Master student Raphael Ripamonti)
- Analysis of EGF-induced Erk1/2 activation
- Preliminary studies to determine a potential role of *Nedd4-1* in cancer-associated fibroblasts (not included in thesis chapter)
- Experimental design together with S.W.
- Design of the figures and writing of the manuscript together with S.W.

## **Abstract**

Nedd4-1 is an evolutionarily highly conserved and ubiquitously expressed HECT E3 ubiquitin ligase with reported functions in organ development, tissue repair and cancer. However, the cell type-specific functions of Nedd4-1 in these processes remain to be identified. Here we show severe growth retardation as well as defects in various organs of late embryos and newborn mice lacking Nedd4-1 in mesenchymal cells, which cause early postnatal lethality. Bone and lung abnormalities were particularly pronounced in the mutant mice. Their skin showed a strongly reduced dermal cellularity and concomitantly impaired keratinocyte differentiation, resulting in a hyperthickened cornified layer. Mechanistically, the developmental defects are likely to result from reduced proliferation and migration of Nedd4-1-deficient fibroblasts as revealed by knock-down studies in cultured cells. These results identify cell-autonomous and non-cell-autonomous functions of Nedd4-1 in mesenchymal cells during organ development.

## Introduction

Ubiquitination of proteins plays a key role in the control of various cellular signaling pathways. It is an energy-dependent process, which involves the covalent attachment and sequential transfer of activated ubiquitin to different proteins, resulting in their mono-, multi-mono- or poly-ubiquitination [94]. The specificity of the ubiquitination process is mainly determined by the final step in this pathway, the transfer of ubiquitin to the target protein, which is achieved by ubiquitin ligases (E3). These enzymes include three subfamilies, the HECT, RING and RBR E3 ligases. In spite of the increasing knowledge on these enzymes and their mechanisms of action, the functions of most E3 ligases in organ development, repair and disease are still poorly understood. This is also the case for the Nedd4 subfamily of HECT E3 ligases.

NEDD4-1 is the founding member of this family, which in total includes nine proteins. The *Nedd4-1* gene was first cloned from mouse embryos in 1992 [114]. "Nedd" stands for "Neural precursor cell expressed developmentally down-regulated", which obtained its name from the down-regulated expression in the murine central nervous system during development [114]. It is an evolutionarily highly conserved protein and ubiquitously expressed in mammalian tissues. Mice with a global *Nedd4-1* knockout showed neonatal lethality, accompanied by delayed embryonic development, reduced body weight and growth [121]. Embryonic fibroblasts isolated from these mice had an impaired mitogenic activity [121], but it is unclear if and to what extent the knockout in fibroblasts or other cell types contributes to the severe developmental defects of these mice. Another independently generated *Nedd4-1* knockout mouse line exhibited embryonic lethality, and the embryos had severe vascular malformations and impaired development of the dendrites and the heart [120]. On the other hand, overexpression of NEDD4-1 occurs in different types of cancer and other human diseases [127, 171]. A genome-wide association study showed that a single nucleotide polymorphism in the *NEDD4-1* gene is associated with keloid scars. A possible role of Nedd4-1 in the pathogenesis of these benign fibrotic skin tumors has been reported [144, 172], but its function in skin fibroblasts is still largely unknown. Therefore, we generated mice lacking Nedd4-1 in mesenchymal cells and established cultured fibroblasts with Nedd4-1 knock-down. Analysis of the Nedd4-1-deficient mice and cells revealed a crucial role of this protein in the control of



fibroblast proliferation and migration *in vitro* and a key function in mesenchymal cells during embryonic development.

## Results

### **Severe developmental defects and early postnatal lethality in mice lacking Nedd4-1 in mesenchymal cells**

We previously identified Nedd4-1 in keratinocytes as a key regulator of epidermal homeostasis and wound repair. These studies also revealed that *Nedd4-1* is expressed at even higher levels in dermal fibroblasts compared to epidermal keratinocytes, and fibroblasts in murine skin strongly expressed this protein (Yan et al., in preparation). This is consistent with previously published single cell RNA-sequencing data from embryonic day 14.5 (E14.5) mouse skin, which showed strong expression of *Nedd4-1* in dermal fibroblasts at this stage [158].

To unravel the function of *Nedd4-1* in fibroblasts *in vivo*, we generated mice with a mesenchyme-specific knockout of this gene by mating mice expressing Cre recombinase under control of the collagen 1 alpha 2 promoter (*Col1a2-Cre*) mice [148] with mice harboring floxed *Nedd4-1* alleles [146] (Supplementary Fig. S1A and B). Based on the activity of the *Col1a2* promoter, this should result in a loss of Nedd4-1 in cells of mesenchymal origin, including fibroblasts of different organs. PCR genotyping results are shown in Supplementary Fig. S1C. The efficient knockout of Nedd4-1 in the dermis of newborn mice was demonstrated by qRT-PCR. Furthermore, immunofluorescence staining of back skin from adult mice confirmed the loss of Nedd4-1 in dermal cells of the homozygous knockout mice (*fl/fl;Cre*), while the epidermis was still strongly positive (Supplementary Fig. S1D and E).

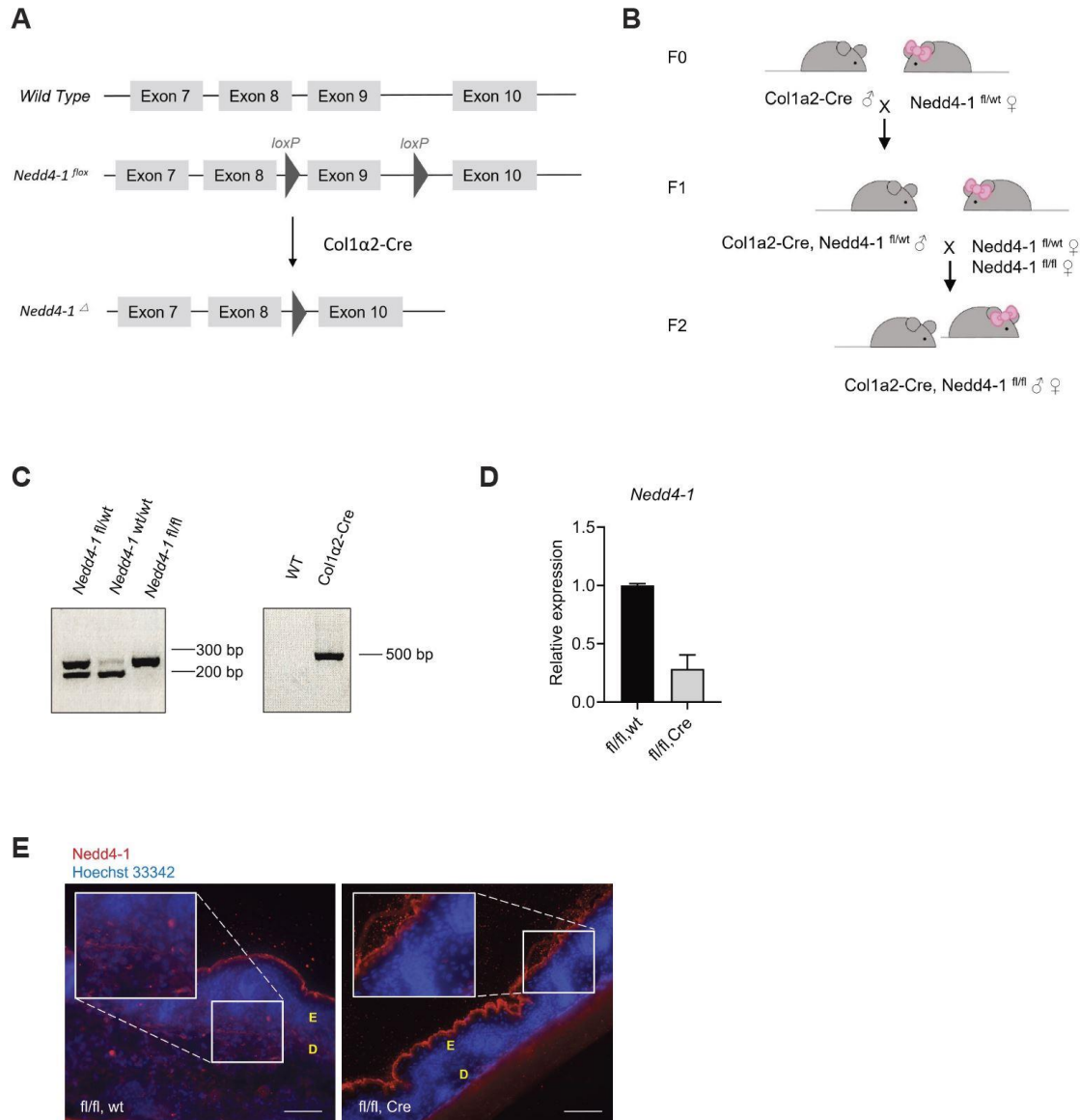


**Fig. S1 Generation of Col1a2Cre-Nedd4-1 mice**

(A,B) Schematic representation of the *Nedd4-1* targeting strategy (A) [146], and breeding scheme (B) for the generation of mice lacking *Nedd4-1* in mesenchymal cells.

(C) Genotyping PCR of DNA from WT (wt/wt), heterozygous (fl/wt), and homozygous (fl/fl) conditional *Nedd4-1* knockout mice using primers detecting the *Nedd4-1* wild-type (wt) and floxed (fl) alleles (left panel). The weak upper band in the middle lane results from a minor contamination. PCR analysis using primers for the *Cre* transgene is shown in the right panel.

(D) qRT-PCR for *Nedd4-1* relative to *Rps29* using RNA samples from dermis of newborn control (fl/fl;wt) and homozygous (fl/fl;Cre) *Nedd4-1* knockout mice. N = 2-3 mice per genotype. Bar graphs show mean  $\pm$  SEM. Expression level in one control (fl/fl;wt) mouse was set to 1.

(E) Representative immunofluorescence staining of back skin from adult control (fl/fl;wt) and homozygous (fl/fl;Cre) *Nedd4-1* knockout mice for *Nedd4-1* (red). Nuclei were counterstained with Hoechst (blue). The white rectangle indicates the area that is shown at higher magnification. E: Epidermis; D: Dermis. Magnification bars: 100  $\mu$ m.

The progeny of the breedings showed an unexpected ratio of the different genotypes after weaning (Table 1). We did not observe any homozygous mutant mice at this stage, suggesting pre- or early postnatal lethality and/or cannibalism by the mothers. By contrast, mice with a heterozygous knockout of *Nedd4-1* were found in all litters. They were viable and fertile and did not show obvious abnormalities. To determine if the homozygous mice survive until late embryonic development, we set up timed matings. We obtained the knockout embryos at the expected Mendelian ratio at E18.5 (Table 2). However, they were much smaller compared to their control littermates (Fig. 1A). This was reflected by their reduced body weight (Fig. 1B). Herovici stainings showed various developmental abnormalities (Fig. S2). Defects in the bones were particularly obvious, and the stainings suggest a reduction in bone mineral density and trabecular bone volume as well as abnormal ossification within the cartilage primordium of the scapula (Fig. S2A, B). Furthermore, the spinal cord appeared hypocellular and severely malformed (Fig. S2C). The cartilage primordium of the lower half of the vertebral centrum showed reduced collagen deposition (blue) (Fig. S2D). In addition, the mutant mice had lung abnormalities with an obvious reduction in the number of alveoli (Fig. S2E), which may cause respiratory failure immediately after birth.

### ***Nedd4-1* in mesenchymal cells is important for skin development**

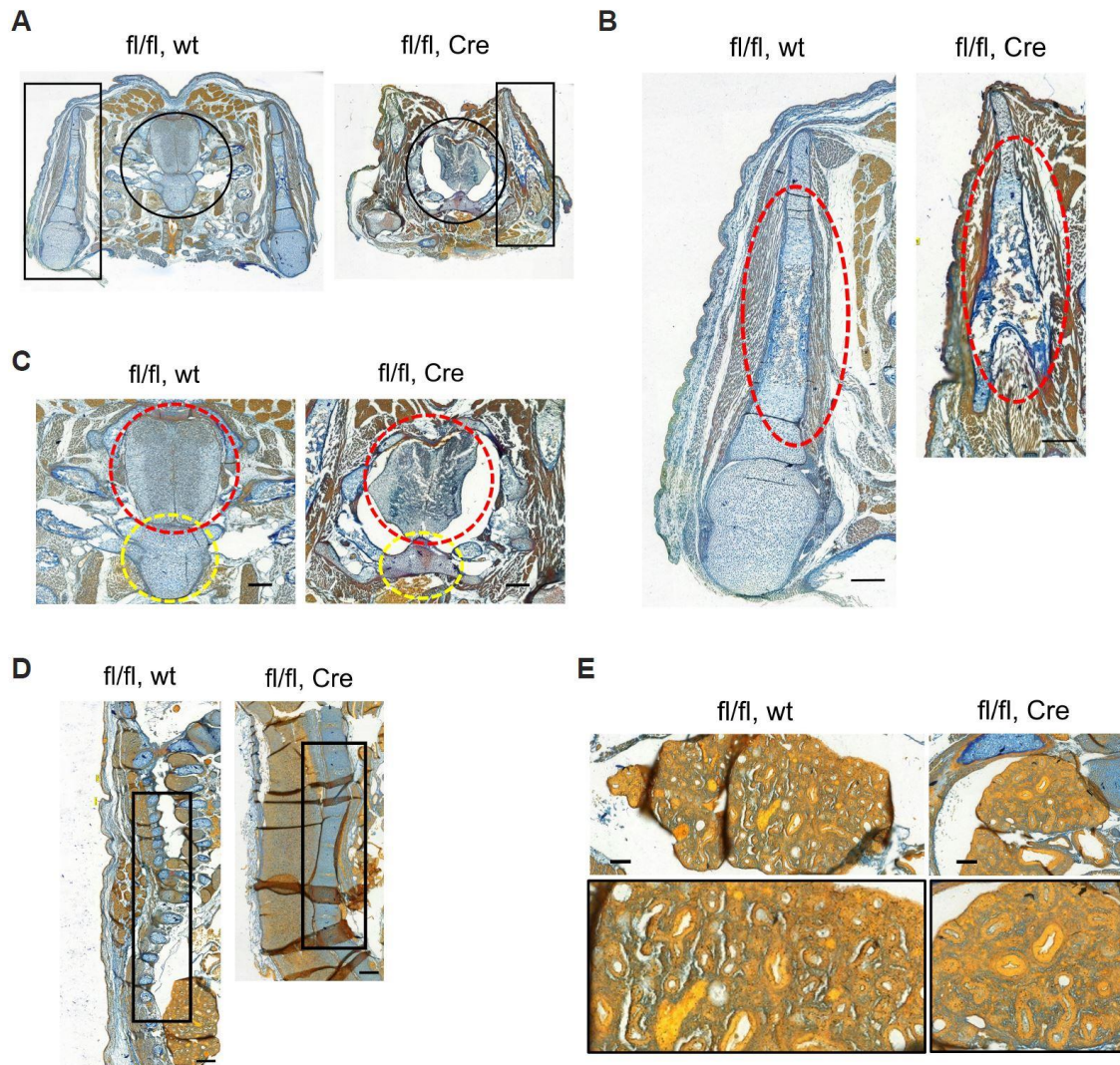
Because of our specific interest in the role of *Nedd4-1* in dermal fibroblasts, we focused our analysis on the skin phenotype. Here, we observed a reduction in dermal cellularity and extracellular matrix (ECM) density (Fig. 1C-E). Interestingly, however, the epidermis was significantly thicker in *Nedd4-1* knockout embryos, in particular the cornified layer (Fig. 1D-F).

**Table 1: Distribution of genotypes of mice after weaning**

	fl/wt,wt	fl/fl,wt	fl/wt,Cre	fl/fl,Cre
Expected Mendelian ratio (%)	25	25	25	25
Observed ratio (%)	50.00	16.67	33.33	0.00
Number of mice	6	2	4	0

**Table 2: Distribution of genotypes of E18.5 embryos**

	fl/wt,wt	fl/fl,wt	fl/wt,Cre	fl/fl,Cre
Expected Mendelian ratio (%)	25	25	25	25
Observed ratio (%)	15.00	25.00	40.00	20.00
Number of mice	3	5	8	4



**Supplementary Fig. S2 Developmental abnormalities in E18.5 *Nedd4-1* knockout embryos**

(A) Herovici staining of cross sections of Ctrl (fl/fl;wt), and homozygous (fl/fl;Cre) *Nedd4-1* knockout embryos at E18.5. Areas, which are marked with a black rectangle, are shown at higher magnification in (B). Areas, which are marked with a black circle, are shown at higher magnification in (C).

(B) Herovici staining of cross sections; red circles indicate the area showing ossification within cartilage primordium of the scapula.

(C) Spinal cord in upper cervical region (red circle) and cartilage primordium of the lower half of centrum of vertebrae (yellow circle).

(D) Herovici staining of longitudinal sections showing the vertebrae of Ctrl (fl/fl;wt) and homozygous (fl/fl;Cre) *Nedd4-1* knockout embryos. Black rectangle indicates the odontoid cartilage primordium of vertebrae.

(E) Herovici staining of lung sections from Ctr (fl/fl;wt) and homozygous (fl/fl;Cre) *Nedd4-1* knockout embryos. Areas, which are marked with a black rectangle, are shown at higher magnification below.

Magnification bars: 200  $\mu$ m (B, C, D), 100  $\mu$ m (E).



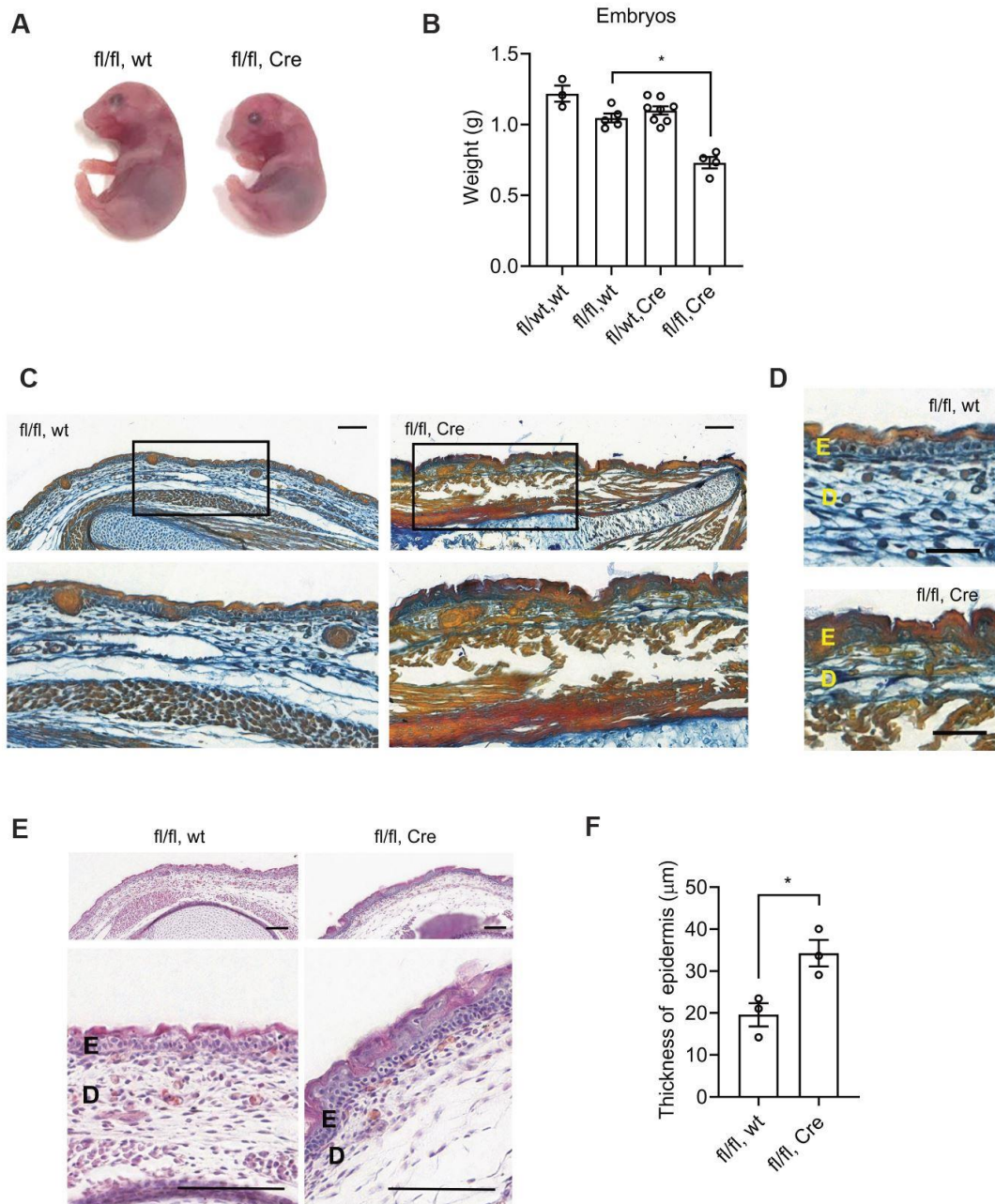


**Fig. 1 Growth retardation and impaired skin morphogenesis in mice lacking Nedd4-1 in mesenchymal cells**

(A, B) Macroscopic appearance (A) and body weight (B) of Ctr (fl/fl;wt) and homozygous (fl/fl;Cre) *Nedd4-1* knockout embryos at E18.5. N = 3-8 embryos per genotype.

(C) Herovici staining of back skin of E18.5 Ctr (fl/fl;wt) and homozygous (fl/fl;Cre) *Nedd4-1* knockout embryos. Areas, which are marked with a black rectangle, are shown at higher magnification below. Enlarged areas are shown in (D), E: Epidermis; D: Dermis.

(E, F) Hematoxylin/eosin staining (E) and quantification of epidermal thickness (F) of back skin from Ctr (fl/fl;wt) and homozygous (fl/fl;Cre) *Nedd4-1* knockout embryos at E18.5. Bar graph shows mean +/- SEM. N = 3 mice per genotype.

Bar graphs shows mean  $\pm$  SEM. \*P<0.05 Mann-Whitney U test (B) Student's t-test (F).

We next checked the litters immediately after birth and identified a few knockout pups (Table 3). They were very small, and their skin seemed to have more wrinkles (Fig. 2A). They appeared much less motile than control mice and had to be sacrificed immediately due to animal welfare regulations. Consistent with the findings obtained with E18.5 embryos, the newborn mice had a significantly reduced body weight (Fig. 2B). Analysis of their skin with antibodies against different epidermal differentiation markers revealed a much broader staining for the late epidermal differentiation markers loricrin and filaggrin (Fig. 2C). By contrast, expression of the early differentiation marker keratin 10 (K10) was strongly reduced and showed a patchy expression pattern (Fig. 2C). These findings suggest that *Nedd4-1* in fibroblasts indirectly affects epidermal differentiation. This may result from the reduced cellularity in the dermis (Fig. 1D and E), and concomitant reduction in the production of paracrine-acting factors. Consistent with the reduced cell number, Ki67 staining revealed strongly reduced dermal cell proliferation in *Nedd4-1* knockout mice (Fig. 2D). In addition, there were less mature blood vessels in the dermis of *Nedd4-1* knockout mice as revealed by the almost complete absence of alpha smooth muscle actin ( $\alpha$ -SMA)-positive vascular smooth muscle cells (Fig. 2E). It remains to be determined if the total number of blood vessels is also affected.

**Table.3 Distribution of genotypes in newborn mice**

	fl/wt,wt	fl/fl,wt	fl/wt,Cre	fl/fl,Cre
Expected Mendelian ratio (%)	25	25	25	25
Birth ratio (%)	29.41	29.41	17.65	23.53
Number of mice	5	5	3	4

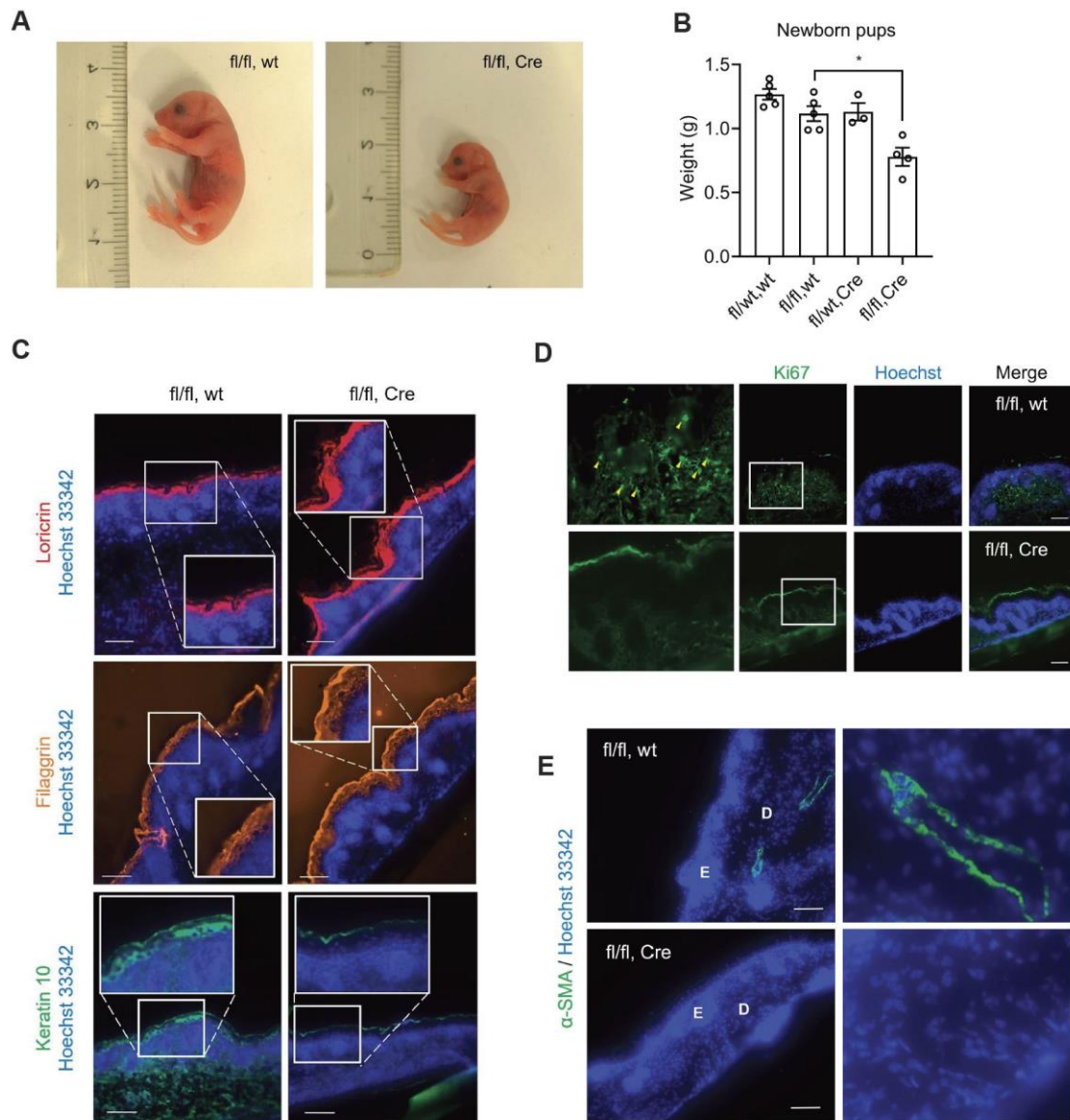


**Fig. 2 Knockout of *Nedd4-1* in mesenchymal cells affects the development of dermis and epidermis**

(A, B) Macroscopic appearance (A) and body weight (B) of newborn Ctr (fl/fl;wt) and homozygous (fl/fl;Cre) *Nedd4-1* knockout mice. Bar graph indicates mean $\pm$  SEM. N = 3-5 mice per genotype. \*P<0.05 Mann-Whitney U test.

(C) Representative immunofluorescence stainings of back skin sections from newborn Ctr (fl/fl;wt) and homozygous (fl/fl;Cre) *Nedd4-1* knockout mice for loricrin, filaggrin, and keratin 10 (K10). Nuclei were counterstained with Hoechst (blue). Higher magnifications are shown in the white rectangles.

(D) Representative photomicrographs of Ki67-stained skin sections from newborn Ctr (fl/fl;wt) and homozygous (fl/fl;Cre) *Nedd4-1* knockout mice. Higher magnifications are shown on the left. Ki67-positive cells in the dermis are indicated with yellow arrowheads.



(E) Representative immunofluorescence stainings of skin sections from newborn Ctr (fl/fl;wt) and homozygous (fl/fl;Cre) *Nedd4-1* knockout mice for  $\alpha$ -smooth muscle actin ( $\alpha$ -SMA). Nuclei were counterstained with Hoechst (blue). Higher magnifications are shown on the right.

Magnification bars: 100  $\mu$ m.

### **Knock-down of Nedd4-1 impairs proliferation and migration of fibroblasts**

To unravel the cellular mechanisms underlying the abnormalities seen Col1a2Cre-*Nedd4-1* mice, we knocked down Nedd4-1 in primary skin fibroblasts from neonatal mice. The efficient knock-down of this protein upon transfection with two different siRNAs was verified by Western blot analysis and immunofluorescence staining (Fig. 3A and B). Knock-down of Nedd4-1 significantly reduced the proliferation rate of fibroblasts (Fig. 3C and D), their migratory capacity in scratch assays (Fig. 3E and F), and their capability to contract collagen gels (Fig. 3G and H).

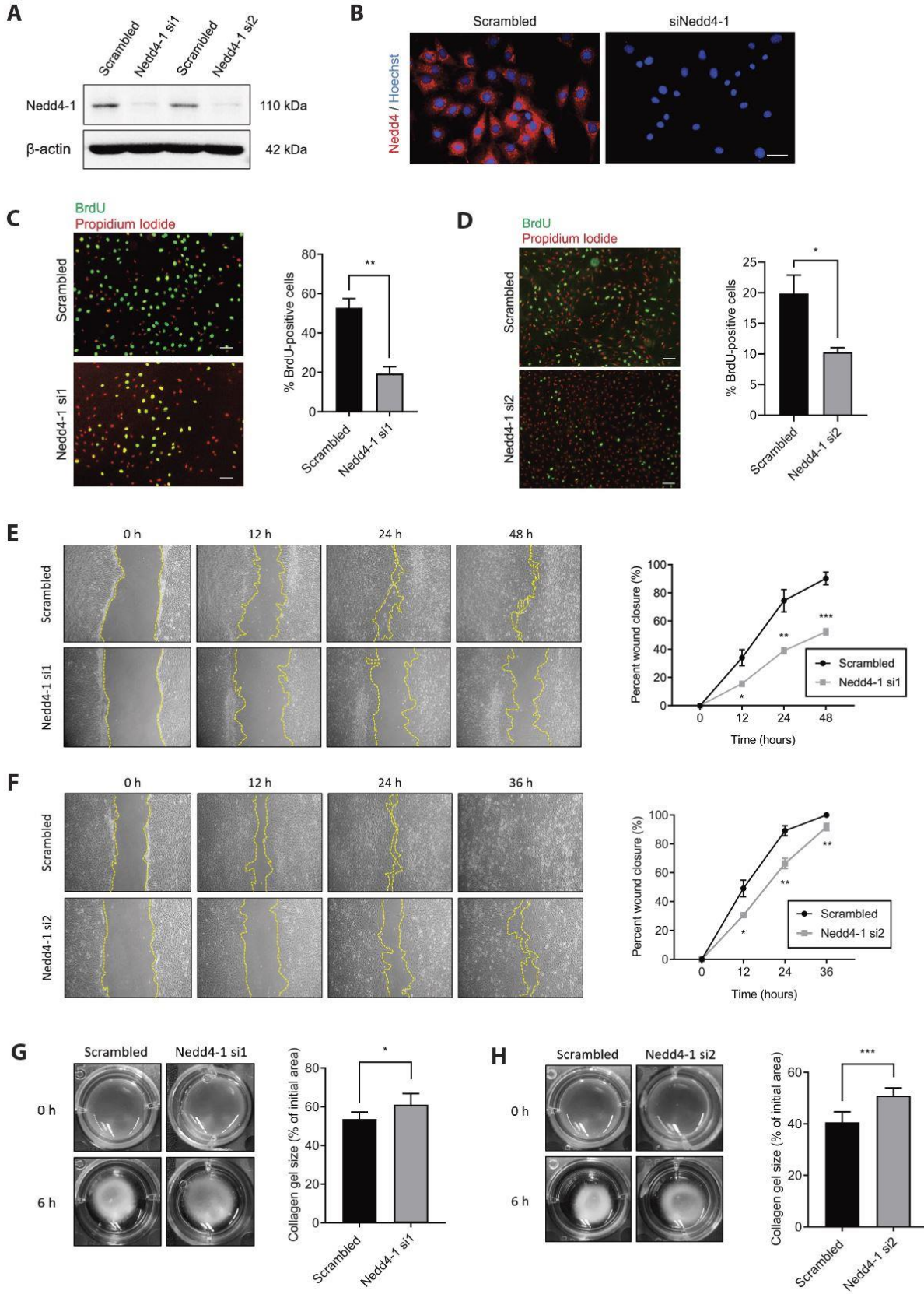


**Fig. 3 Transient knock-down of Nedd4-1 affects different fibroblast functions *in vitro***

(A) Western blot analysis of lysates from primary murine fibroblasts transfected with Nedd4-1 or scrambled siRNAs using antibodies against Nedd4-1 and  $\beta$ -actin (loading control).

(B) Representative photomicrographs of Nedd4-1 immunofluorescence staining of fibroblasts transfected with Nedd4-1 or scrambled siRNA (red). Nuclei were counterstained with Hoechst (blue).

(C, D) Representative photomicrographs of BrdU-stained primary murine fibroblasts (green) transfected with Nedd4-1 si1 (C), Nedd4-1 si2 (D) or scrambled siRNA. Nuclei were counterstained with propidium iodide (red). Quantification of BrdU-positive keratinocytes is shown in the graphs. For each siRNA (scrambled, si1 or si2) treatment: N = 3 for each siRNA using cells from 3 different mice.

(E, F) Representative photomicrographs of scratch wounded primary murine fibroblasts transfected with Nedd4-1 si1 (E), Nedd4-1 si2(F) or scrambled siRNA and treated with mitomycin C to inhibit cell proliferation. The open area devoid of cells was measured immediately after (0h) and 12h, 24h, and 36h or 48h post scratch wounding. Quantification of the percentage of scratch closure at the indicated time points is shown in the graph. For each siRNA (scrambled, si1 or si2) treatment: N = 2-3 cell cultures from 2-3 different mice, n = 2 dishes per culture.

(G,H) Representative photomicrographs of collagen gels containing primary murine fibroblasts transfected with Nedd4-1 si1 (G), Nedd4-1 si2(H) or scrambled siRNA. The gel area was measured immediately (0h) and 6h after gel polymerization. Quantification of the percentage of the original collagen gel area at the indicated time points is shown in the graph. For each siRNA (scrambled, si1 or si2) treatment: N = 3 cell cultures from 3 different mice, n = 2 dishes per culture.

Bar graphs show mean  $\pm$  SEM. \*P < 0.05, \*\*P < 0.01, \*\*\*P < 0.001 (Student's t-test). Magnification bars: 100 $\mu$ m.

We also generated spontaneously immortalized murine fibroblast cell lines with stable shRNA-mediated knock-down of *Nedd4-1* (Fig. 4A). While cell morphology and viability of fibroblasts were not significantly affected by the *Nedd4-1* knock-down under normal culture conditions (Fig. 4B and C), the proliferation rate of two different cell lines and their migratory capacity in a circular wound closure assay and in a chemotactic transwell migration assay were strongly reduced (Fig. 4 D-F).

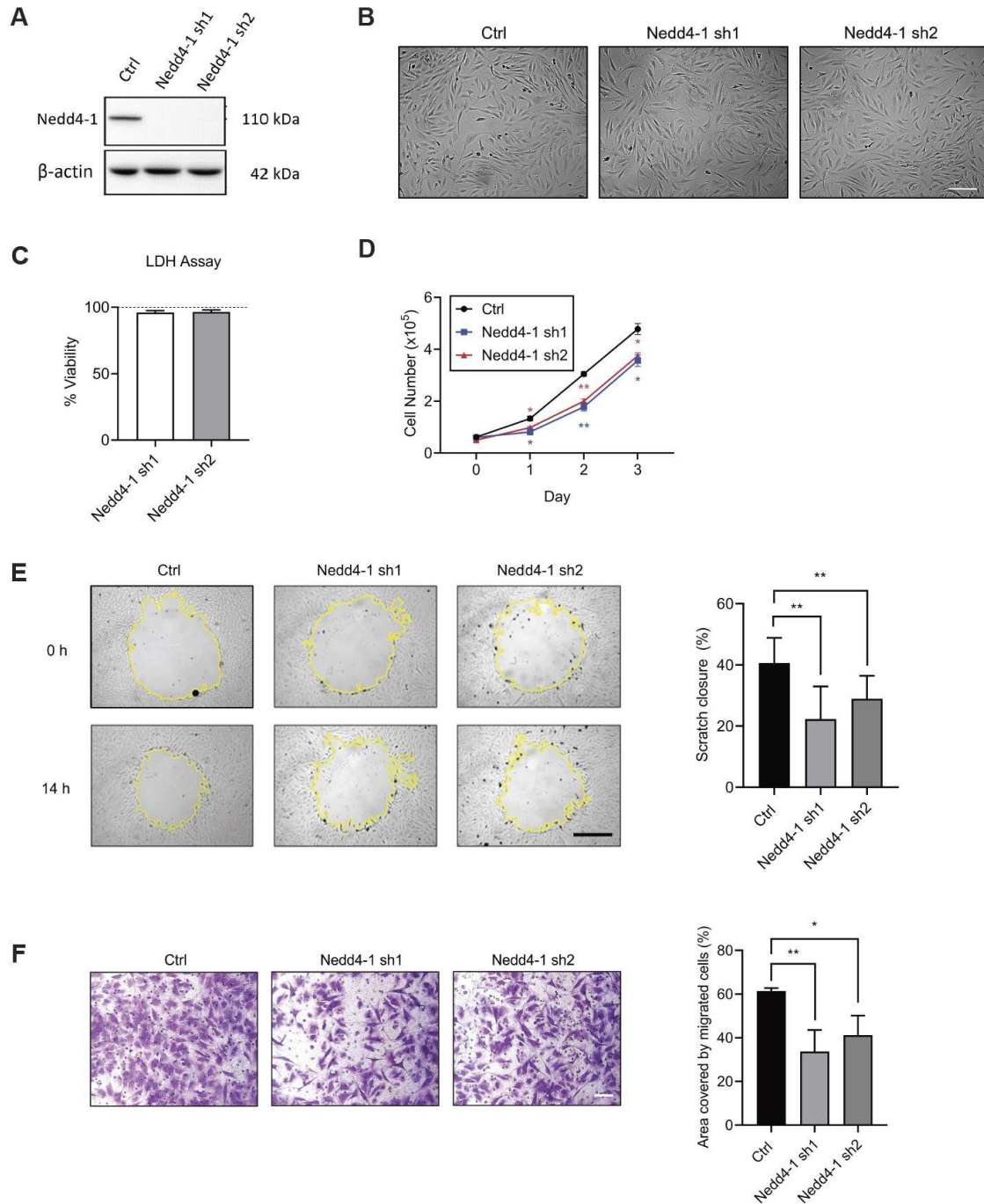


**Fig. 4 Knock-down of *Nedd4-1* inhibits fibroblast proliferation and migration**

(A) Western blot analysis for Nedd4-1 and  $\beta$ -actin (loading control) using lysates of immortalized murine fibroblasts transduced with lentiviruses expressing two different *Nedd4-1* shRNAs (sh1 and sh2) or cells transduced with a viral vector expressing ctrl shRNA (Ctrl).

(B) Morphology of Ctrl and *Nedd4-1* knock-down fibroblast lines under normal culture conditions.

(C) Fibroblast lines with *Nedd4-1* knock-down were cultured under normal conditions. The media were analyzed for LDH levels in the supernatant using an LDH cytotoxicity assay. Graph shows % viability relative to control cells. N = 6 dishes from each cell line.

(D) The total number of *Nedd4-1* knock-down and control fibroblasts was counted every 24h after seeding in 12-well-plates and maintenance under normal culture conditions. N =3 dishes from each cell line.

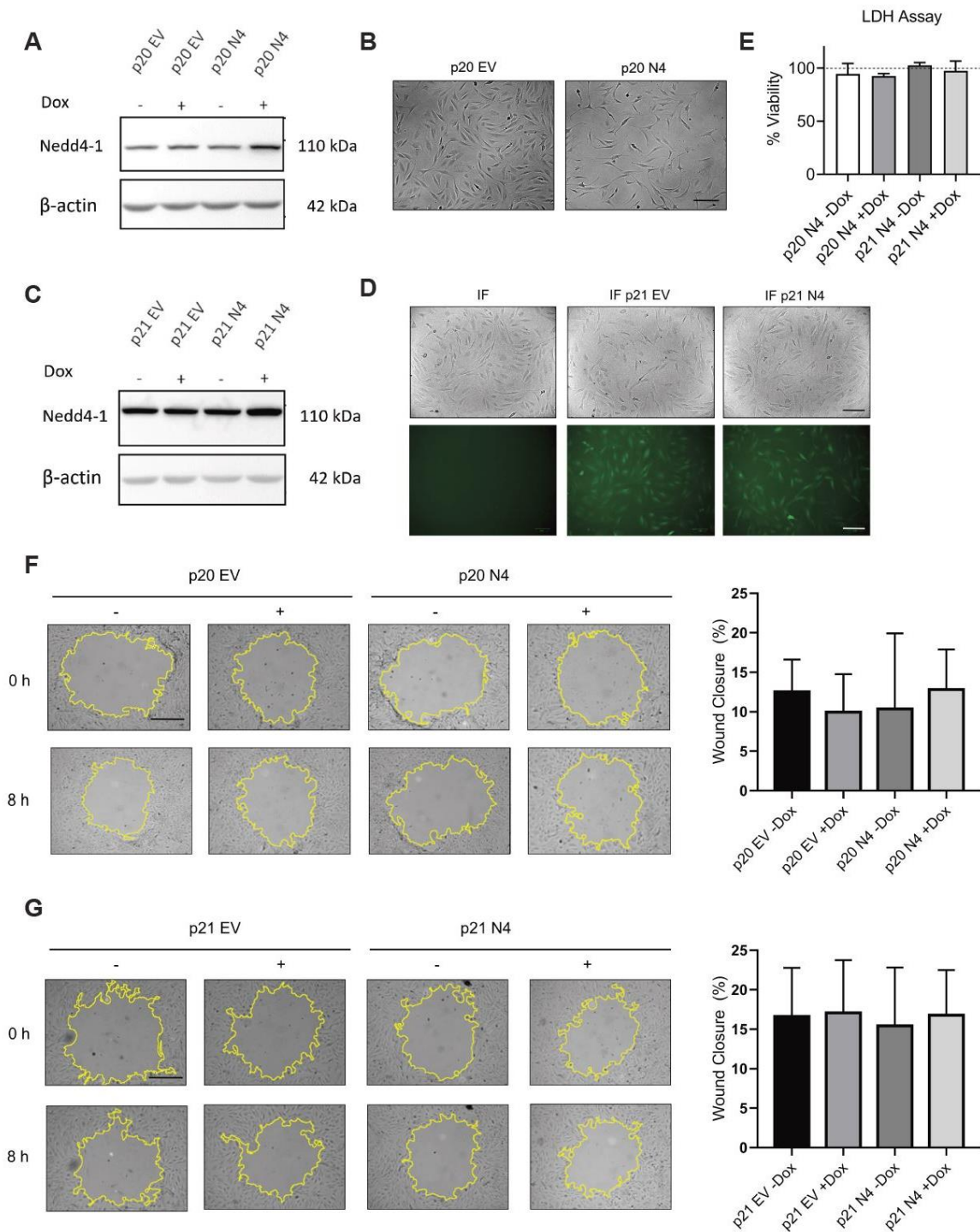
(E) Cell migration was determined using a circular wound closure assay. Representative images of the circular wounds are shown (left). Graph shows quantification of the wounded area covered by migrated cells. N = 4-10 dishes from each cell line.

(F) Cell migration was determined using Millipore transwell chambers. Representative images of the bottom surface are shown (left). Graph shows quantification of the area covered by migrated cells. N = 3 dishes from each cell line.

Bar graphs show mean $\pm$  SEM. \*P<0.05; \*\*P<0.01 (Student's t-test).

Magnification bars: 200  $\mu$ m (B), 500  $\mu$ m (E) and 100  $\mu$ m (F).

In contrast to the severe consequences of *Nedd4-1* knock-down, doxycycline-inducible overexpression of *Nedd4-1* using two different lentiviral vectors, which allow selection by puromycin treatment or flow cytometry for eGFP, did not affect cell morphology, viability, or the migratory capability of cells under normal culture conditions (Fig. S3A-G). However, we only obtained cell lines with approximately 2-fold overexpression of *Nedd4-1* (Fig. S3A), suggesting that higher *Nedd4-1* levels may be detrimental.



**Supplementary Fig. S3 Mild overexpression of Nedd4-1 does not influence fibroblast morphology, viability and migration**

(A) Western blot analysis for Nedd4-1 and  $\beta$ -actin (loading control) using lysates of immortalized murine fibroblasts transduced with lentiviruses allowing doxycycline-induced overexpression of Nedd4-1 (p20 N4)



or cells transduced with an empty vector (p20 EV). Cells were treated with doxycycline (+) or vehicle (DMSO) only (-). p20: pInducer20.

**(B)** Morphology of p20 N4 and p20 EV fibroblasts under normal culture conditions.

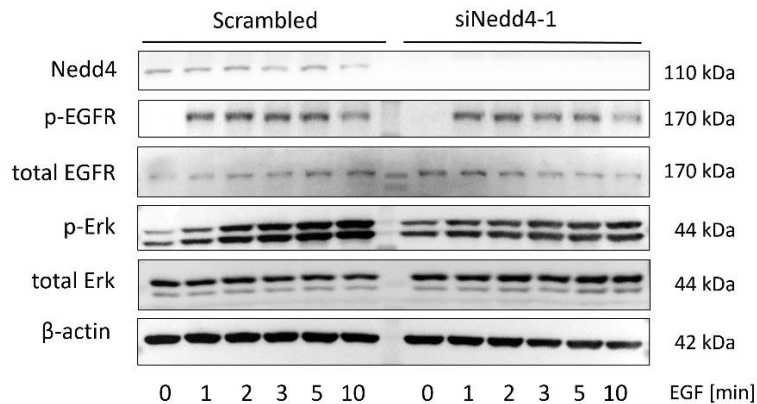
**(C)** Western blot analysis for Nedd4-1 and  $\beta$ -actin (loading control) using lysates of immortalized murine fibroblasts transduced with lentiviruses overexpressing of Nedd4-1 (p21 N4) or cells transduced with an empty vector (p21 EV). Cells were incubated in medium with doxycycline (+) or vehicle only (-). p21: pInducer21.

**(D)** Representative images of the non-transduced immortalized fibroblast cell line (IF) and the transduced and subsequently sorted eGFP-positive cell lines (IF p21 EV and IF p21 N4).

**(E)** Fibroblast cell lines with inducible overexpression of Nedd4-1 were cultured under normal culture conditions and incubated in medium with doxycycline (+) or vehicle only (-). Media were analyzed for LDH levels in the supernatant using an LDH cytotoxicity assay. Bars show % viability relative to control cells. N = 6 dishes from each cell line.

**(F, G)** Migration of Nedd4-1 overexpressing or control fibroblast cell lines was determined using a circular wound closure assay. Representative images of the circular wounds are shown (left). Graph shows quantification of the area covered by migrated cells after 8 h. N = 7-13 dishes from each cell line.

Magnification bars: 200  $\mu$ m (**B, D**), 500  $\mu$ m (**F, G**).



#### Supplementary Fig. S4

Serum-starved primary mouse fibroblasts were treated with epidermal growth factor (EGF) (10 ng/ml) for 0, 1, 2, 3, 5 and 10 min. Cell lysates were analyzed by Western blot for Nedd4-1, total and phosphorylated EGF receptor (EGFR) and total and phosphorylated Erk1/2.  $\beta$ -actin was used as an additional loading control.

## Discussion

In this study we identified key functions of Nedd4-1 in mesenchymal cells in the development of different tissues and organs. While mice with heterozygous knockout of *Nedd4-1* did not reveal obvious abnormalities and were viable and fertile, the progeny of our breedings showed an unexpected ratio of the different genotypes upon weaning, with a complete lack of homozygous knockout mice. Close observation of the knockout mice after birth showed that they complete embryonic development, but most likely die immediately after birth, possibly from respiratory failure. Thus, the newborn mice that we observed were very small, had severe malformations and showed obvious immobility and breathing problems. Therefore, we sacrificed them immediately according to animal welfare regulations.

Previous studies using *Nedd4-1* knockout mice identified important functions of this protein in the development of different tissues and organs. Two independently generated *Nedd4-1* cKO mouse lines exhibited embryonic lethality with significant vascular malformations and heart development defects or neonatal lethality, which was accompanied by delayed embryonic development, reduced body weight and growth [121, 122]. Embryonic fibroblasts isolated from those mice had an impaired mitogenic activity [121]. All these findings indicate that Nedd4-1 is necessary for cell proliferation and organ development. Considering these previous findings, the early lethality of our Col1a2-*Nedd4-1* mutant mice, in which the deletion of *Nedd4-1* occurred in mesenchymal cells of various organs, did not come as a surprise. Besides various other abnormalities, our preliminary data suggest that bone and lung development are particularly impaired in Col1a2cre-*Nedd4-1* mice, which may lead to movement problems and respiratory failure. The lung phenotype is consistent with the abnormalities seen in mice with global *Nedd4-1* knockout [121], suggesting that mesenchymal cells are the major players in this phenotype. In the future, it will be important to further characterize the different tissues and organs in Col1a2cre-*Nedd4-1* mice, e.g. by staining for various cell type-specific marker proteins and analysis of proliferation and apoptosis.

In the skin, we observed reduced dermal cellularity and a less dense ECM. The latter may be a consequence of the reduced number of fibroblasts. However, it is also possible that



fibroblasts produce less ECM upon loss of Nedd4-1, which should be analyzed in *Nedd4-1* knockout or knock-down fibroblasts. Interestingly, we also observed major epidermal abnormalities in the mutant mice, in particular accelerated terminal differentiation of keratinocytes and a concomitant increase in the thickness of the cornified layer. These abnormalities may result in an impairment of the epidermal barrier function, thereby leading to enhanced transepidermal water loss. This may provide an additional explanation for the postnatal death of the animals. It seems likely that the reduced number of dermal fibroblasts and possibly an impaired activity of these cells result in a deficiency in ECM and/or paracrine-acting growth factors, which are important for normal keratinocyte differentiation [44]. In the future, this should be tested in 3D organotypic cultures with Nedd4-1-deficient fibroblasts and wild-type keratinocytes. Finally, it will be important to unravel the function of Nedd4-1 in mesenchymal cells in tissue homeostasis and repair, which will require mice with an inducible knockout in these cells. Such mice were obtained within the frame of this project, but they have not been analyzed so far. Finally, future studies should identify the targets of Nedd4-1, which are responsible for the fibroblast phenotype of the knockout mice. It has previously been shown that knockout of Nedd4-1 results in impaired signaling by the insulin and insulin-like growth factor receptors in immortalized embryonic fibroblasts, which is at least in part mediated by enhanced expression of the adaptor protein Grb10 [121]. It remains to be determined if signaling by these receptors is also affected in primary fibroblasts from neonatal mice or in fibroblasts with Nedd4-1 knock-down. In addition to a possible role of insulin receptor signaling, our previous studies demonstrated that Erk1/2 activation by the epidermal growth factor receptor is reduced and more transient in Nedd4-1-deficient hepatocytes and keratinocytes [50] (Yan et al., in preparation), and our preliminary data suggest a similar deficiency in Nedd4-1 knock-down fibroblasts (Supplementary Fig. 4). In summary, our study uncovered important functions of this E3 ligase in mesenchymal cells in the development of various tissues and organs, which will have to be further characterized in follow-up studies.

## Materials and Methods

### Mouse Lines and Genotyping

Mice expressing Cre recombinase under the control of the promoter/enhancer unit of the gene encoding the  $\alpha 2$  chain of collagen type I (Col1a2-Cre mice) [148] were mated with mice harboring floxed alleles of the *Nedd4-1* gene [146]. All mice were in C57BL/6 genetic background. We only used male Col1a2-Cre mice for matings to avoid global deletion, which is frequently seen when female mice of this line are used [169].

For genotyping, DNA was extracted from toe biopsies and amplified by PCR using the KAPA2G FAST Genotyping Mix (Kapa Biosystems, Wilmington, MA) and the primers shown in Supplementary Table S1.

Mice were housed under specific pathogen-free (SPF) conditions and maintained according to Swiss animal protection guidelines. All animal experiments had been approved by the local veterinary authorities (Kantonales Veterinäramt Zürich, Switzerland).

### Timed Pregnancy

Pregnant *Nedd4-1 fl/fl* female mice, which had been mated with *Nedd4-1 fl/wt*, *Cre* male mice, were sacrificed at E18.5 and the uteri were isolated and placed in ice-cold phosphate-buffered saline (PBS). Embryos were decapitated and fixed in 4% paraformaldehyde overnight, dehydrated, embedded in paraffin, and sectioned (7  $\mu$ m).

### Separation of epidermis and dermis

Newborn pups were sacrificed by decapitation, and appendages were surgically removed with scissors (tails were lysed for genotyping). From the isolated skin, the fat was gently scraped off using a scalpel. Then, the skin was incubated in 0.25% dispase (ThermoFisher, Waltham, MA) solution at 37°C for 1h. Subsequently, the epidermis was gently separated from the dermis and the samples were immediately snap-frozen in liquid nitrogen and stored at -80°C.

### **5-Bromo-2'-deoxyurine (BrdU) Incorporation Assay**

BrdU was added to the cell culture medium at a final concentration of 10  $\mu\text{M}$ , and cells were incubated for 2 h at 37°C and 5% CO<sub>2</sub>. After washing with PBS they were fixed for 10 min at room temperature with 4% paraformaldehyde (PFA). Cells were then permeabilized using 0.1% Triton-X 100 in PBS, followed by incubation with 2M HCl for 30 min. The HCl solution was removed and cells were incubated with boric buffer (100 mM boric acid, 75 mM NaCl, 25 mM sodium tetraborate, pH 8.5) for 5 min. Blocking was performed using 1% BSA for 10 min, followed by incubation with the FITC-coupled BrdU antibody at 4°C overnight. Cells were counterstained using propidium iodide (#P4170, Sigma, Munich, Germany).

### **Histology and Histomorphometry**

Tissue samples were fixed in 4% phosphate buffered PFA or 95% ethanol/1% acetic acid for 24 h at 4°C, processed, and embedded in paraffin. Alternatively, they were immediately frozen in tissue freezing medium® (Leica Biosystems, Wetzlar, Germany). Tissue blocks were sectioned (7  $\mu\text{m}$ ) and stained with hematoxylin and eosin or using the Herovici procedure [173].

### **Immunofluorescence and Immunohistochemistry**

Tissue sections were deparaffinized and rehydrated, or fixed with cold methanol (in case of frozen sections). Non-specific binding sites were blocked with PBS/12% BSA/0.025% NP-40 for 1 h at room temperature, and sections were then incubated overnight at 4 °C with the primary antibodies (Supplementary Table S2) diluted in the same buffer. If needed, antigen retrieval was performed prior to the blocking procedure by cooking in citrate buffer (1 h at 95 °C). After three washes with PBST (1× PBS/0.1% Triton-X100), slides were incubated for 1 h with secondary antibodies and Hoechst 33342 (#B2261, Sigma), washed with PBST and mounted with Vectashield mounting medium (Vector Laboratories, Burlingame, CA). All secondary antibodies were from Jackson ImmunoResearch, West Grove, PA.

Cultured cells were fixed for 10 min with cold 4% PFA, washed twice with PBS, and treated as described above for tissue sections. They were mounted with Mowiol (Hoechst, Frankfurt, Germany).

### **RNA Isolation and qRT–PCR Analysis**

RNA was isolated from cultured cells using the RNeasy Kit (74106, Qiagen, Hilden, Germany) according to the manufacturer's instructions and reverse transcribed using the iScript™ cDNA synthesis kit (# 1708890, BioRad, Hercules, CA). Quantitative PCR was performed using the LightCycler® 480 SYBR Green I Master reaction mix (04707516001, Roche, Rotkreuz, Switzerland) as previously described [169]. Data were quantified using second derivative maximum analysis and normalized to the expression levels of the housekeeping gene *Rps29*. Primers used for qRT PCR are listed in Supplementary Table S3.

### **Preparation of Protein Lysates and Western Blot Analysis**

Cells were trypsinized, centrifuged and lysed in RIPA lysis buffer containing Complete Protease Inhibitor Cocktail (#11836170001, Roche) and PhosSTOP Phosphatase Inhibitor Cocktail (Roche). Lysates were cleared by sonication and centrifugation, snap-frozen, and stored at -80°C. The protein concentration was determined using the BCA Protein assay (#23225, ThermoFisher Scientific). Proteins were separated by SDS-PAGE and transferred onto nitrocellulose membranes. Antibodies are listed in Supplementary Table S2 and used according to the manufacturer's instructions. Corresponding secondary antibodies were coupled to horseradish peroxidase (HRP) and the signal was visualized using WesternBright ECL HRP substrate (#K-12045-D50, Witec AG, Sursee, Switzerland) and detected using the Fusion Solo S imaging system (Vilber Lourmat, Eberhardzell, Germany). Bands were quantified using ImageJ software (National Institutes of Health, Bethesda, MD).

### **Isolation and Culture of Primary Dermal Fibroblasts**

Isolation and cultivation of murine primary dermal fibroblasts from 2-4 day-old mice was performed as previously described [169]. The dermis was separated from the epidermis by incubating with a 5% trypsin/EDTA solution for 1 h at 37 °C and gently peeling off the epidermal layer. The dermis was then minced into small pieces and incubated with 2.5 ml of a collagenase type II solution (500 U/ml; Worthington Biochemical Corporation, Lakewood, NJ) for 1 h at 37 °C with manual agitation every 15 min. The cell suspension was poured through a 100 µm cell strainer and centrifuged at 1,200 r.p.m. for 5 min. The resulting cell pellet was re-suspended in 8 ml of fibroblast medium (DMEM, Sigma)/10% fetal bovine serum/penicillin/streptomycin) and seeded into a 10 cm dish. Medium was changed the following day and cells were passaged prior to confluency. Absence of mycoplasma was confirmed by PCR using the PCR Mycoplasma Test Kit I/C (PromoKine, Heidelberg, Germany).

### **Lentivirus Transduction of Cultured Cells**

Immortalized mouse fibroblasts MEFs (kindly provided by Dr. Paul Hiebert) were cultured in 6 cm culture dishes and transduced at 30-50 % confluency. 4 ml virus-containing medium was mixed with 1 ml fresh culture medium and polybrene (final concentration 8 µg/ml) and filtered through a 0.45 µm syringe filter to remove cellular debris and particles. The culture medium was removed, and 4 ml of the filtered virus-containing medium was added dropwise to the cells. After overnight incubation, the virus-containing medium was replaced by fresh culture medium. Forty-eight hours later, cells transduced with viruses containing the pLKO.1 vector [151] were selected for 2 weeks in medium containing 2 µg/ml puromycin (Sigma). The shRNAs used are listed in Supplementary Table S4. Cells transduced with pInducer20 viral vectors [174] were selected for 2 weeks in medium containing 1500 µg/ml G-418 (Sigma). Cells transduced with pInducer21 viral vectors [174] were selected by FACS using eGFP as selection marker in an ARIA III cell sorter (BD Biosciences, Franklin Lakes, NJ, Laser: Blue 488 nm). Cells were treated with 1 µg/ml doxycycline in DMSO to induce the overexpression.

### **siRNA-Mediated Knockdown**

Primary mouse fibroblasts were transfected with siRNAs (Axolabs, Kulmbach, Germany) using Lipofectamine RNAiMAX (# 13778150, Thermo Fisher Scientific) according to the manufacturer's instructions. Experiments were performed 48h after siRNA transfection. The siRNA duplexes used are listed in Supplementary Table S5.

### ***In Vitro* Cell Migration Assay**

Cells were grown to 100% confluency in culture medium, and treated with 10 µg/ml mitomycin C (Sigma) for 2 h to inhibit proliferation. A scratch was made into the cell layer of each well using a sterile 200 µl pipette tip. Dead cells and debris were removed with pre-warmed PBS, and fresh pre-warmed culture medium was added. Alternatively, cells were seeded into 24-well plates, grown to 100% confluency, and treated with 10 µg/ml mitomycin C for 2 h. A circular wound was introduced into each well with a 200 µl pipette tip (without filter) mounted on a vacuum pump. The pipette tip was moved perpendicularly on top of the cell monolayer, and the vacuum pump was applied for 5 sec. The medium of each well was replaced with serum-containing medium. Pictures were acquired with an Axiovert 200 inverted microscope (Carl Zeiss Inc., Oberkochen, Germany; bright field, 10x magnification) at different time points. Wound closure was determined using ImageJ software with the MRI wound healing tool plugin.

### **Transwell Migration Assay**

Cells were cultured in 6 cm culture dishes in DMEM/10% FBS until they were 80-90% confluent and subsequently incubated in starvation medium (DMEM / 0% FCS or FBS) for 24 h. Adherent cells were trypsinized, centrifuged, counted with a hemocytometer, and resuspended in starvation medium to reach a final concentration of  $4 \times 10^5$  cells/ml. 250 µl cell suspension was transferred into a transwell plate (6.5 mm Transwell® chambers with 8.0 µm pore polycarbonate membrane inserts (Corning, New York, NY; 105 cells/well). After 1 h of incubation, the inserts were transferred 24-well plates containing 650 µl serum-containing culture medium per well. Cells were incubated for several hours, washed twice with PBS, and fixed with cold 100% methanol for 15 min at room temperature. Cell layers were covered with 0.5 % crystal violet solution (500 mg crystal violet, 25 ml methanol, 75 ml H<sub>2</sub>O) for 10 min and washed twice with PBS. Cells

on the upper layer were removed with cotton swabs. The transwell inserts were allowed to dry for 2 h, and the dried membranes were removed with a scalpel blade. The cell-free side of the membrane was placed onto a microscope slide and the cell-containing side was mounted with Mowiol (Sigma). Images of the migrated cells were taken with an Axioskop 2 inverted light microscope (Carl Zeiss GmbH) at 20x magnification. The areas covered by cells on the transwell membrane were measured using ImageJ software with the colour deconvolution plugin.

### Collagen Gel Contraction Assay

Fibroblasts were seeded into a 10 cm dish and cultured in DMEM/10% FBS until they reached 75 - 90% confluency. One ml of 1% BSA was added to each of the wells in a 24-well plate and incubated for at least 30 min at 37°C. While the 24-well plates were incubated with 1% BSA, the gel solutions were prepared in 1.5 ml tubes (one tube for each gel). The collagen gel recipe for one 500 µl gel (one tube) is shown below. The final collagen concentration of the gel was ~1 mg/ml.

Component	Volume
0.2 M HEPES buffer, pH 8.0	120 µl
DMEM	26 µl
Sterile H <sub>2</sub> O	16 µl
TeloCol® Collagen Solution (3.1 mg/ml)	198 µl
Cells at 4.2 x 10 <sup>5</sup> cells/ml	240 µl

The collagen solution was kept on ice until use. HEPES, DMEM and sterile Milli-Q H<sub>2</sub>O were added to each tube (one tube for one well of a 24-well plate). Cells were then trypsinized, centrifuged, and the cell pellet was re-suspended in 500 µl medium. Ten µl of the cell-containing medium from each tube was used to count the cell number using a haemocytometer. The total number of cells was divided by 4.2 x 10<sup>5</sup> to calculate the required final volume. The appropriate amount of medium was added to each tube (which contains the initial 500 µl re-suspended cells) so obtain the cell number in each well. The 1% BSA solution was removed from the 24-well plate. Then, 198 µl of the collagen

solution was added to each of the tubes (one tube for one well of 24-well plate), and 240  $\mu$ l of the cells at  $4.2 \times 10^5$  cells/ml were added to the tubes containing the gel mixtures. The gel mixtures were quickly, but gently mixed, and 500  $\mu$ l of the mixture was added to the appropriate wells in the 24-well plate. The 24-well plate containing the gels was incubated at 37°C for 30 min until the gels were fully solidified. 500  $\mu$ l cell culture medium was then added to the wells containing the gels. Gels were photographed together with a ruler at 0 h and at different time points thereafter (e.g. 2, 24, 48 h).

### Statistical Analysis

Statistical analysis was performed using the GraphPad Prism 8 software (GraphPad Software Inc, San Diego, CA). Quantitative data are expressed as mean  $\pm$  SEM. Testing for statistically significant differences between two experimental groups was performed using Student's t-test or non-parametric Mann-Whitney U test for two-tailed, unpaired comparison at a confidence level starting at 95% ( $p < 0.05$ ). \* $P < 0.05$ , \*\* $P < 0.01$ , and \*\*\* $P < 0.001$ .

### Supplementary Table S1: Primers used for Genotyping

	Forward sequence 5'→3'	Reverse sequence 5'→3'
<i>Nedd4-1</i> floxed	GTACATTTTAGTTCATGG TTCTCACAGG	CAGAGGTCACATGGCTGTGGG
<i>Col1a2-Cre</i>	TTAGCACCCACGGCAGCA GGAG	CAGGCCAGATCTCCTGTGCAGCA T

### Supplementary Table S2: Antibodies

Antibody	Source	Catalog No.
Anti- $\beta$ -Actin	Sigma	#A5316
Anti-Nedd4	BD Biosciences	#611480
Anti-Nedd4	Abcam, Cambridge, UK	#ab27979
Anti-mouse IgG HRP conjugate	Promega, Fitchburg, MA	#W402B
Anti-rabbit IgG HRP conjugate	Promega	#W4011
Mouse anti-keratin 10	DAKO, Glostrup, Denmark	#M7002
Rabbit anti-loricrin	BAbCo, Richmond, CA	#PRB-145P
Anti-filaggrin	BioLegend, San Diego, CA	#PRB-417P
Mouse anti- $\alpha$ SMA-FITC	Sigma	#F3777



Anti-Ki67	Abcam	#Ab15580
Anti-pErk1/2	Cell Signaling, Danvers, MA	#9101S
Anti-total Erk1/2	Cell Signaling	#9102S
Anti-pEGFR	Cell Signaling	#cs3777
Anti-total EGFR	Santa Cruz, Santa Cruz, CA	#sc-03

**Supplementary Table S3.** Primers used for qRT-PCR

Target gene	Forward sequence 5'→3'	Reverse sequence 5'→3'
<i>Nedd4-1</i>	CACACACCTGCTTCAATCGC	GGGAAGAGCCAGTGACCATC
<i>Rps29</i>	GGTCACCAGCAGCTCTAGTG	GTCCAACCTTAATGAAGCCTATGTCC

**Supplementary Table S4.** shRNA sequences

	Mature antisense 5'→3'
Nedd4-1 shRNA 1	AATCCTCCAGAATGTTTGCGC
Nedd4-1 shRNA 2	ATTCATGGTTTACGTAGTAGG

**Supplementary Table S5.** siRNA sequences

	Forward sequence 5'→3'	Reverse sequence 5'→3'
Nedd4-1 siRNA 1	acAGAUuAAGcGAuuuucudTsdT	AGAAAUUCGCUuAAUCUGUdTsdT
Nedd4-1 siRNA 2	gacAccGcAuucuuuucGAdTsdT	UCGAAAAGAAUGCGGUGUCdTsdT
Scrambled siRNA	AGGuAGuGuAAucGccuuGdTsdT	cAAGGcGAuuAcAcuAccudTsdT

## **Acknowledgements**

We thank Dr. Paul Hiebert for invaluable experimental help. This work was supported by the Swiss National Science Foundation (310030\_132884 and 31003A-169204/1 to S.W) and a Chinese Government Predoctoral Fellowship (to S.Y.)

## **Author Contributions:**

S.Y., R. R. and M.C. performed experiments and analyzed the data.

P.A. provided the Col1a2-Cre mice.

H. K. provided *Nedd4-1* floxed mice.

S. Y. wrote the manuscript together with S.W.

S.W. designed and supervised the study, wrote the manuscript together with S.Y. and provided the funding.

All authors made important suggestions to the manuscript.

## 5. Discussion and Outlook

NEDD4-1 is an evolutionarily highly conserved and ubiquitously expressed HECT E3 ubiquitin ligase with important functions in organ development, tissue homeostasis, repair and cancer [143, 175]. Surprisingly, however, its function in the skin has been poorly characterized. To determine the role of Nedd4-1 in the major resident cell types of the skin, I generated mice lacking this protein either in keratinocytes or in mesenchymal cells, including fibroblasts of the skin. In addition, functional studies were performed using cultured keratinocytes and fibroblasts with Nedd4-1 knock-down. The results obtained in this thesis project identify crucial functions of Nedd4-1 in skin development, homeostasis and repair.

### 5.1 Role of Nedd4-1 in keratinocytes

#### 5.1.1 Keratinocyte-derived Nedd4-1 in skin development and homeostasis

Previous work of our laboratory identified an important function of Nedd4-1 in hepatocytes for liver regeneration [50]. Therefore, it was of interest to find out if Nedd4-1 deficiency in other types of epithelial cells also affects the repair process. We focused on the skin, since the knowledge about Nedd4-1 function in this tissue is extremely limited.

Mice lacking Nedd4-1 in keratinocytes and outer root sheath cells of the hair follicles, which were obtained by breeding of the *Nedd4-1* floxed mice with K5-Cre mice, reached adulthood without apparent health and fertility problems. Interestingly, however, the percentage of knockout mice in the litters upon weaning and genotyping was lower than the expected Mendelian ratio. This suggests embryonic or early perinatal death of some knockout mice, which should be further investigated in the future. The K5cre-*Nedd4-1* mice, which survived, were significantly smaller and had a lower body weight at the weaning age, but this difference was no longer observed in adult mice. The phenotype could result from the knockout of *Nedd4-1* in the oral epithelium, tongue, esophagus and forestomach, since the K5 promoter is also active in epithelial cells of these tissues [176]. The absence of Nedd4-1 might negatively influence the proliferation and differentiation of those epithelial cells, potentially resulting in malnutrition. A detailed histological analysis of these tissues will be required to test this hypothesis. Alternatively, the mice may have a transient defect in the epidermal barrier, resulting in enhanced water loss that could affect whole-body homeostasis. Such a defect could also provide an explanation for a potential early

perinatal lethality of some mice. A possible effect of Nedd4-1 deficiency on the epidermal barrier is supported by the reduced expression of the late epidermal differentiation marker loricrin in neonatal and adult mice, indicating a defect in terminal keratinocyte differentiation. In particular, we observed enhanced transepidermal water loss in adult mice, demonstrating a defect in the inside-out barrier of the epidermis. In the future, it will be interesting to measure transepidermal water loss in the mutant mice immediately after birth and at the weaning age and to determine if the inside-out barrier is also affected. This could be studied with late embryos or neonatal mice using a toluidine blue penetration assay [177, 178].

Adult K5cre-Nedd4-1 cKO mice showed epidermal abnormalities with a thinner epidermis, which most likely results from the impaired keratinocyte proliferation that we detected *in vivo* and *in vitro*. By contrast, the number of apoptotic cells was equally low in mice of both genotypes. Besides, we did not observe abnormal expression of differentiation-specific keratins. However, and consistent with the results obtained with neonatal skin, expression of the late differentiation marker loricrin was strongly reduced in the epidermis, again pointing to a defect in terminal keratinocyte differentiation. It is as yet unclear how Nedd4-1 influences terminal keratinocyte differentiation, and the identification of the responsible targets will be an important task for the future.

At ten weeks of age and thus at a time point when hair follicles are in the telogen phase in control mice, patchy hair growth was seen in shaved K5cre-Nedd4-1 mice. Histological analysis of the skin at this stage indeed identified anagen hair follicles in female K5cre-Nedd4-1, but only very rarely in control mice, indicating alterations in the progression through the hair cycle. Analysis of the hair follicles at different stages of postembryonic development, which are characteristic for the different phases of the hair cycle [23, 25], will reveal at which stage the hair cycle is perturbed in K5cre-Nedd4-1 mice. Interestingly, we noticed that the expression of K15, a hair follicle bulge stem cell marker, was almost completely absent in the hair follicles of female K5cre-Nedd4-1 mice at P71 (10 weeks of age). This will have to be verified with more mice and at different stages of postembryonic development. It will also be important to analyze the expression of additional hair follicle bulge stem cell markers, such as CD34 [179]. However, it seems unlikely that the bulge stem cells are lost over time, since we did not detect obvious hair loss upon aging. It is also unclear if the reduced K15 expression is a cause or a consequence of the defect in hair cycling.

Overall, these studies revealed a role of Nedd4-1 in skin development and homeostasis, although its loss in keratinocytes did not result in severe postnatal abnormalities. It may well be that other ubiquitin ligases compensate for the loss of Nedd4-1 in this tissue, and such a compensatory

effect may be more pronounced in adult mice compared to mice at and prior to the weaning age. A major candidate for such a compensatory effect is closely related Nedd4-2 (Nedd4L) [117]. A phylogenetic analysis shows that Nedd4-1 is the most primitive protein of the Nedd4 family, while Nedd4-2 appeared later, possibly as a result of gene duplication. All vertebrates have *Nedd4-1* and *Nedd4-2* genes. Nedd4-1 and Nedd4-2 share the same E2 ubiquitin-conjugating enzymes. Both Nedd4-1 and Nedd4-2 regulate ubiquitin-mediated trafficking, lysosomal or proteasomal degradation, and nuclear translocation of multiple proteins. Due to the similar affinity of WW domains in Nedd4-1 and Nedd4-2, they regulate some common targets, for example, the epithelial sodium channel (ENaC) [110, 180-182]. Redundancy/compensation between both proteins has indeed been demonstrated for the regulation of Wnt signaling and stem cell priming in the intestine through the degradation of Lgr5. This was revealed by the more severe phenotype of double compared to single knockout mice [130]. A similar genetic approach will unravel if Nedd4-1 and Nedd4-2 have overlapping functions in keratinocytes.

### 5.1.2 Keratinocyte-derived Nedd4-1 in wound healing

Histological and histomorphometric analysis of 3-day wounds revealed a delay in wound repair at this early stage in *Nedd4-1* cKO mice. In particular, the length of the wound epidermis was significantly reduced. This reflects a defect in keratinocyte migration, since the migration of keratinocytes precedes the proliferation of these cells, and proliferation of 3-day wound keratinocytes is still low [47]. At later stages of healing, keratinocytes behind the migrating epidermal tongue start to hyperproliferate, and this process was strongly reduced in the *Nedd4-1* cKO mice at day five after wounding. Therefore, less proliferating keratinocytes are available to refill the wound, resulting in delayed wound re-epithelialization.

Cutaneous wound healing involves a large number of tightly regulated growth factor and cytokine signals. Loss of Nedd4-1 might affect the expression/secretion of these growth factors and cytokines and/or their efficient signaling, thereby causing impaired wound healing. In the future, it will be interesting to determine if the loss of Nedd4-1 reduces the levels or activities of major growth factors and their receptors involved in wound re-epithelialization. Importantly we already showed that EGF receptor signaling is affected in Nedd4-1-deficient keratinocytes as revealed by the reduced and more transient Erk1/2 activation upon EGF-stimulation (see 5.4.1). This is important, since the EGFR is highly expressed in wound keratinocytes [175, 183], and its loss strongly affected wound re-epithelialization [184]. *Vice versa*, treatment of wounds with EGF or other members of the EGF family promoted wound healing in rodents [185, 186], and heparin-binding EGF acted synergistically with IGF-1, another growth factor present in the wound fluid, in

stimulating keratinocyte proliferation *in vitro* [187]. Impaired wound healing is also associated with abnormal expression of IGFs and their receptors [164, 188], which are expressed by keratinocytes, macrophages and some other inflammatory cells during wound healing [189]. Exogenous IGF-I also promoted wound healing in rodents, especially in combination with other growth factors [190]. Loss of Nedd4-1 may well cause impaired IGF-1 signaling in keratinocytes, as previously demonstrated for embryonic fibroblasts and HEK 293T cells [121, 191]. However, the upregulation of Nedd4-1 caused IGF-1 receptor protein degradation in neurons, resulting in neurodegeneration [192]. Therefore, it should be determined in the future if and how Nedd4-1 affects IGF-1 signaling in keratinocytes.

Surprisingly, loss of Nedd4-1 in keratinocytes also caused impaired wound contraction, a process that involves the action of fibroblasts/myofibroblasts. Therefore, it seems likely that keratinocytes produce secreted factors in a Nedd4-1-dependent manner, which affect the underlying fibroblasts. Our preliminary experiments suggest that the number of blood vessels is not significantly altered in the mutant mice, but a potential effect on fibroblasts/myofibroblasts remains to be determined. Future studies, such as co-culture of keratinocytes and fibroblasts, could determine if the impaired contraction is indeed associated with alterations in the keratinocyte/fibroblast cross-talk and if they are a consequence of defective fibroblast-myofibroblast differentiation. This would point to a potential role of the major myofibroblast-inducing factor, TGF- $\beta$  [164], in this phenotype. In addition, it will be interesting to see if other cells of the granulation tissue are also affected by the loss of Nedd4-1 in keratinocytes, including different types of immune cells.

Despite the delay in wound healing, the wounds eventually healed in the *Nedd4-1* cKO mice, suggesting that Nedd4-1 is dispensable for wound re-epithelialization. However, we cannot fully exclude the possibility that a few keratinocytes, which have escaped recombination, mainly contributed to re-epithelialization. This will require immunostaining of wounds from control and *Nedd4-1* cKO mice for Nedd4-1, RNAscope *in situ* hybridization and/or qRT-PCR analysis for *Nedd4-1* using RNA from isolated wound epidermis. Preliminary immunostainings were so far inconclusive, possibly because of the suboptimal quality of the available antibodies and their possible cross-reactivity with Nedd4-2. Therefore, it will be interesting to determine if the latter is upregulated in the wound epidermis of the K5cre-*Nedd4-1* cKO mice and may thus compensate for the lack of Nedd4-1.

There is as yet limited information on the role of ubiquitin ligases in mammalian wound healing, and our finding highlight the importance of protein ubiquitination in the process. Therefore, strategies to promote and maintain the activity of Nedd4-1 could be developed as a potential

therapeutic for the treatment of impaired wound healing. Our finding that fibroblasts also require Nedd4-1 for efficient proliferation and migration further supports such an approach.

The results obtained in this study were all obtained with mouse wounds and cultured mouse cells, and the relevance of our findings for the human situation remains to be determined. However, Nedd4-1 proteins in mice and humans are highly homologous, and they share about 86% protein sequence identity [193]. This high homology between the mouse and human proteins strongly suggests that the wound healing promoting activity of NEDD4-1 is conserved in humans. Interestingly, immunohistochemical staining showed that NEDD4-1 is ubiquitously expressed in normal human skin and particularly abundant in the granular cell layer of the epidermis and in dermal fibroblasts. In the future, the knock-down experiments in cultured keratinocytes and fibroblasts should be repeated with primary human cells. Most importantly, it will be interesting to determine the expression of NEDD4-1 in acute and chronic human wounds using immunofluorescence staining. Reduced expression of NEDD4-1 in chronic vs. acute human wounds would provide a further rationale for the use of compounds that promote NEDD4-1 expression or its activity for the treatment of impaired healing.

### 5.1.3 Nedd4-1 in UV-induced apoptosis

In addition to its role in wound healing, we also identified a previously unrecognized function of Nedd4-1 in the UVB response of keratinocytes. Thus, the number of apoptotic cells was strongly increased in the epidermis of *Nedd4-1* cKO mice upon UVB irradiation, indicating that Nedd4-1 protects keratinocytes from UV-induced apoptosis. This is most likely a cell-autonomous phenotype, which should be tested by UV irradiation of cultured primary keratinocytes from the mutant mice or of keratinocytes with Nedd4-1 knock-down. The role of Nedd4-1 in the protection from apoptosis is consistent with findings from others, who demonstrated increased apoptosis of bladder cancer cells upon knock-down of NEDD4-1, combined with reduced proliferation and migration of these cells [194]. In this study, knockdown of NEDD4-1 reduced the levels of the tumor suppressor PTEN and increased the levels of Notch-1. Future work should determine if Nedd4-1 protects keratinocytes and other cells from additional pro-apoptotic stimuli, such as DNA-damaging agents.

The targets of Nedd4-1, which are responsible for its UVB-protecting effect, are as yet unknown. It may involve different proteins, e.g., RNA polymerase II, which was shown to be ubiquitinated by Nedd4-1 in response to UV-induced DNA damage [195] or the impaired EGFR signaling, since UVB irradiation of keratinocytes activates the EGFR [196].

While our results revealed an anti-apoptotic role of Nedd4-1 after UVB irradiation of keratinocytes, it may promote apoptosis in other cells and under different conditions. Thus, NEDD4-1 directly ubiquitinated caspase-9 in the Patched complex, which is required for Patched-mediated apoptosis [197]. Furthermore, “sensitive to apoptosis gene” (SAG) was initially identified as a potential NEDD4-1 substrate in a proteomics study [198] and validated by another group [199], who showed that this protein mediates NEDD4-1-induced chemosensitization of cancer cells. Therefore, the role of NEDD4-1 in apoptosis is likely to be cell-type and context-dependent.

## 5.2 Role of Nedd4-1 in fibroblasts

To obtain mice lacking Nedd4-1 in fibroblasts, we used Col1a2-Cre mice, which induce the deletion of floxed gene loci in all mesenchymal cells [148]. These Cre mice were used because mice that selectively target skin fibroblasts are unfortunately not available. While mice with heterozygous knockout of *Nedd4-1* did not reveal apparent abnormalities and were viable and fertile, the progeny of our breedings showed an unexpected ratio of the different genotypes at the weaning age, and the double mutant mice died *in utero* or shortly after birth.

Previous studies using *Nedd4-1* knockout mice identified important functions of this protein in the development of different tissues and organs. Two independently generated *Nedd4-1* knockout mouse lines exhibited embryonic lethality with significant vascular malformations and heart development defects or neonatal lethality, which was accompanied by delayed embryonic development, reduced body weight and growth [121, 122]. Embryonic fibroblasts isolated from those mice had an impaired mitogenic activity [121]. All these findings indicate that Nedd4-1 is necessary for cell proliferation and organ development. Considering these previous findings, the early lethality of our Col1a2-*Nedd4-1* cKO mice, in which the deletion of *Nedd4-1* occurred in mesenchymal cells of various organs, did not come as a surprise.

To determine if the knockout mice survive until late gestation, timed matings were set up, and embryos were analyzed at day 18.5 of pregnancy. Here, we obtained the knockout embryos at the expected Mendelian ratio. We also obtained newborn knockout pups, but they were very small and had difficulties in moving. Therefore, they had to be sacrificed immediately due to animal welfare regulations. Histological analysis of the E18.5 embryos showed severe developmental defects in several organs. Besides various other abnormalities, our preliminary data suggest that lung development is impaired in Col1a2cre-*Nedd4-1* cKO mice, which may lead to respiratory failure. To further test this possibility, a more detailed analysis of the embryonic lung will be required, including immunostaining of the lung alveoli for several alveolar markers, analysis of



cell proliferation in the lung mesenchyme and adjacent epithelium using Ki67 staining, and immunostaining for different extracellular matrix proteins, including collagen type 1. It may well be that the deficiency in *Nedd4-1* inhibits the proliferation of fibroblasts in the lung and other organs as suggested by our *in vitro* experiments and the published study [121]. In the skin, we observed reduced dermal cellularity and a less dense ECM. These abnormalities could also be explained by the impaired migration and proliferation of fibroblasts. It remains to be determined if the effect on the matrix is simply a consequence of a reduced number of fibroblasts or if matrix production is impaired in *Nedd4-1*-deficient fibroblasts. This should be tested in 2D or 3D cell culture models. Here, equal numbers of control and *Nedd4-1*-deficient fibroblasts should be seeded, and the amount of deposited ECM proteins should be quantified.

Additional tissues that should be further characterized in the future are bone and heart, since they appeared histologically abnormal in the E18.5 embryos. This will require a detailed analysis of the embryos at different stages of development. Impaired bone development could be a direct consequence of the deletion of *Nedd4-1* in osteoblasts, since the *Col1a2* promoter is active in these cells during development [148]. Alternatively, fibroblasts of the bone may be affected, resulting - for example - in alterations of ECM. Bone cells express high levels of IGF-1, and local and especially endocrine IGF-1 actions are involved in regulating bone growth [200]. Since *Nedd4-1* is an important regulator of IGF-1 and insulin signaling [121], this mechanism may indirectly contribute to the bone abnormalities. Overall the mutant mice offer the possibility to study the role of *Nedd4-1* in mesenchymal cells in the development of different tissues and organs.

To overcome the lethality of *Col1a2cre-Nedd4-1 cKO* mice and to study *Nedd4-1* function in the adult organism, we also generated a tamoxifen-inducible mesenchyme-specific *Nedd4-1* knockout (*Col1a2-CreER*) mouse line [201]. Upon activation of a Cre recombinase–human estrogen receptor fusion protein with tamoxifen, Cre activity is induced, resulting in the deletion of the transgene in mesenchymal cells in a time-controlled manner [201]. Deletion of the gene in adult mice prior to and at different time points after wounding would allow us to study *Nedd4-1* function in fibroblasts at different stages of postembryonic development as well as during wound healing and scar formation. Unfortunately, we could not characterize these mice for time reasons, but this is an important task for the future.

## 5.3 Potential role of Nedd4-1 in skin cancer

Several findings obtained in this study point to a potential role of Nedd4-1 in skin carcinogenesis. These include the important function of this protein in keratinocyte and fibroblast proliferation and migration as well as in the protection from UVB-induced apoptosis. All these results suggest a pro-tumorigenic function of Nedd4-1 in keratinocytes and possibly also in fibroblasts by promoting the formation of cancer-associated fibroblasts (CAFs). Consistent with a potential pro-tumorigenic effect of Nedd4-1, it was shown to activate important signaling pathways involved in tumorigenesis, such as the TGF- $\beta$ , EGF, IGF, vascular endothelial growth factor, stromal cell-derived factor-1, and TNF- $\alpha$  signaling pathways [143, 202]. Furthermore, data from the Human Protein Atlas suggest that NEDD4-1 overexpression is a marker for poor prognosis in renal and lung cancer (<https://www.proteinatlas.org/ENSG00000069869-NEDD4/pathology>). Therefore, it will be interesting to determine if the loss of Nedd4-1 in keratinocytes and/or fibroblasts protects from the development of chemically- or UV-induced skin tumors. These studies could be performed with the *K5cre-Nedd4-1* mice and the *Col1a2-ER-Nedd4-1* cKO mice. In addition, we could generate squamous cell carcinoma (SCC) cell lines with NEDD4-1 knock-down or knockout or overexpression and determine their tumor-forming potential in mouse xenograft experiments. Similar studies could also be performed with NEDD4-1-deficient and control fibroblasts, and co-injection of these cells with wild-type SCC cells. In a preliminary experiment, we injected SCC13 cells together with Nedd4-1 knock-down or control fibroblasts into the ear skin of immuno-deficient NOD/Scid mice. The ear tumor size was slightly smaller in the Nedd4-1 knock-down group, but the difference was not statistically significant (data not shown). It may well be that the siRNA-mediated knock-down was too transient, and therefore, the experiment should be repeated with the cells that constitutively express Nedd4-1 shRNA. In addition to these functional studies, it will be important to analyze *NEDD4-1* expression levels in CAFs of various human tumors based on published CAF RNA sequencing data. If such studies indeed reveal a tumor-promoting effect of NEDD4-1 in the skin, blocking of NEDD4-1 activity using small molecule inhibitors may be a potential strategy for cancer prevention and/or therapy. Such inhibitors are available [203, 204] and have been proposed as anticancer therapeutics [171].

## 5.4 Mechanism of action of Nedd4-1 in skin cells

### 5.4.1 Nedd4-1 regulates skin cell behavior

We found that knock-down of Nedd4-1 reduces proliferation and migration of both keratinocytes and fibroblasts, although the underlying mechanisms are as yet unclear. Our preliminary data suggest alterations in the expression of different cyclins and cyclin-dependent kinase inhibitors in the Nedd4-1 knock-down cells. These cells also exhibited an increase in the number of cells in the G1 phase and a decrease in the total number of cells in the G2 phase (data not shown). Therefore, knock-down of Nedd4-1 might lead to a prolonged G1/S phase, which ultimately reduces the overall proliferation rate. It is as yet unclear if Nedd4-1 directly targets cyclins or other cell cycle regulators or if this is the consequence of the ubiquitination of one or more other proteins.

Another group reported that large tumor suppressor kinase 1 (LATS1) directly binds NEDD4-1, leading to its ubiquitination and subsequent degradation. LATS1 is a serine/threonine kinase acting as a cell cycle regulator, and it is also a negative regulator of YAP1 in the Hippo signaling pathway [205]. Degradation of LATS1 is therefore expected to increase the nuclear accumulation and transcriptional activity of YAP and subsequently promote cell cycle progression. Our preliminary data showed that LATS1 was slightly down-regulated in Nedd4-1 overexpressing cells. Furthermore, Notch-1, an important regulator of keratinocyte differentiation [206], has been shown to interact with NEDD4-1 [207]. This resulted in the ubiquitination of Notch-1, thereby promoting its endocytosis and turnover [207]. It is of particular interest to check if Nedd4-1 targets these potential candidates and regulates these signaling pathways in keratinocytes and/or fibroblasts. While the role of these potential Nedd4-1 targets in the proliferation defect of Nedd4-1-deficient cells has not been tested, we showed that EGF-induced Erk1/2 activation is reduced and more transient in Nedd4-1-deficient keratinocytes and fibroblasts. Due to the important role of EGFR-Erk1/2 signaling in keratinocyte and fibroblast proliferation and migration [161, 162, 208], this finding is likely to explain at least in part the phenotype of the Nedd4-1 knock-down/knockout cells and mice.

It has previously been shown for other cell types, including hepatocytes, that the impaired EGFR signaling results from impaired receptor internalization that is caused by a deficiency in the monoubiquitination of the adaptor protein Eps15 [50, 134, 156, 209]. We found that knock-down of Nedd4-1 did not change the total EGFR and Eps15 levels, but reduced and shortened the EGF-mediated increase in Erk1/2 phosphorylation in cultured keratinocytes and fibroblasts. We noticed

that in keratinocytes, this event happens during the first 10 min, but not at later time points, indicating that it is a transient process. Important future experiments will be to check the internalization of the EGFR and the ubiquitination of Eps15 after EGF stimulation in control and Nedd4-1 knockout/knock-down cells.

Eps15 is not the only adaptor protein involved in EGFR internalization. For example, another UIM-containing protein, Hgs (a mammalian homologue of a yeast vacuolar sorting adaptor), interacts with NEDD4 to target the EGFR receptor for ubiquitination to induce endocytosis [137]. This UIM is often found in endocytic adaptors. In preliminary experiments, we observed punctuated staining of Nedd4-1 in keratinocytes (data not shown), potentially indicating its accumulation in endosomes. Therefore, Nedd4-1 may well affect endocytosis of different transmembrane receptors via the ubiquitination of different adaptor proteins.

#### 5.4.2 Finding targets of Nedd4-1 in skin cells

As described above, the molecular mechanisms of action of Nedd4-1 in skin homeostasis and repair are so far unclear. A role of impaired receptor endocytosis and/or recycling and subsequent alterations in growth factor signaling is likely to be involved, in particular given the important function of ubiquitination at various steps of receptor endocytosis, recycling and/or degradation [210]. The adaptor protein Eps15 is a documented target of Nedd4-1, which regulates receptor endocytosis. However, it is unlikely that impaired Eps15 ubiquitination is the only cause of the *in vitro* and *in vivo* phenotypes that we observed. Therefore, it will be important to identify other Nedd4-1 targets in fibroblasts and keratinocytes and to analyze their precise intracellular localization and function. From the literature and also our data, we know that Nedd4-1 mainly localizes in the cytoplasm. Furthermore, it is also localized in the perinuclear region [119]. To further investigate the subcellular localization of Nedd4-1, nuclear/cytoplasmic fractionation of keratinocytes and fibroblasts and isolation of endosomes and other organelles should be performed. In particular, an unbiased screen should be performed to identify its targets in keratinocytes and fibroblasts. This could involve the approaches described below.

a.) To identify Nedd4-1 binding partners (including its ubiquitinated substrates), we could perform a pulldown of Nedd4-1 using a specific antibody, followed by the identification of interacting proteins by mass spectrometry. BioID technology and APEX2 tagging assay could also be good options to identify binding partners of Nedd4-1 [211, 212]. When studying proteins that interact with Nedd4-1, its subcellular location, ubiquitination reaction duration and any

treatments of the cells need to be considered. Sometimes the interaction and concomitant ubiquitination might be transient and only occur under certain stimulation conditions. For example, Nedd4-1 targets Eps15 at the cell membrane to regulate EGFR internalization after EGF stimulation. Therefore, a potential Nedd4-1-Eps15 interaction could be studied using isolated cell membranes prior to and following EGF treatment.

b.) In a second step, it has to be tested if the identified binding partners are indeed ubiquitination substrates. Based on the techniques mentioned above to identify the ubiquitinated proteins, such approaches could be facilitated by the use of tagged ubiquitin derivatives (e.g., biotinylated, His-, GST-, Myc-, Flag- or HA-tagged ubiquitin) [213], or using commercially available affinity reagents.

To specifically identify those binding partners, which are also ubiquitinated, additionally, an affinity purification approach called ligase-trapping could be performed. Here, an E3-ligase polyubiquitin-binding domain fusion is used, and proteins that bind to the ligase trap are captured. Affinity purification is subsequently performed under denaturing conditions to enrich proteins that are conjugated with a histidine-tagged ubiquitin. The latter can then be identified by mass spectrometry [214].

An alternative option is the use of the UbiQapture-Q matrix, which allows specific capturing of ubiquitinated proteins [215, 216]. This technology could be used for the isolation of mono-, multi-, and polyubiquitinated targets. Another method called Ubiquitin-Activated Interaction Traps (UBAITs) can also be used to trap covalent interactions between ubiquitin and target proteins [217]. By adding inhibitors for deubiquitinating enzymes (e.g., N-ethylmaleimide) and proteasome inhibitors (e.g., MG-132 or epoxomicin), the yield of ubiquitinated proteins could be increased [218].

c.) In addition to the identification of ubiquitinated substrates, it is important to determine if they are mono-, multi-mono- or poly-ubiquitinated and to identify the ubiquitinated sites in the substrates. For this purpose, link-specific antibodies against M1, K11, K27, K48 and K63 linkages are available, and high-affinity specific affimers have been generated against K6 and K33/K11 linkages [219]. Alternatively, certain ubiquitination sites in the protein could be mutated.

The most powerful approach for the identification of ubiquitinated proteins is ubiquitin proteomics, a mass spectrometry-based approach [220], which allows to determine the topology of the polyubiquitin chains and ubiquitination sites of the protein [221]. For this purpose, an anti-Gyl-Gly (GG) remnant (K (Lys)- $\epsilon$ -GG)-specific antibody has been used [222, 223]. This antibody recognizes the GG remnants that are attached to conjugated Lys specifically. Then, after trypsin

digestion, ubiquitinated peptides can be enriched by immunoprecipitation and analyzed by MS. The ubiquitin modification is shown in unique mass spectrometry spectra. In addition, a new technique includes a simple chemical labeling and analysis using a Quadrupole-Time-Of-Flight (Q-TOF) mass spectrometer to analyze ubiquitinated proteins [224]. Combining liquid chromatography with tandem MS, it could quantify both the precursor and the product, enhancing the isopeptide detection. This allows the identification and quantification of ubiquitinated proteins [225].

d.) For the polyubiquitinated targets of Nedd4-1, which are subsequently degraded via the proteasome, we could perform quantitative proteomics using lysates from Nedd4-1 knock-down or knockout cells or cells treated with a Nedd4-1 inhibitor. This should be performed in the presence or absence of a proteasome inhibitor. Proteins, which increase in cells with Nedd4-1 loss-of-function in a proteasome-dependent manner are potential polyubiquitination targets. Their Nedd4-1-dependent polyubiquitination could then be verified by immunoprecipitation of the protein of interest, followed by Western blot analysis for ubiquitin. Such experiments could also be performed with predicted ubiquitination targets.

These studies would provide important insight into the roles and mechanisms of action of Nedd4-1 in different cell types and under different conditions. They should be complemented by the analysis of upstream regulators of Nedd4-1 under these circumstances.

## 5.5 Conclusion

The data obtained in this thesis project identified various novel functions of Nedd4-1 in skin development and homeostasis. We identified a crucial function of Nedd4-1 in mesenchymal cells in embryonic development and organogenesis. In addition, we demonstrate important roles of this protein in tissue repair and UV response, suggesting targeting NEDD4-1 as a strategy for the treatment of impaired wound healing and other skin diseases.

# Complete Bibliography

1. Tobin, D.J., *Biochemistry of human skin--our brain on the outside*. Chem Soc Rev, 2006. **35**(1): p. 52-67.
2. Fuchs, E., *Scratching the surface of skin development*. Nature, 2007. **445**(7130): p. 834-42.
3. Arnold, S.J. and E.J. Robertson, *Making a commitment: cell lineage allocation and axis patterning in the early mouse embryo*. Nat Rev Mol Cell Biol, 2009. **10**(2): p. 91-103.
4. Yousef, H., M. Alhajj, and S. Sharma, *Anatomy, Skin (Integument), Epidermis*, in *StatPearls*. 2020: Treasure Island (FL).
5. Pasparakis, M., I. Haase, and F.O. Nestle, *Mechanisms regulating skin immunity and inflammation*. Nat Rev Immunol, 2014. **14**(5): p. 289-301.
6. Pastar, I., et al., *Epithelialization in Wound Healing: A Comprehensive Review*. Adv Wound Care (New Rochelle), 2014. **3**(7): p. 445-464.
7. Lamouille, S., J. Xu, and R. Derynck, *Molecular mechanisms of epithelial-mesenchymal transition*. Nat Rev Mol Cell Biol, 2014. **15**(3): p. 178-96.
8. Simpson, C.L., D.M. Patel, and K.J. Green, *Deconstructing the skin: cytoarchitectural determinants of epidermal morphogenesis*. Nat Rev Mol Cell Biol, 2011. **12**(9): p. 565-80.
9. Alonso, L. and E. Fuchs, *Stem cells of the skin epithelium*. Proc Natl Acad Sci U S A, 2003. **100** Suppl 1: p. 11830-5.
10. Moll, I., et al., *Human Merkel cells--aspects of cell biology, distribution and functions*. Eur J Cell Biol, 2005. **84**(2-3): p. 259-71.
11. Sidhu, G.S., P. Chandra, and N.D. Cassai, *Merkel cells, normal and neoplastic: an update*. Ultrastruct Pathol, 2005. **29**(3-4): p. 287-94.
12. Deckers, J., H. Hammad, and E. Hoste, *Langerhans Cells: Sensing the Environment in Health and Disease*. Front Immunol, 2018. **9**: p. 93.
13. Fuchs, E. and S. Raghavan, *Getting under the skin of epidermal morphogenesis*. Nat Rev Genet, 2002. **3**(3): p. 199-209.
14. Denecker, G., et al., *Caspase-14 reveals its secrets*. J Cell Biol, 2008. **180**(3): p. 451-8.
15. Kabashima, K., et al., *The immunological anatomy of the skin*. Nat Rev Immunol, 2019. **19**(1): p. 19-30.
16. Rognoni, E. and F.M. Watt, *Skin Cell Heterogeneity in Development, Wound Healing, and Cancer*. Trends Cell Biol, 2018. **28**(9): p. 709-722.
17. Thulabandu, V., D. Chen, and R.P. Atit, *Dermal fibroblast in cutaneous development and healing*. Wiley Interdiscip Rev Dev Biol, 2018. **7**(2).
18. Werner, S., et al., *The function of KGF in morphogenesis of epithelium and reepithelialization of wounds*. Science, 1994. **266**(5186): p. 819-22.
19. Werner, S., et al., *Large induction of keratinocyte growth factor expression in the dermis during wound healing*. Proc Natl Acad Sci U S A, 1992. **89**(15): p. 6896-900.
20. Visscher, M. and V. Narendran, *The Ontogeny of Skin*. Adv Wound Care (New Rochelle), 2014. **3**(4): p. 291-303.
21. Paus, R. and G. Cotsarelis, *The biology of hair follicles*. N Engl J Med, 1999. **341**(7): p. 491-7.
22. Stenn, K.S., et al., *Hair follicle growth controls*. Dermatol Clin, 1996. **14**(4): p. 543-58.
23. Stenn, K.S. and R. Paus, *Controls of hair follicle cycling*. Physiol Rev, 2001. **81**(1): p. 449-494.
24. Morris, R.J., et al., *Capturing and profiling adult hair follicle stem cells*. Nat Biotechnol, 2004. **22**(4): p. 411-7.

25. Muller-Rover, S., et al., *A comprehensive guide for the accurate classification of murine hair follicles in distinct hair cycle stages*. J Invest Dermatol, 2001. **117**(1): p. 3-15.
26. Alonso, L. and E. Fuchs, *The hair cycle*. J Cell Sci, 2006. **119**(Pt 3): p. 391-3.
27. Zouboulis, C.C., *Acne and sebaceous gland function*. Clin Dermatol, 2004. **22**(5): p. 360-6.
28. Saga, K., *Structure and function of human sweat glands studied with histochemistry and cytochemistry*. Prog Histochem Cytochem, 2002. **37**(4): p. 323-86.
29. Proksch, E., J.M. Brandner, and J.M. Jensen, *The skin: an indispensable barrier*. Exp Dermatol, 2008. **17**(12): p. 1063-72.
30. Baroni, A., et al., *Structure and function of the epidermis related to barrier properties*. Clin Dermatol, 2012. **30**(3): p. 257-62.
31. Madison, K.C., *Barrier function of the skin: "la raison d'etre" of the epidermis*. J Invest Dermatol, 2003. **121**(2): p. 231-41.
32. Mostafa, W.Z. and R.A. Hegazy, *Vitamin D and the skin: Focus on a complex relationship: A review*. J Adv Res, 2015. **6**(6): p. 793-804.
33. Zielins, E.R., et al., *The role of stem cells in limb regeneration*. Organogenesis, 2016. **12**(1): p. 16-27.
34. Longaker, M.T., et al., *Studies in fetal wound healing, VI. Second and early third trimester fetal wounds demonstrate rapid collagen deposition without scar formation*. J Pediatr Surg, 1990. **25**(1): p. 63-8; discussion 68-9.
35. Velnar, T., T. Bailey, and V. Smrkolj, *The wound healing process: an overview of the cellular and molecular mechanisms*. J Int Med Res, 2009. **37**(5): p. 1528-42.
36. Hubner, G., et al., *Differential regulation of pro-inflammatory cytokines during wound healing in normal and glucocorticoid-treated mice*. Cytokine, 1996. **8**(7): p. 548-56.
37. Singer, A.J. and R.A. Clark, *Cutaneous wound healing*. N Engl J Med, 1999. **341**(10): p. 738-46.
38. Garlick, J.A. and L.B. Taichman, *Fate of human keratinocytes during reepithelialization in an organotypic culture model*. Lab Invest, 1994. **70**(6): p. 916-24.
39. Litjens, S.H., J.M. de Pereda, and A. Sonnenberg, *Current insights into the formation and breakdown of hemidesmosomes*. Trends Cell Biol, 2006. **16**(7): p. 376-83.
40. Raja, et al., *Wound re-epithelialization: modulating keratinocyte migration in wound healing*. Front Biosci, 2007. **12**: p. 2849-68.
41. Hertle, M.D., et al., *Aberrant integrin expression during epidermal wound healing and in psoriatic epidermis*. J Clin Invest, 1992. **89**(6): p. 1892-901.
42. Paladini, R.D., et al., *Onset of re-epithelialization after skin injury correlates with a reorganization of keratin filaments in wound edge keratinocytes: defining a potential role for keratin 16*. J Cell Biol, 1996. **132**(3): p. 381-97.
43. Opalenik, S.R. and J.M. Davidson, *Fibroblast differentiation of bone marrow-derived cells during wound repair*. FASEB J, 2005. **19**(11): p. 1561-3.
44. Werner, S., T. Krieg, and H. Smola, *Keratinocyte-fibroblast interactions in wound healing*. J Invest Dermatol, 2007. **127**(5): p. 998-1008.
45. Lovvorn, H.N., 3rd, et al., *Relative distribution and crosslinking of collagen distinguish fetal from adult sheep wound repair*. J Pediatr Surg, 1999. **34**(1): p. 218-23.
46. Levenson, S.M., et al., *The Healing of Rat Skin Wounds*. Ann Surg, 1965. **161**: p. 293-308.
47. Gurtner, G.C., et al., *Wound repair and regeneration*. Nature, 2008. **453**(7193): p. 314-21.
48. Eriksson, A., et al., *PDGF alpha- and beta-receptors activate unique and common signal transduction pathways*. EMBO J, 1992. **11**(2): p. 543-50.
49. Frank, S., M. Madlener, and S. Werner, *Transforming growth factors beta1, beta2, and beta3 and their receptors are differentially regulated during normal and impaired wound healing*. J Biol Chem, 1996. **271**(17): p. 10188-93.



50. Bachofner, M., et al., *Large-Scale Quantitative Proteomics Identifies the Ubiquitin Ligase Nedd4-1 as an Essential Regulator of Liver Regeneration*. Dev Cell, 2017. **42**(6): p. 616-625 e8.
51. Mead, M.N., *Benefits of sunlight: a bright spot for human health*. Environ Health Perspect, 2008. **116**(4): p. A160-7.
52. Polefka, T.G., et al., *Effects of solar radiation on the skin*. J Cosmet Dermatol, 2012. **11**(2): p. 134-43.
53. Svobodova, A., D. Walterova, and J. Vostalova, *Ultraviolet light induced alteration to the skin*. Biomed Pap Med Fac Univ Palacky Olomouc Czech Repub, 2006. **150**(1): p. 25-38.
54. Maverakis, E., et al., *Light, including ultraviolet*. J Autoimmun, 2010. **34**(3): p. J247-57.
55. Schroeder, P., J. Haendeler, and J. Krutmann, *The role of near infrared radiation in photoaging of the skin*. Exp Gerontol, 2008. **43**(7): p. 629-32.
56. Krutmann, J., *Ultraviolet A radiation-induced biological effects in human skin: relevance for photoaging and photodermatitis*. J Dermatol Sci, 2000. **23 Suppl 1**: p. S22-6.
57. Phan, T.A., et al., *Spectral and dose dependence of ultraviolet radiation-induced immunosuppression*. Front Biosci, 2006. **11**: p. 394-411.
58. Helfrich, Y.R., D.L. Sachs, and J.J. Voorhees, *Overview of skin aging and photoaging*. Dermatol Nurs, 2008. **20**(3): p. 177-83; quiz 184.
59. Matsumura, Y. and H.N. Ananthaswamy, *Toxic effects of ultraviolet radiation on the skin*. Toxicol Appl Pharmacol, 2004. **195**(3): p. 298-308.
60. Wondrak, G.T., M.K. Jacobson, and E.L. Jacobson, *Endogenous UVA-photosensitizers: mediators of skin photodamage and novel targets for skin photoprotection*. Photochem Photobiol Sci, 2006. **5**(2): p. 215-37.
61. Lee, C.H., et al., *Molecular Mechanisms of UV-Induced Apoptosis and Its Effects on Skin Residential Cells: The Implication in UV-Based Phototherapy*. Int J Mol Sci, 2013. **14**(3): p. 6414-35.
62. Yokoyama, H. and R. Mizutani, *Structural biology of DNA (6-4) photoproducts formed by ultraviolet radiation and interactions with their binding proteins*. Int J Mol Sci, 2014. **15**(11): p. 20321-38.
63. D'Errico, M., et al., *Cell type and DNA damage specific response of human skin cells to environmental agents*. Mutat Res, 2007. **614**(1-2): p. 37-47.
64. Pfeifer, G.P., *Formation and processing of UV photoproducts: effects of DNA sequence and chromatin environment*. Photochem Photobiol, 1997. **65**(2): p. 270-83.
65. Schoppy, D.W., Y. Ruzankina, and E.J. Brown, *Removing all obstacles: a critical role for p53 in promoting tissue renewal*. Cell Cycle, 2010. **9**(7): p. 1313-9.
66. Zhan, Q., et al., *Abrogation of p53 function affects gadd gene responses to DNA base-damaging agents and starvation*. DNA Cell Biol, 1996. **15**(10): p. 805-15.
67. Pincelli, C. and A. Marconi, *Keratinocyte stem cells: friends and foes*. J Cell Physiol, 2010. **225**(2): p. 310-5.
68. Bang, B., et al., *In vivo UVB irradiation induces clustering of Fas (CD95) on human epidermal cells*. Exp Dermatol, 2003. **12**(6): p. 791-8.
69. Tobin, D., M. van Hogerlinden, and R. Toftgard, *UVB-induced association of tumor necrosis factor (TNF) receptor 1/TNF receptor-associated factor-2 mediates activation of Rel proteins*. Proc Natl Acad Sci U S A, 1998. **95**(2): p. 565-9.
70. Qin, J.Z., et al., *Pathways involved in proliferating, senescent and immortalized keratinocyte cell death mediated by two different TRAIL preparations*. Exp Dermatol, 2002. **11**(6): p. 573-83.
71. Qin, J.Z., et al., *Low-dose UV-radiation sensitizes keratinocytes to TRAIL-induced apoptosis*. J Cell Physiol, 2004. **200**(1): p. 155-66.

72. Kroemer, G., *The proto-oncogene Bcl-2 and its role in regulating apoptosis*. Nat Med, 1997. **3**(6): p. 614-20.
73. Riedl, S.J. and G.S. Salvesen, *The apoptosome: signalling platform of cell death*. Nat Rev Mol Cell Biol, 2007. **8**(5): p. 405-13.
74. Assefa, Z., et al., *Ultraviolet B radiation-induced apoptosis in human keratinocytes: cytosolic activation of procaspase-8 and the role of Bcl-2*. FEBS Lett, 2003. **540**(1-3): p. 125-32.
75. Van Laethem, A., et al., *Activation of p38 MAPK is required for Bax translocation to mitochondria, cytochrome c release and apoptosis induced by UVB irradiation in human keratinocytes*. FASEB J, 2004. **18**(15): p. 1946-8.
76. Lee, C.H., et al., *Effects and interactions of low doses of arsenic and UVB on keratinocyte apoptosis*. Chem Res Toxicol, 2004. **17**(9): p. 1199-205.
77. Birch-Machin, M.A. and H. Swalwell, *How mitochondria record the effects of UV exposure and oxidative stress using human skin as a model tissue*. Mutagenesis, 2010. **25**(2): p. 101-7.
78. Lai, W.W., et al., *Synergistic phototoxic effects of glycolic acid in a human keratinocyte cell line (HaCaT)*. J Dermatol Sci, 2011. **64**(3): p. 191-8.
79. Liu, C.Y., C.F. Lee, and Y.H. Wei, *Role of reactive oxygen species-elicited apoptosis in the pathophysiology of mitochondrial and neurodegenerative diseases associated with mitochondrial DNA mutations*. J Formos Med Assoc, 2009. **108**(8): p. 599-611.
80. Paz, M.L., et al., *Mitochondrial dysfunction and cellular stress progression after ultraviolet B irradiation in human keratinocytes*. Photodermatol Photoimmunol Photomed, 2008. **24**(3): p. 115-22.
81. Schroeder, P., et al., *Partial depletion of mitochondrial DNA from human skin fibroblasts induces a gene expression profile reminiscent of photoaged skin*. J Invest Dermatol, 2008. **128**(9): p. 2297-303.
82. Ziegler, A., et al., *Sunburn and p53 in the onset of skin cancer*. Nature, 1994. **372**(6508): p. 773-6.
83. Pierceall, W.E., M.L. Kripke, and H.N. Ananthaswamy, *N-ras mutation in ultraviolet radiation-induced murine skin cancers*. Cancer Res, 1992. **52**(14): p. 3946-51.
84. Holley, A.K. and D.K. St Clair, *Watching the watcher: regulation of p53 by mitochondria*. Future Oncol, 2009. **5**(1): p. 117-30.
85. Wu, Y., et al., *Regulation of Bax activation and apoptotic response to UV irradiation by p53 transcription-dependent and -independent pathways*. Cancer Lett, 2008. **271**(2): p. 231-9.
86. Brady, C.A. and L.D. Attardi, *p53 at a glance*. J Cell Sci, 2010. **123**(Pt 15): p. 2527-32.
87. Jain, A.K. and M.C. Barton, *Making sense of ubiquitin ligases that regulate p53*. Cancer Biol Ther, 2010. **10**(7): p. 665-72.
88. Wade, M., Y.V. Wang, and G.M. Wahl, *The p53 orchestra: Mdm2 and Mdmx set the tone*. Trends Cell Biol, 2010. **20**(5): p. 299-309.
89. Huang, H. and D.J. Tindall, *Regulation of FOXO protein stability via ubiquitination and proteasome degradation*. Biochim Biophys Acta, 2011. **1813**(11): p. 1961-4.
90. Marine, J.C. and G. Lozano, *Mdm2-mediated ubiquitylation: p53 and beyond*. Cell Death Differ, 2010. **17**(1): p. 93-102.
91. Zhu, Y., et al., *Ribosomal protein S7 is both a regulator and a substrate of MDM2*. Mol Cell, 2009. **35**(3): p. 316-26.
92. Inuzuka, H., et al., *Phosphorylation by casein kinase I promotes the turnover of the Mdm2 oncoprotein via the SCF(beta-TRCP) ubiquitin ligase*. Cancer Cell, 2010. **18**(2): p. 147-59.
93. Melino, G., R.A. Knight, and G. Cesareni, *Degradation of p63 by Itch*. Cell Cycle, 2006. **5**(16): p. 1735-9.
94. Hershko, A. and A. Ciechanover, *The ubiquitin system*. Annu Rev Biochem, 1998. **67**: p. 425-79.

95. Hicke, L. and R. Dunn, *Regulation of membrane protein transport by ubiquitin and ubiquitin-binding proteins*. Annu Rev Cell Dev Biol, 2003. **19**: p. 141-72.
96. Komander, D. and M. Rape, *The ubiquitin code*. Annu Rev Biochem, 2012. **81**: p. 203-29.
97. Metzger, M.B., et al., *RING-type E3 ligases: master manipulators of E2 ubiquitin-conjugating enzymes and ubiquitination*. Biochim Biophys Acta, 2014. **1843**(1): p. 47-60.
98. Li, W., et al., *Genome-wide and functional annotation of human E3 ubiquitin ligases identifies MULAN, a mitochondrial E3 that regulates the organelle's dynamics and signaling*. PLoS One, 2008. **3**(1): p. e1487.
99. Huijbregtse, J.M., et al., *A family of proteins structurally and functionally related to the E6-AP ubiquitin-protein ligase*. Proc Natl Acad Sci U S A, 1995. **92**(11): p. 5249.
100. Huang, L., et al., *Structure of an E6AP-Ubch7 complex: insights into ubiquitination by the E2-E3 enzyme cascade*. Science, 1999. **286**(5443): p. 1321-6.
101. Galan, J.M. and R. Haguenaer-Tsapis, *Ubiquitin lys63 is involved in ubiquitination of a yeast plasma membrane protein*. EMBO J, 1997. **16**(19): p. 5847-54.
102. Plant, P.J., et al., *Apical membrane targeting of Nedd4 is mediated by an association of its C2 domain with annexin XIIIb*. J Cell Biol, 2000. **149**(7): p. 1473-84.
103. Dunn, R., et al., *The C2 domain of the Rsp5 ubiquitin ligase binds membrane phosphoinositides and directs ubiquitination of endosomal cargo*. J Cell Biol, 2004. **165**(1): p. 135-44.
104. Staub, O., et al., *WW domains of Nedd4 bind to the proline-rich PY motifs in the epithelial Na<sup>+</sup> channel deleted in Liddle's syndrome*. EMBO J, 1996. **15**(10): p. 2371-80.
105. Kanelis, V., D. Rotin, and J.D. Forman-Kay, *Solution structure of a Nedd4 WW domain-ENaC peptide complex*. Nat Struct Biol, 2001. **8**(5): p. 407-12.
106. Scheffner, M. and S. Kumar, *Mammalian HECT ubiquitin-protein ligases: biological and pathophysiological aspects*. Biochim Biophys Acta, 2014. **1843**(1): p. 61-74.
107. Ingham, R.J., G. Gish, and T. Pawson, *The Nedd4 family of E3 ubiquitin ligases: functional diversity within a common modular architecture*. Oncogene, 2004. **23**(11): p. 1972-84.
108. Marchler-Bauer, A., et al., *CDD: a database of conserved domain alignments with links to domain three-dimensional structure*. Nucleic Acids Res, 2002. **30**(1): p. 281-3.
109. Marchler-Bauer, A., et al., *CDD: a curated Entrez database of conserved domain alignments*. Nucleic Acids Res, 2003. **31**(1): p. 383-7.
110. Harvey, K.F., et al., *The Nedd4-like protein KIAA0439 is a potential regulator of the epithelial sodium channel*. J Biol Chem, 2001. **276**(11): p. 8597-601.
111. Kamynina, E., C. Tauxe, and O. Staub, *Distinct characteristics of two human Nedd4 proteins with respect to epithelial Na<sup>+</sup> channel regulation*. Am J Physiol Renal Physiol, 2001. **281**(3): p. F469-77.
112. Fotia, A.B., et al., *The role of individual Nedd4-2 (KIAA0439) WW domains in binding and regulating epithelial sodium channels*. FASEB J, 2003. **17**(1): p. 70-2.
113. Goel, P., J.A. Manning, and S. Kumar, *NEDD4-2 (NEDD4L): the ubiquitin ligase for multiple membrane proteins*. Gene, 2015. **557**(1): p. 1-10.
114. Kumar, S., Y. Tomooka, and M. Noda, *Identification of a set of genes with developmentally down-regulated expression in the mouse brain*. Biochem Biophys Res Commun, 1992. **185**(3): p. 1155-61.
115. Bork, P. and M. Sudol, *The WW domain: a signalling site in dystrophin?* Trends Biochem Sci, 1994. **19**(12): p. 531-3.
116. Morrione, A., et al., *mGrb10 interacts with Nedd4*. J Biol Chem, 1999. **274**(34): p. 24094-9.
117. Yang, B. and S. Kumar, *Nedd4 and Nedd4-2: closely related ubiquitin-protein ligases with distinct physiological functions*. Cell Death Differ, 2010. **17**(1): p. 68-77.

118. Sudol, M., et al., *Characterization of a novel protein-binding module--the WW domain*. FEBS Lett, 1995. **369**(1): p. 67-71.
119. Anan, T., et al., *Human ubiquitin-protein ligase Nedd4: expression, subcellular localization and selective interaction with ubiquitin-conjugating enzymes*. Genes Cells, 1998. **3**(11): p. 751-63.
120. Putz, U., et al., *Nedd4 family-interacting protein 1 (Ndfip1) is required for the exosomal secretion of Nedd4 family proteins*. J Biol Chem, 2008. **283**(47): p. 32621-7.
121. Cao, X.R., et al., *Nedd4 controls animal growth by regulating IGF-1 signaling*. Sci Signal, 2008. **1**(38): p. ra5.
122. Fouladkou, F., et al., *The ubiquitin ligase Nedd4-1 is required for heart development and is a suppressor of thrombospondin-1*. J Biol Chem, 2010. **285**(9): p. 6770-80.
123. Luhtala, S., et al., *Clinicopathological and prognostic correlations of HER3 expression and its degradation regulators, NEDD4-1 and NRDP1, in primary breast cancer*. BMC Cancer, 2018. **18**(1): p. 1045.
124. Huang, Z., et al., *The E3 ubiquitin ligase NEDD4 negatively regulates HER3/ErbB3 level and signaling*. Oncogene, 2015. **34**(9): p. 1105-15.
125. Zhang, J., et al., *Diosgenin inhibits the expression of NEDD4 in prostate cancer cells*. Am J Transl Res, 2019. **11**(6): p. 3461-3471.
126. Guo, Y., et al., *NEDD4 Negatively Regulates G1TR via Ubiquitination in Immune Microenvironment of Melanoma*. Onco Targets Ther, 2019. **12**: p. 10629-10637.
127. Wang, Z.W., et al., *NEDD4 E3 ligase: Functions and mechanism in human cancer*. Semin Cancer Biol, 2020.
128. Gu, Y., et al., *Microarray analysis and functional characterization revealed NEDD4-mediated cardiomyocyte autophagy induced by angiotensin II*. Cell Stress Chaperones, 2019. **24**(1): p. 203-212.
129. Xu, J., et al., *NEDD4 protects vascular endothelial cells against Angiotensin II-induced cell death via enhancement of XPO1-mediated nuclear export*. Exp Cell Res, 2019. **383**(1): p. 111505.
130. Novellasdemunt, L., et al., *NEDD4 and NEDD4L regulate Wnt signalling and intestinal stem cell priming by degrading LGR5 receptor*. EMBO J, 2020. **39**(3): p. e102771.
131. Verma, N., et al., *Targeting of PYK2 Synergizes with EGFR Antagonists in Basal-like TNBC and Circumvents HER3-Associated Resistance via the NEDD4-NDRG1 Axis*. Cancer Res, 2017. **77**(1): p. 86-99.
132. Shao, G., et al., *The E3 ubiquitin ligase NEDD4 mediates cell migration signaling of EGFR in lung cancer cells*. Mol Cancer, 2018. **17**(1): p. 24.
133. Lin, Q., et al., *HECT E3 ubiquitin ligase Nedd4-1 ubiquitinates ACK and regulates epidermal growth factor (EGF)-induced degradation of EGF receptor and ACK*. Mol Cell Biol, 2010. **30**(6): p. 1541-54.
134. Polo, S., et al., *A single motif responsible for ubiquitin recognition and monoubiquitination in endocytic proteins*. Nature, 2002. **416**(6879): p. 451-5.
135. Woelk, T., et al., *Molecular mechanisms of coupled monoubiquitination*. Nat Cell Biol, 2006. **8**(11): p. 1246-54.
136. Hoeller, D., et al., *Regulation of ubiquitin-binding proteins by monoubiquitination*. Nat Cell Biol, 2006. **8**(2): p. 163-9.
137. Katz, M., et al., *Ligand-independent degradation of epidermal growth factor receptor involves receptor ubiquitylation and Hgs, an adaptor whose ubiquitin-interacting motif targets ubiquitylation by Nedd4*. Traffic, 2002. **3**(10): p. 740-51.
138. Pak, Y., et al., *Transport of LAPTM5 to lysosomes requires association with the ubiquitin ligase Nedd4, but not LAPTM5 ubiquitination*. J Cell Biol, 2006. **175**(4): p. 631-45.

139. Tan, X., et al., *LAPTM4B is a PtdIns(4,5)P2 effector that regulates EGFR signaling, lysosomal sorting, and degradation*. EMBO J, 2015. **34**(4): p. 475-90.
140. Ma, S., et al., *The Hippo Pathway: Biology and Pathophysiology*. Annu Rev Biochem, 2019. **88**: p. 577-604.
141. Park, J.H., et al., *YOD1 Deubiquitinates NEDD4 Involved in the Hippo Signaling Pathway*. Cell Physiol Biochem, 2020. **54**(1): p. 1-14.
142. Jeon, S.A., D.W. Kim, and J.Y. Cho, *Neural precursor cell-expressed, developmentally down-regulated 4 (NEDD4) regulates hydrogen peroxide-induced cell proliferation and death through inhibition of Hippo signaling*. FASEB J, 2019. **33**(12): p. 14772-14783.
143. Huang, X., et al., *The many substrates and functions of NEDD4-1*. Cell Death Dis, 2019. **10**(12): p. 904.
144. Chung, S., et al., *Possible involvement of NEDD4 in keloid formation; its critical role in fibroblast proliferation and collagen production*. Proc Jpn Acad Ser B Phys Biol Sci, 2011. **87**(8): p. 563-73.
145. Wang, Y., et al., *STAT3 operates as a novel transcription factor that regulates NEDD4 in Keloid*. Biochem Biophys Res Commun, 2019. **518**(4): p. 638-643.
146. Kawabe, H., et al., *Regulation of Rap2A by the ubiquitin ligase Nedd4-1 controls neurite development*. Neuron, 2010. **65**(3): p. 358-72.
147. Ramirez, A., et al., *A keratin K5Cre transgenic line appropriate for tissue-specific or generalized Cre-mediated recombination*. Genesis, 2004. **39**(1): p. 52-7.
148. Florin, L., et al., *Cre recombinase-mediated gene targeting of mesenchymal cells*. Genesis, 2004. **38**(3): p. 139-44.
149. Zheng, B., et al., *Ligand-dependent genetic recombination in fibroblasts : a potentially powerful technique for investigating gene function in fibrosis*. Am J Pathol, 2002. **160**(5): p. 1609-17.
150. Yang, J., et al., *Fibroblast growth factor receptors 1 and 2 in keratinocytes control the epidermal barrier and cutaneous homeostasis*. J Cell Biol, 2010. **188**(6): p. 935-52.
151. Stewart, S.A., et al., *Lentivirus-delivered stable gene silencing by RNAi in primary cells*. RNA, 2003. **9**(4): p. 493-501.
152. Martin, P., *Wound healing--aiming for perfect skin regeneration*. Science, 1997. **276**(5309): p. 75-81.
153. Eming, S.A., P. Martin, and M. Tomic-Canic, *Wound repair and regeneration: mechanisms, signaling, and translation*. Sci Transl Med, 2014. **6**(265): p. 265sr6.
154. Sen, C.K., et al., *Human skin wounds: a major and snowballing threat to public health and the economy*. Wound Repair Regen, 2009. **17**(6): p. 763-71.
155. Michalopoulos, G.K., *Liver regeneration*. J Cell Physiol, 2007. **213**(2): p. 286-300.
156. Boase, N.A. and S. Kumar, *NEDD4: The founding member of a family of ubiquitin-protein ligases*. Gene, 2015. **557**(2): p. 113-22.
157. Fujita, M., et al., *NEDD4 Is Involved in Inflammation Development during Keloid Formation*. J Invest Dermatol, 2019. **139**(2): p. 333-341.
158. Sennett, R., et al., *An Integrated Transcriptome Atlas of Embryonic Hair Follicle Progenitors, Their Niche, and the Developing Skin*. Dev Cell, 2015. **34**(5): p. 577-91.
159. Rezza, A., et al., *Signaling Networks among Stem Cell Precursors, Transit-Amplifying Progenitors, and their Niche in Developing Hair Follicles*. Cell Rep, 2016. **14**(12): p. 3001-18.
160. Liu, Y., et al., *Keratin 15 promoter targets putative epithelial stem cells in the hair follicle bulge*. J Invest Dermatol, 2003. **121**(5): p. 963-8.
161. Haase, I., et al., *Regulation of keratinocyte shape, migration and wound epithelialization by IGF-1- and EGF-dependent signalling pathways*. J Cell Sci, 2003. **116**(Pt 15): p. 3227-38.
162. Shibata, S., et al., *Adiponectin regulates cutaneous wound healing by promoting keratinocyte proliferation and migration via the ERK signaling pathway*. J Immunol, 2012. **189**(6): p. 3231-41.

163. Urwyler-Rosselet, C., et al., *Keratinocyte-Specific Ablation of RIPK4 Allows Epidermal Cornification but Impairs Skin Barrier Formation*. J Invest Dermatol, 2018. **138**(6): p. 1268-1278.
164. Werner, S. and R. Grose, *Regulation of wound healing by growth factors and cytokines*. Physiol Rev, 2003. **83**(3): p. 835-70.
165. Ming, M., et al., *UVB-induced ERK/AKT-dependent PTEN suppression promotes survival of epidermal keratinocytes*. Oncogene, 2010. **29**(4): p. 492-502.
166. Peus, D., et al., *H2O2 is required for UVB-induced EGF receptor and downstream signaling pathway activation*. Free Radic Biol Med, 1999. **27**(11-12): p. 1197-202.
167. Uchiyama, A., et al., *SOX2 Epidermal Overexpression Promotes Cutaneous Wound Healing via Activation of EGFR/MEK/ERK Signaling Mediated by EGFR Ligands*. J Invest Dermatol, 2019. **139**(8): p. 1809-1820 e8.
168. Schafer, M., et al., *Nrf2: a central regulator of UV protection in the epidermis*. Cell Cycle, 2010. **9**(15): p. 2917-8.
169. Hiebert, P., et al., *Nrf2-Mediated Fibroblast Reprogramming Drives Cellular Senescence by Targeting the Matrisome*. Dev Cell, 2018. **46**(2): p. 145-161 e10.
170. Telorack, M., et al., *A Glutathione-Nrf2-Thioredoxin Cross-Talk Ensures Keratinocyte Survival and Efficient Wound Repair*. PLoS Genet, 2016. **12**(1): p. e1005800.
171. Ye, X., et al., *NEDD4: a promising target for cancer therapy*. Curr Cancer Drug Targets, 2014. **14**(6): p. 549-56.
172. Zhao, Y., et al., *NEDD4 single nucleotide polymorphism rs2271289 is associated with keloids in Chinese Han population*. Am J Transl Res, 2016. **8**(2): p. 544-55.
173. Herovici, C., [*Picropolychrome: histological staining technic intended for the study of normal and pathological connective tissue*]. Rev Fr Etud Clin Biol, 1963. **8**: p. 88-9.
174. Meerbrey, K.L., et al., *The pINDUCER lentiviral toolkit for inducible RNA interference in vitro and in vivo*. Proc Natl Acad Sci U S A, 2011. **108**(9): p. 3665-70.
175. Wenczak, B.A., J.B. Lynch, and L.B. Nanney, *Epidermal growth factor receptor distribution in burn wounds. Implications for growth factor-mediated repair*. J Clin Invest, 1992. **90**(6): p. 2392-401.
176. Ramirez, A., et al., *Sequences 5' of the bovine keratin 5 gene direct tissue- and cell-type-specific expression of a lacZ gene in the adult and during development*. Differentiation, 1994. **58**(1): p. 53-64.
177. Hardman, M.J., et al., *Patterned acquisition of skin barrier function during development*. Development, 1998. **125**(8): p. 1541-52.
178. Schmitz, A., et al., *Assessing the in vivo epidermal barrier in mice: dye penetration assays*. J Invest Dermatol, 2015. **135**(2): p. 1-4.
179. Trempus, C.S., et al., *Enrichment for living murine keratinocytes from the hair follicle bulge with the cell surface marker CD34*. J Invest Dermatol, 2003. **120**(4): p. 501-11.
180. Harvey, K.F., et al., *All three WW domains of murine Nedd4 are involved in the regulation of epithelial sodium channels by intracellular Na<sup>+</sup>*. J Biol Chem, 1999. **274**(18): p. 12525-30.
181. Kamynina, E., et al., *A novel mouse Nedd4 protein suppresses the activity of the epithelial Na<sup>+</sup> channel*. FASEB J, 2001. **15**(1): p. 204-214.
182. Snyder, P.M., J.C. Steines, and D.R. Olson, *Relative contribution of Nedd4 and Nedd4-2 to ENaC regulation in epithelia determined by RNA interference*. J Biol Chem, 2004. **279**(6): p. 5042-6.
183. Stoscheck, C.M., L.B. Nanney, and L.E. King, Jr., *Quantitative determination of EGF-R during epidermal wound healing*. J Invest Dermatol, 1992. **99**(5): p. 645-9.
184. Repertinger, S.K., et al., *EGFR enhances early healing after cutaneous incisional wounding*. J Invest Dermatol, 2004. **123**(5): p. 982-9.
185. Greenhalgh, D.G., *The role of growth factors in wound healing*. J Trauma, 1996. **41**(1): p. 159-67.

186. Steed, D.L., *Modifying the wound healing response with exogenous growth factors*. Clin Plast Surg, 1998. **25**(3): p. 397-405.
187. Marikovsky, M., et al., *Wound fluid-derived heparin-binding EGF-like growth factor (HB-EGF) is synergistic with insulin-like growth factor-I for Balb/MK keratinocyte proliferation*. J Invest Dermatol, 1996. **106**(4): p. 616-21.
188. Bitar, M.S., *Insulin and glucocorticoid-dependent suppression of the IGF-I system in diabetic wounds*. Surgery, 2000. **127**(6): p. 687-95.
189. Gartner, M.H., J.D. Benson, and M.D. Caldwell, *Insulin-like growth factors I and II expression in the healing wound*. J Surg Res, 1992. **52**(4): p. 389-94.
190. Lynch, S.E., R.B. Colvin, and H.N. Antoniades, *Growth factors in wound healing. Single and synergistic effects on partial thickness porcine skin wounds*. J Clin Invest, 1989. **84**(2): p. 640-6.
191. Fukushima, T., et al., *Nedd4-induced monoubiquitination of IRS-2 enhances IGF signalling and mitogenic activity*. Nat Commun, 2015. **6**: p. 6780.
192. Kwak, Y.D., et al., *Upregulation of the E3 ligase NEDD4-1 by oxidative stress degrades IGF-1 receptor protein in neurodegeneration*. J Neurosci, 2012. **32**(32): p. 10971-81.
193. Kumar, S., et al., *cDNA cloning, expression analysis, and mapping of the mouse Nedd4 gene*. Genomics, 1997. **40**(3): p. 435-43.
194. Wen, W., et al., *Inhibition of NEDD4 inhibits cell growth and invasion and induces cell apoptosis in bladder cancer cells*. Cell Cycle, 2017. **16**(16): p. 1509-1514.
195. Anindya, R., O. Aygun, and J.Q. Svejstrup, *Damage-induced ubiquitylation of human RNA polymerase II by the ubiquitin ligase Nedd4, but not Cockayne syndrome proteins or BRCA1*. Mol Cell, 2007. **28**(3): p. 386-97.
196. El-Abaseri, T.B., S. Putta, and L.A. Hansen, *Ultraviolet irradiation induces keratinocyte proliferation and epidermal hyperplasia through the activation of the epidermal growth factor receptor*. Carcinogenesis, 2006. **27**(2): p. 225-31.
197. Fombonne, J., et al., *Patched dependence receptor triggers apoptosis through ubiquitination of caspase-9*. Proc Natl Acad Sci U S A, 2012. **109**(26): p. 10510-5.
198. Persaud, A., et al., *Comparison of substrate specificity of the ubiquitin ligases Nedd4 and Nedd4-2 using proteome arrays*. Mol Syst Biol, 2009. **5**: p. 333.
199. Zhou, W., et al., *SAG/RBX2 is a novel substrate of NEDD4-1 E3 ubiquitin ligase and mediates NEDD4-1 induced chemosensitization*. Oncotarget, 2014. **5**(16): p. 6746-55.
200. Govoni, K.E., et al., *Conditional deletion of insulin-like growth factor-I in collagen type 1alpha2-expressing cells results in postnatal lethality and a dramatic reduction in bone accretion*. Endocrinology, 2007. **148**(12): p. 5706-15.
201. Feil, R., et al., *Ligand-activated site-specific recombination in mice*. Proc Natl Acad Sci U S A, 1996. **93**(20): p. 10887-90.
202. Chen, C. and L.E. Matesic, *The Nedd4-like family of E3 ubiquitin ligases and cancer*. Cancer Metastasis Rev, 2007. **26**(3-4): p. 587-604.
203. Kathman, S.G., et al., *A Small Molecule That Switches a Ubiquitin Ligase From a Processive to a Distributive Enzymatic Mechanism*. J Am Chem Soc, 2015. **137**(39): p. 12442-5.
204. Quirrit, J.G., et al., *Indole-3-carbinol (I3C) analogues are potent small molecule inhibitors of NEDD4-1 ubiquitin ligase activity that disrupt proliferation of human melanoma cells*. Biochem Pharmacol, 2017. **127**: p. 13-27.
205. Salah, Z., et al., *NEDD4 E3 ligase inhibits the activity of the Hippo pathway by targeting LATS1 for degradation*. Cell Cycle, 2013. **12**(24): p. 3817-23.
206. Lefort, K. and G.P. Dotto, *Notch signaling in the integrated control of keratinocyte growth/differentiation and tumor suppression*. Semin Cancer Biol, 2004. **14**(5): p. 374-86.

207. Sakata, T., et al., *Drosophila Nedd4 regulates endocytosis of notch and suppresses its ligand-independent activation*. *Curr Biol*, 2004. **14**(24): p. 2228-36.
208. Kimura, H., et al., *EGF positively regulates the proliferation and migration, and negatively regulates the myofibroblast differentiation of periodontal ligament-derived endothelial progenitor cells through MEK/ERK- and JNK-dependent signals*. *Cell Physiol Biochem*, 2013. **32**(4): p. 899-914.
209. Savio, M.G., et al., *USP9X Controls EGFR Fate by Deubiquitinating the Endocytic Adaptor Eps15*. *Curr Biol*, 2016. **26**(2): p. 173-183.
210. Marmor, M.D. and Y. Yarden, *Role of protein ubiquitylation in regulating endocytosis of receptor tyrosine kinases*. *Oncogene*, 2004. **23**(11): p. 2057-70.
211. Hung, V., et al., *Spatially resolved proteomic mapping in living cells with the engineered peroxidase APEX2*. *Nat Protoc*, 2016. **11**(3): p. 456-75.
212. Hesketh, G.G., et al., *Parallel Exploration of Interaction Space by BioID and Affinity Purification Coupled to Mass Spectrometry*. *Methods Mol Biol*, 2017. **1550**: p. 115-136.
213. Callis, J. and R. Ling, *Preparation, characterization, and use of tagged ubiquitins*. *Methods Enzymol*, 2005. **399**: p. 51-64.
214. Mark, K.G., T.B. Loveless, and D.P. Toczyski, *Isolation of ubiquitinated substrates by tandem affinity purification of E3 ligase-polyubiquitin-binding domain fusions (ligase traps)*. *Nat Protoc*, 2016. **11**(2): p. 291-301.
215. Lomonosova, E., J. Ryerse, and G. Chinnadurai, *BAX/BAK-independent mitoptosis during cell death induced by proteasome inhibition?* *Mol Cancer Res*, 2009. **7**(8): p. 1268-84.
216. Yoon, J.H., et al., *Activin receptor-like kinase5 inhibition suppresses mouse melanoma by ubiquitin degradation of Smad4, thereby derepressing eomesodermin in cytotoxic T lymphocytes*. *EMBO Mol Med*, 2013. **5**(11): p. 1720-39.
217. O'Connor, H.F., et al., *Ubiquitin-Activated Interaction Traps (UBAITs): Tools for Capturing Protein-Protein Interactions*. *Methods Mol Biol*, 2018. **1844**: p. 85-100.
218. Altun, M., et al., *Activity-based chemical proteomics accelerates inhibitor development for deubiquitylating enzymes*. *Chem Biol*, 2011. **18**(11): p. 1401-12.
219. Michel, M.A., et al., *Ubiquitin Linkage-Specific Affimers Reveal Insights into K6-Linked Ubiquitin Signaling*. *Mol Cell*, 2017. **68**(1): p. 233-246 e5.
220. Beaudette, P., O. Popp, and G. Dittmar, *Proteomic techniques to probe the ubiquitin landscape*. *Proteomics*, 2016. **16**(2): p. 273-87.
221. Kliza, K., et al., *Internally tagged ubiquitin: a tool to identify linear polyubiquitin-modified proteins by mass spectrometry*. *Nat Methods*, 2017. **14**(5): p. 504-512.
222. Udeshi, N.D., et al., *Large-scale identification of ubiquitination sites by mass spectrometry*. *Nat Protoc*, 2013. **8**(10): p. 1950-60.
223. Udeshi, N.D., et al., *Refined preparation and use of anti-diglycine remnant (K-epsilon-GG) antibody enables routine quantification of 10,000s of ubiquitination sites in single proteomics experiments*. *Mol Cell Proteomics*, 2013. **12**(3): p. 825-31.
224. Chicooree, N. and J.R. Griffiths, *A Combined Chemical Derivatization/Mass Spectrometric Method for the Enhanced Detection and Relative Quantification of Protein Ubiquitination*. *Methods Mol Biol*, 2019. **1977**: p. 17-24.
225. Swayden, M., et al., *Profiling Ubiquitin and Ubiquitin-like Dependent Post-translational Modifications and Identification of Significant Alterations*. *J Vis Exp*, 2019(153).



# Curriculum Vitae

## Personal information

Name: Shen Yan  
Date and place of birth: 25<sup>th</sup> December 1989, Beijing, China  
Nationality: Chinese  
Address: Otto-Stern-Weg 7, 8093 Zurich, Switzerland  
E-mail: shen.yan@biol.ethz.ch

## Education

2016.2-2020.11 PhD thesis  
Swiss Federal Institute of Technology (ETH) Zurich, Switzerland  
“Molecular and Translational Biomedicine” (MTB) Ph.D. program  
Life Science Zurich Graduate School (LSZGS)

2012.9-2015.6 Master of Natural Science in Cell Biology  
State Key Laboratory of Cellular Stress Biology  
Xiamen University, China

2008.9-2012.7 Bachelor of Science in Biochemistry and Biotechnology  
Xiamen University, China

## Publications

**Yan S**, Ripamonti R, Ben-Yehuda Greenwald M, Kawabe H, and Werner S. "NEDD4-1 is a key regulator of epidermal homeostasis, wound repair and UV response." *Manuscript in preparation*.

**Yan S**, Ripamonti R, Angel P, Kawabe H, Cangkrama M and Werner S. "Nedd4-1 is a key regulator of fibroblast function in vitro and during mouse development." *Manuscript in preparation*.

Wu RS\*, Hong JJ\*, Wu JF\*, **Yan S\***, Wu D, Liu N, Liu QF, Wu QW, Xie YY, Liu YJ, Zheng ZZ, Chan EC, Zhang ZM and Li BA. "OVOL2 antagonizes TGF-beta signaling to regulate epithelial to mesenchymal transition during mammary tumor metastasis." *Oncotarget*, 2017. 8(24): p. 39401-39416. \*Equal contribution

Wang ZH, Li Z, Hu M, Yang QJ, **Yan S**, Wu RS, Li BA and Guo M. "Ovol2 gene inhibits the Epithelial-to-Mesenchymal Transition in lung adenocarcinoma by transcriptionally repressing Twist1." *Gene*, 2017. 600: p. 1-8.